論文 / 著書情報
Article / Book Information

題目(和文)	グルタミン代謝に関連したトランスポーターの認識に基づき腫瘍選択的に相互作用する機能性高分子の開発
Title(English)	Development of Glutamine-Functionalized Polymers with Tumor-Selective Interaction Capacity by Sensing Dense Glutaminolysis-Related Transporters
著者(和文)	山田直生
Author(English)	Naoki Yamada
出典(和文)	学位:博士(工学), 学位授与機関:東京工業大学, 報告番号:甲第10658号, 授与年月日:2017年9月20日, 学位の種別:課程博士, 審査員:西山 伸宏,上田 宏,山口 猛央,宍戸 厚,丸山 厚
Citation(English)	Degree:Doctor (Engineering), Conferring organization: Tokyo Institute of Technology, Report number:甲第10658号, Conferred date:2017/9/20, Degree Type:Course doctor, Examiner:,,,,
学位種別(和文)	博士論文
Type(English)	Doctoral Thesis

博士論文

Development of Glutamine-Functionalized Polymers with Tumor-Selective Interaction Capacity by Sensing Dense Glutaminolysis-Related Transporters

(グルタミン代謝に関連したトランスポーターの認識に基づき腫瘍選択的に相互作用する機能性高分子の開発)

山田 直生

Table of contents

Chapter 1. General introduction

1.1 Drug Delivery System for Cancer Therapy

Cancer is a leading cause of death in the world. For effective cancer therapy, tremendous efforts have been made to develop novel therapeutic/diagnostic techniques. Among them, drug delivery system (DDS), a technique for tissue/cell selective delivery of therapeutic agents, is one of the noteworthy techniques. In conventional chemotherapy, anticancer drugs distribute non-specifically in whole body, leading to severe side effects. In contrast, DDS allows selective delivery of drugs to disease sites, thereby showing enhanced therapeutic efficacy and reduced side effects [1,2]. As drug carries for tumor-targeted DDS, nano-sized materials (e.g., polymeric micelles, liposomes, dendrimers, and polymer-drug conjugates) [3-6] have recently attracted considerable attentions because these nano-sized materials selectively accumulate in tumor tissue by two different but connected ways: passive targeting and active targeting.

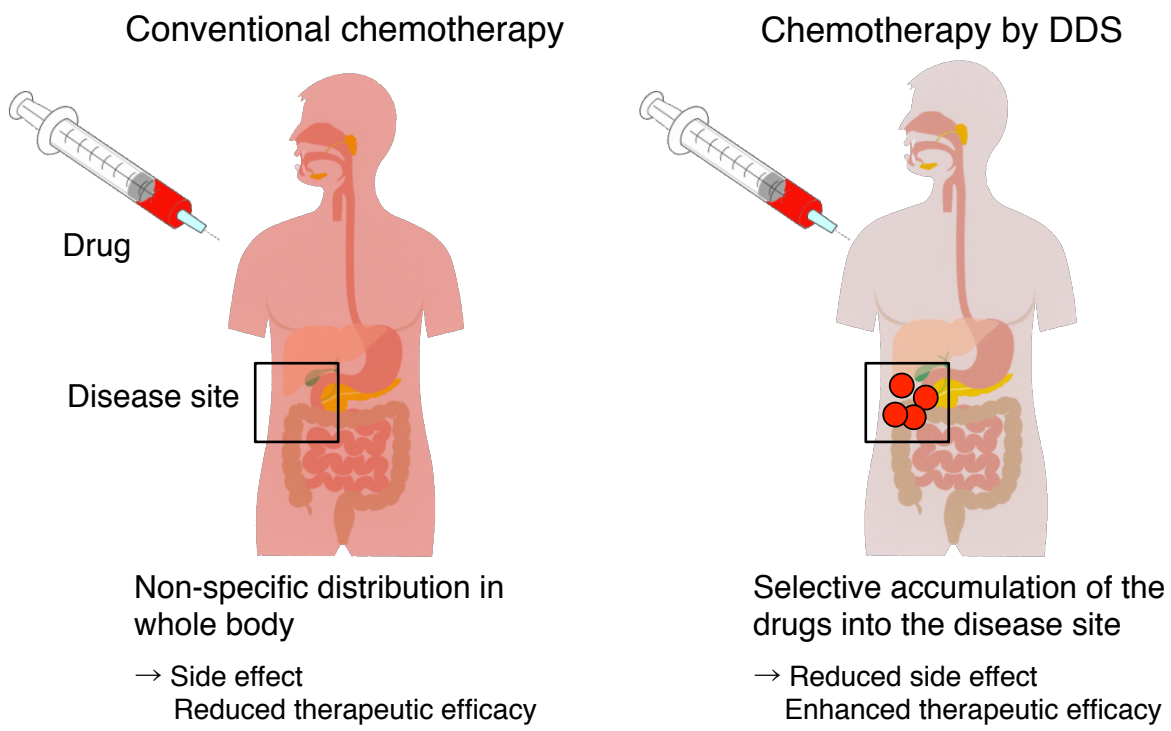

Figure 1-1. Schematic illustrations of drug delivery systems.

In conventional chemotherapy, the administrated drugs distribute non-specifically in whole body, leading to cause severe side effect. In contrast, DDS allows the selective accumulation of the administrated drugs into the disease site, thereby reducing the side effect and enhancing the therapeutic efficacy.

1.1.1 Passive targeting

Compared to normal blood vessels, tumor blood vessels show abnormal structure probably due to their formation under excessive angiogenesis [7-10]. In particular, tumor blood vessels have gaps between endothelial cells, deficient pericytes coverage, and discontinuous basement membrane, leading to an enhanced vascular permeability [8]. Thus, nano-sized drug carriers selectively penetrate into tumor tissues through the leaky blood vessels (Figure 1-2 a) while the penetration of nano-sized drug carriers in normal tissues is inhibited because of the tight junction between endothelial cells in normal blood vessels. In addition, because tumor tissues have deficient lymphatic drainages system, the nano-sized

drug carriers penetrated into tumor tissues are unlikely to be eliminated, thereby showing longer retention in the tumor tissues. This passive targeting mechanism is called the enhanced permeability and retention effect (EPR effect) [11-13], and is fundamental strategy for tumor-targeted drug delivery. Indeed, based on the EPR effect, nano-sized drug carriers including liposomes and polymeric micelles achieved increased accumulation of drugs and therapeutic efficacy [14-20].

Although the EPR effect contributes to the extravasation of the nano-sized drug carriers, it dose not affect the cellular uptake efficiency of the drug carriers. To further improve the therapeutic efficacy of the drug carriers, a methodology that can improve the cellular uptake efficiency as well as tumor accumulation of the drug carriers should be developed. Moreover, because the EPR effect is depend on the tumor type [21, 22], the passive targeting is not effective for all tumors. To overcome these problems, active targeting strategy has been developed.

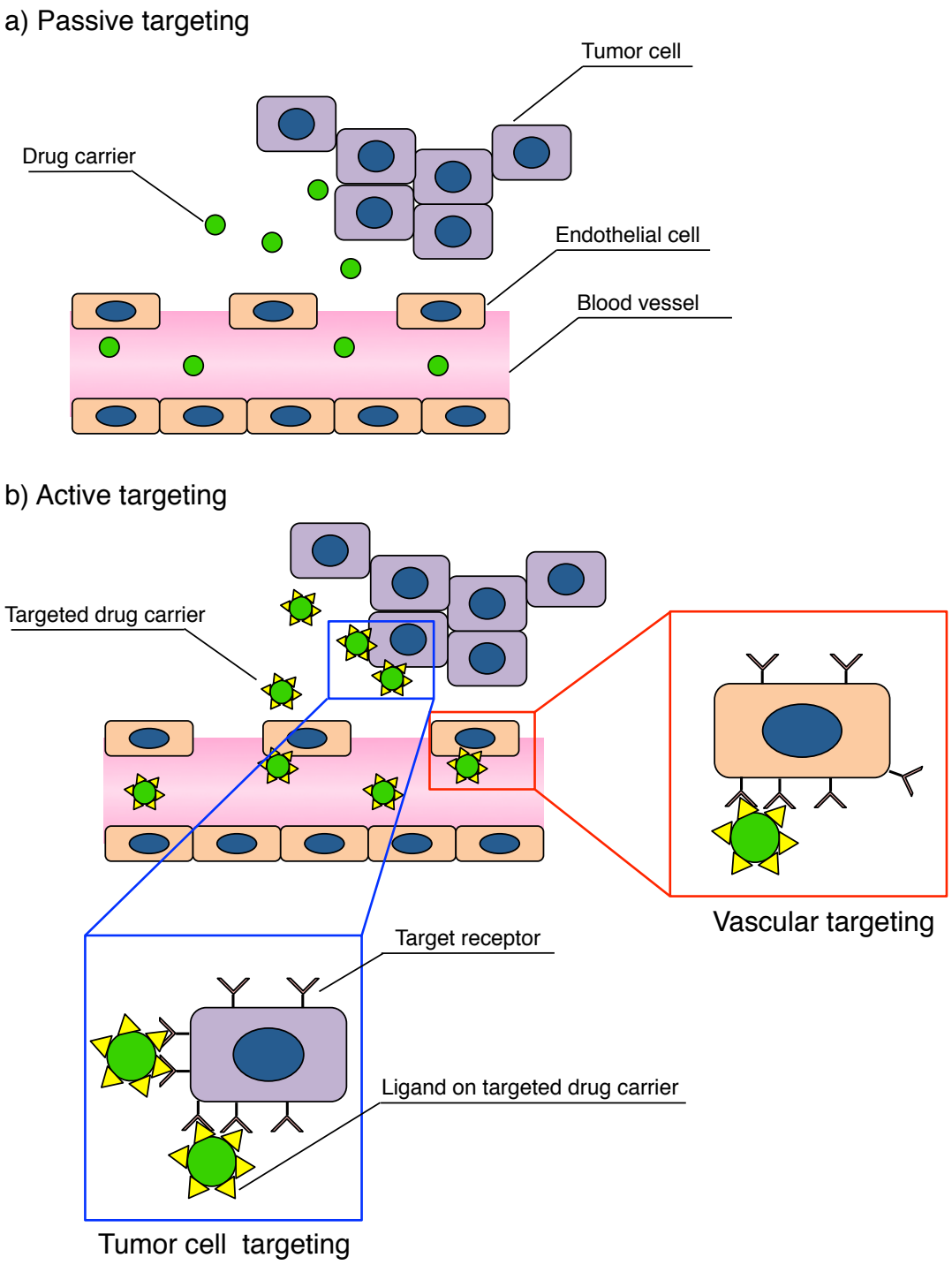

Figure 1-2. Schematic illustrations of passive and active targeting for tumor tissue.

(a) In passive targeting strategy, nano-sized drug carries selectively penetrate into tumor tissues through the leaky blood vessels. (b) In tumor cell targeting strategy (blue box), the nano-sized drug carriers having ligand molecules on the surface (targeted drug carrier) first extravasate into tumor tissue by the EPR effect, and then interact with the target receptors on tumor cells for facilitated cellular uptake. In vascular targeting strategy (red box), the targeted carriers should bind to endothelial cells in the tumor tissue to kill angiogenic blood vessels.

1.1.2 Active targeting

In active targeting strategy, nano-sized drug carriers have targeting ligand molecules on their surfaces to bind the appropriate receptors on the target sites (Figure 1-1 b). The role of ligand molecules is slightly different depend on the target sites.

For tumor cell targeting (as shown in a blue box in Figure 1-2 b), the ligand molecules should facilitate the cellular internalization of the drug carriers because the major objective of tumor cell targeting is improving the cellular uptake efficiency of the drug carriers. As discussed in passive targeting strategy, nano-sized drug carriers first penetrate into tumor tissues based on the EPR effect, and then the drug carriers may be taken up by the tumor cells but some of them stay in stroma or interstitial area in tumor tissues because of high interstitial pressure [23, 24]. The drug carriers internalized by tumor cells can kill the tumor cells; however, the entrapped drug carriers in stroma will be broken before reaching to tumor cells, leading to a decrease of antitumor efficacy of the drugs [25]. Therefore, it is important to increase cellular uptake of the drug carriers to improve therapeutic efficacy of the drugs. This objective can be achieved by tumor cell targeting strategy using ligand molecules that can bind to target receptors on the tumor cells. The folate receptor is one of the examples for the targets of tumor cell targeting. Folic acid is a ligand molecule to the folate receptor, and folic acid-modified nano-sized materials could interact with folate receptor with high affinity and be internalized into the cells by receptor-mediated endocytosis [26]. Another examples of the targets are carbohydrate antigens that are overexpressed on tumor cells due to the abnormal glycosylation [27]. Lectins are proteins that can strongly and specifically bind to certain carbohydrates, thus they are used as targeting ligands for carbohydrate antigens [28].

On the other hand, for tumor vascular targeting (as shown in a red box in figure 1-2 b), the ligand molecules should interact with the target receptor on the endothelial cells in tumor vasculature. This strategy is particularly effective to treat poorly permeable tumor because the drug carriers attached to the endothelial cells can exert their therapeutic efficacy by destroying the tumor vasculatures for starving the tumor tissues. The $\alpha_v\beta_3$ integrin, which is a receptor for extracellular matrix, is known to be overexpressed on endothelial cells in tumor angiogenic sites [29, 30]. Cyclic Arg-Gly-Asp peptide (cRGD) is frequently used as a ligand molecule for this $\alpha_v\beta_3$ integrin in DDS. Indeed, cRGD modified nanoparticles showed enhanced antitumor effect to glioblastoma, which is characterized by poorly permeable tumor blood vessels [31, 32].

Among ligand molecules developed so far, antibodies are attracting considerable attention as potent ligands because of their high affinity to the targets (dissociation constant is nM to pM range) with specificity. Utilizing this high affinity and target specificity of antibodies, antibody drug conjugates (ADCs) are developed as a new class of anticancer drugs for targeted therapy and showed potent antitumor effect [33]. To date, three ADCs are on the market and more than 30 ADCs are in clinical trials [34], indicating the potency of antibodies as ligands. On the other hand, antibodies have disadvantages as ligands: limitation of cancer specific targets (antigens) and high production cost. HER2 is one of the well-known antigens overexpressed in breast cancer; however, the HER2-positive ratio is 15-20% in total breast cancer patients [35]. Furthermore, antibodies are generally produced by biological systems, thereby limiting facile large-scale production and increasing the production cost. Folate and transferrin are potent ligands (dissociation constant is 1-300 nM for folate and 1-10 nM for transferrin) that can be produced at a low cost [36]. However, these ligands also

have problems. For example, both folate- and transferrin-decollated drug carriers showed undesired accumulation in the liver because their receptors express almost whole tissues including liver [36]. Furthermore, the folate receptor showed various expression level depend on cancer type, indicating low versatility [26]. Thus, novel potent ligand molecules for active targeting should possess these important characteristics: high affinity to the targets, low production cost, and enhanced cancer selectivity. With regard to the production cost, chemically synthesized ligands are promising candidates because they are easily produced in large scale and therefore the producing cost of the ligands can be low. In terms of cancer selectivity, one promising approach is developing the ligands that can sense the difference of the target density. In conventional ligands developments, one ligand molecule should bind tightly to one target protein. Although the target proteins generally overexpress in tumor tissue, the ligands developed in such direction potentially interact with the other healthy tissues expressing the target proteins. To avoid this problem, novel ligands should change their affinity to cells depend on the density of the target proteins.

1.2 Metabolic Alternation in Cancer Cells

Cancer cells reprogram their metabolic pathways due to their genetic and/or epigenetic alternations [37, 38]. Elevated glycolysis in the presence of oxygen, also known as Warburg effect or aerobic glycolysis, is one of the well-known metabolic alterations in cancer cells and was first described in 1924 by Otto Warburg [38, 39]. This Warburg effect explains a change of adenosine triphosphate (ATP) production pathway from glucose. In differentiated cells, glucose is first metabolized to pyruvate and most of the resultant pyruvate is further metabolized in the mitochondria to produce ATP through the tricarboxylic acid (TCA) cycle and oxidative phosphorylation [37, 39, 40]. Because the oxidative phosphorylation requires oxygen, this metabolic process is carried out in the presence of oxygen. However, in cancer cells, even with sufficient level of oxygen, the pyruvate derived from glucose is metabolized in glycolysis pathway, which generates ATP and lactate (Figure 1-3). Although the glycolysis pathway allows rapid ATP production compared to the oxidative phosphorylation, the ATP production efficiency of aerobic glycolysis is far less than that of oxidative phosphorylation (the aerobic glycolysis produces ~2 mol ATP/mol glucose while the oxidative phosphorylation produces ~36 mol ATP/mol glucose) [39]. Thus, to yield enough ATP for the growth and survival, cancer cells overexpress glucose transporters (e.g., GLUT1) and show augmented glucose uptake. Focusing on these characteristics, glucose derivatives were developed to target such disease sites. Indeed, ^{18}F-fluorodeoxyglucose successfully visualized tumor tissue in clinical studies [41, 42], indicating the potential of cancer-related metabolisms as a diagnostic/therapeutic target.

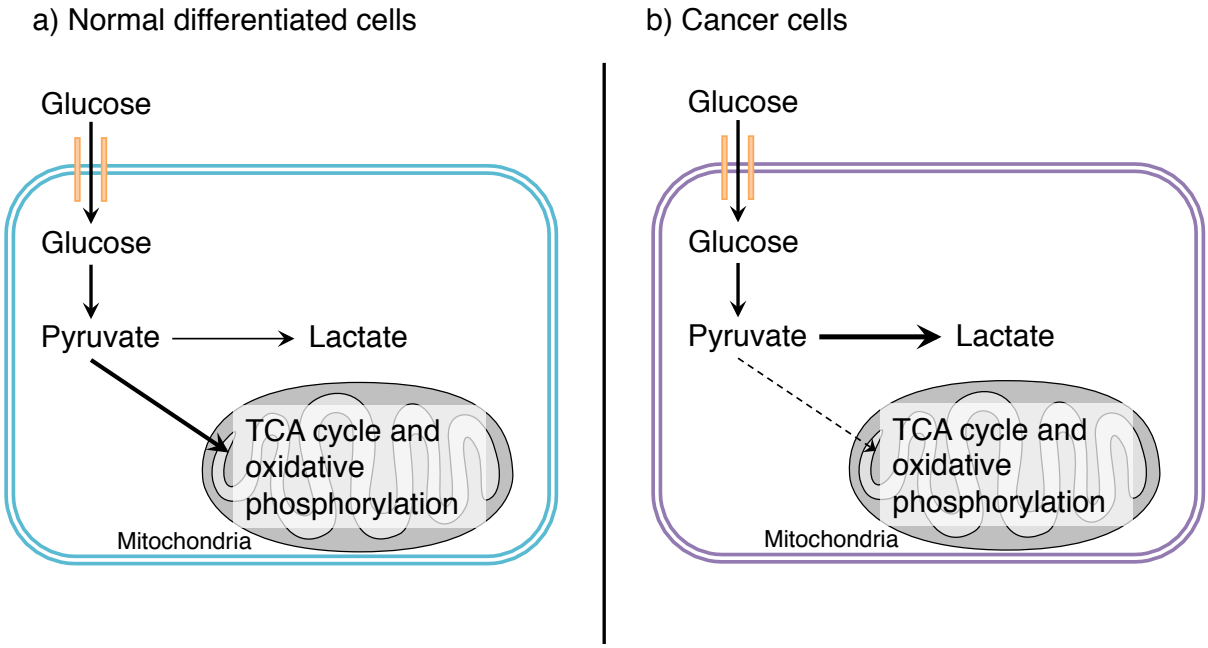

Figure 1-3. Glucose metabolism in differentiated cells and cancer cells.

In normal differentiated cells, glucose is first metabolized to pyruvate via glycolysis pathway and then most of that pyruvate is oxidized in mitochondria to generate ATP. In contrast, cancer cells metabolize most of glucose in glycolysis pathway.

In addition to this Warburg effect, recent advances in metabolite analysis have revealed the other cancer-related metabolism including lipid synthesis, fatty acids oxidation, and amino acids metabolisms over the past decade [38, 43, 44]. Among them, elevated glutamine metabolism (glutaminolysis) has recently attracted much attention because this glutaminolysis plays crucial roles for tumor growth and survival as described in the following section.

1.2.1 Glutaminolysis in cancer cells

The major function of glutaminolysis in cancer cells is providing alpha-ketoglutarate (α-KG), an intermediate in the TCA cycle (Figure 1-4). As explained by the Warburg effect, cancer cells metabolize glucose in the aerobic glycolysis rather than in

the oxidative phosphorylation, indicating a decreased demand of mitochondrial ATP production in tumor cells. One of the major functions of the TCA cycle is providing the substrates for oxidative phosphorylation; however, the TCA cycle also produces biosynthetic precursors that are essential in cancer cells. Thus, to maintain the functional TCA cycle, cancer cells rely on glutaminolysis: glutamine is first converted to glutamate, and further metabolized to α-KG to replenish the TCA cycle. In addition to this critical role, glutaminolysis also contributes to regulating redox balance by supporting the production of reducing agents such as glutathione (GSH) and nicotinamide adenine dinucleotide phosphate (NADPH) [45].

To satisfy the increased demand of glutamine, cancer cells overexpress glutamine transporters and show augmented glutamine uptake compared to normal cells. Among several glutamine transporters as shown in Table 1-1, system ASC transporter 2 (ASCT2) is considered to be the glutaminolysis-related transporter because ASCT2 overexpression was observed in various kinds of tumor tissues including hepatocellular carcinoma [46], breast cancer [47], prostate cancer [48], and pancreatic cancer [49]. In addition, inhibition of ASCT2 function has resulted in a decrease of glutamine uptake in cancer cells and suppression of tumor cell growth [47, 48, 50]. Furthermore, oncogene Myc up-regulated ASCT2 [51], while its expression was down-regulated by tumor suppressor retinoblastoma protein [52]. ASCT2 is a Na^+-dependent transporter that transports neutral amino acids including glutamine, alanine, and serine [53]. This transporter can transport amino acids bidirectionally; however, it showed asymmetric affinity for amino acids. For example, Michaelis constant (K_m) for extracellular glutamine was reported to be 20-60 μM, while *K*m for intracellular glutamine was reported to be 1.8 mM [53]. Most of internalized ASCT2 by

endocytosis reappeared on cell surface within one hour [54]. Furthermore, an increase of extracellular glutamine concentration enhanced the expression level of ASCT2 [55].

The increased glutamine uptake by overexpressed ASCT2 can be a potential target for tumor therapy/diagnosis. Previous studies have indeed demonstrated the successful *in vivo* tumor imaging using ^{18}F-labeled glutamine analogues [56-59]. Considering this promising potential, glutamine is expected to be used as an ASCT2-targeting ligand molecule. Furthermore, several advantages are attributable by using glutamine as a ligand (Table 1-2). Glutamine-based ligand can be chemically synthesized, leading to facile large-scale synthesis and low production cost. Given that the overexpression of target transporter ASCT2 was reported to be in various tumor cells as aforementioned, the glutamine-based ligand may have versatility. However, development of glutamine-based ligand is still a great challenge probably due to weak binding affinity of glutamine to ASCT2. Indeed, the dissociation constant (K_d) of glutamine to ASCT2 was estimated to be 20 μM [60], whereas K_d value of potent ligand molecules should be tens of nanomolar range [61]. Thus, chemical design of glutamine-functionalized molecules toward improvement of this weak binding affinity and enhancement of ASCT2 density-based cancer selectivity (as discussed in previous section) is prerequisite to utilize glutamine as a novel ligand.

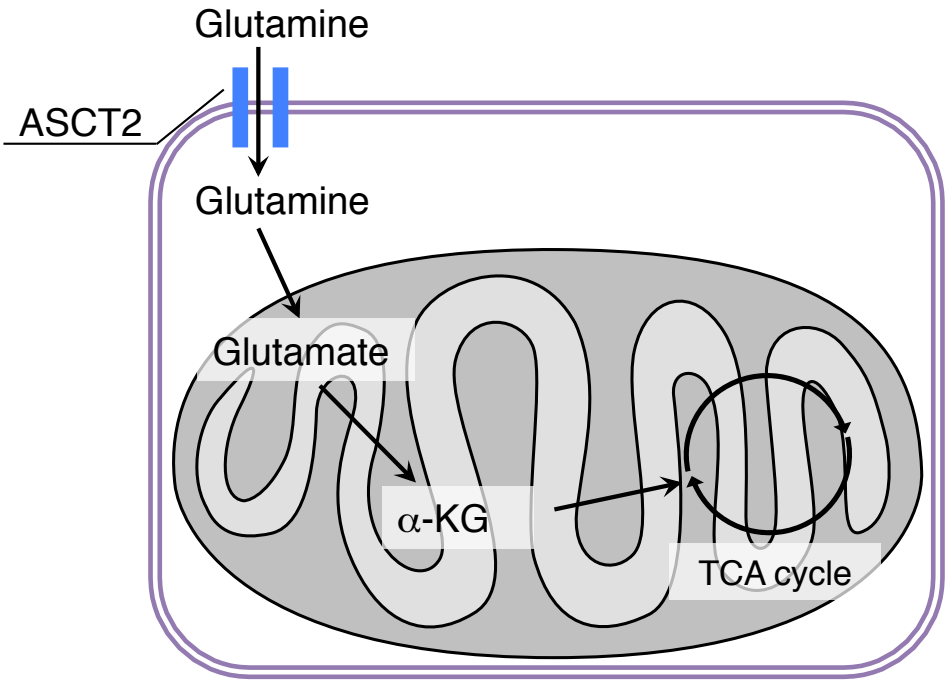

Figure 1-4. Glutaminolysis in cancer cells.

Glutamine is transported into cancer cells by glutamine transporter ASCT2. Then, the glutamine is metabolized to glutamate, and further metabolized to α-KG to maintain the functional TCA cycle

Table 1-1. Classification and characteristics of the glutamine transporters [55].

Family	Member	System	Aliases	Mechanism	Variant	Regulator/ mode
SLC1	*A5*	ASC	ASCT2, ATB0	Na^+-glutamine/ neutral amino acids antiport	Isoform1: NP_005619.1 Isoform 2: NP_001138616.1 Isoform 3: NP_001138617.1	Glutamine/protein expression EGF/trafficking and activity Insulin and IGF/activity mTOR/protein expression Leptin/trafficking and gene expression pRb/protein expression Aldosterone/protein expression
SLC6	*A14*	$B^{(0,+)}$	$ATB^{0,+}$	$2Na^+$-$1Cl^-$-glutamine co-transport (electrogenic)	NP_009162.1	EGF and GH/expression
	A19	B or B^0	B^0AT1	Na^+- glutamine co-transport, (electrogenic)	NP_001003841.1	collectrin (kidney), ACE2/trafficking APN (intestine)/activity and trafficking Leptin/trafficking and gene expression potassium/activity JAK2 (Janus kinase-2)/trafficking PKB-Akt and SGK/trafficking
	A15		B^0AT2	Na^+-glutamine co-transport, (electrogenic)	Isoform 1: NP_877499.1 Isoform 2: NP_060527.2 Isoform 3: NP_001139807.1	
SLC7	*A5*	L	LAT1	glutamine/ large neutral amino acids antiport	NP_003477.4 XP_006721350.1* XP_006721349.1*	4F2hc/trafficking c-Myc/protein expression EAA/protein expression Glucose/up regulation Aldosterone /protein expression insulin/increases mRNA abundance
	A8		LAT2	glutamine/ small neutral amino acids antiport	Isoform 1: NP_036376.2 Isoform 2: NP_877392.1 Isoform 3: NP_001253965.1 Isoform 4: NP_001253966.1	4F2hc/trafficking Aldosterone/protein expression mTORC1/trafficking DHT/protein expression
	A6		y+LAT2	Na^+ -glutamine /cationic amino acids antiport	NP_001070253.1	4F2hc/ trafficking
SLC38	*A1*	A	SNAT1, ATA1, SAT1, NAT2	Na^+-glutamine cotransport (electrogenic)	Isoform 1: NP_001265317.1 Isoform 2: NP_001265319.1	
	A2		SNAT2, ATA2, SAT2, SA1	Na^+-glutamine cotransport (electrogenic)	Isoform 1: NP_061849.2 Isoform 2: XP_005269040.1*Isoform 3: BAG57253.1*	DHT/activity glucagon/expression
	A3	N	SNAT3, SN1, NAT	Na^+-glutamine/H^+antiport (electroneutral)	NP_006832.1	Insulin/trafficking PKC/trafficking Manganese/degradation
	A5		SNAT5, SN2	Na^+-glutamine/H^+ antiport (electroneutral)	Isoform 1: NP_277053.2 Isoform 2: XP_005272752.1*	c-myc/expression
	A7		SNAT7	Na^+-glutamine/H^+antiport (electroneutral)	Isoform 1: NP_060701.1 Isoform 2: XP_006721292.1*	

Table 1-2. Comparison of established ligand molecules and glutamine

Ligand	Targets	Dissociation constant	Production Cost	Disadvantages	References
Antibody	Surface antigens	nM to pM	High	Limitation of the cancer specific antigens High cost	33, 34
Folate	Folate receptors	1-300 nM	Low	Variable expression of folate receptors in cancer cells	26, 36
Transferrin	Transferrin receptors	1-10 nM	Low	Undesired accumulation in liver Inhibition by free transferrin in blood	36
Glutamine	Glutamine transporters (widely expressed in cancer cells)	tens to hundreds μM	Low	Weak affinity to glutamine transporters compared to the above ligands	46-49, 60

1.3 Multivalent Interaction

Multivalent interaction is widely used in biological systems including virus infection and cell-cell interaction [63, 64]. In active targeting DDS, the multivalent interaction is also utilized; multiple presentations of the ligands on the surface of the drug carriers potentially enhance the interaction capacity with the target cells, thereby showing increased accumulation in the target site and enhanced therapeutic efficacy [65]. In addition, because the affinity of multivalent interaction depends on the density of the target receptors on the surface, multivalent interaction is expected to accomplish the selective binding. Previous studies indeed demonstrated the selective binding of the polymer-based multivalent ligand to the surface with certain receptor density [66, 67]. Thus, construction of multivalent

ligands should be a promising strategy for the development of potent ligands molecules for active targeting.

1.4 Significance of This Study

Elevated glutaminolysis has recently attracted much attention as one of the hallmarks of tumor cells; it has been well-documented that this elevated glutaminolysis is accompanied with increased uptake of glutamine mediated by specific glutamine transporters, including ASC transporter 2 (ASCT2). Although the molecular interaction between glutamine and ASCT2 offers great interests to sensing tumor cells, developing glutamine-functionalized molecules with high affinity to tumor cells is still a big challenge because binding affinity of single glutamine to ASCT2 is too weak for this purpose.

In this study, to develop glutamine-functionalized molecules with tumor-selective high affinity, I designed glutamine-functionalized polymer having multiple glutamine moieties at the side chain (Figure 1-5). As a polymer scaffold, poly(L-lysine) (PLys) was selected because PLys can be synthesized by *N*-carboxy anhydride (NCA) polymerization method, which allows facile control of polymer length with narrow molecular weight distribution, and the lysine residue can be modified to have glutamine-like structure *via* amide formation. It should be noted that the γ-amide modification of glutamine is expected to tolerate the ASCT2-glutamine interaction according to the previous studies [68, 69]. The multiple presentation of glutamine would facilitate strong interaction with dense ASCT2 on tumor cell surface by multivalent effect. On the other hand, because multivalent interaction is unlikely to occur on cell surface with low target transporter density [66, 67], weak single

glutamine-transporter interaction may contribute to minimal interaction between the glutamine-functionalized polymer and cells with low ASCT2 density.

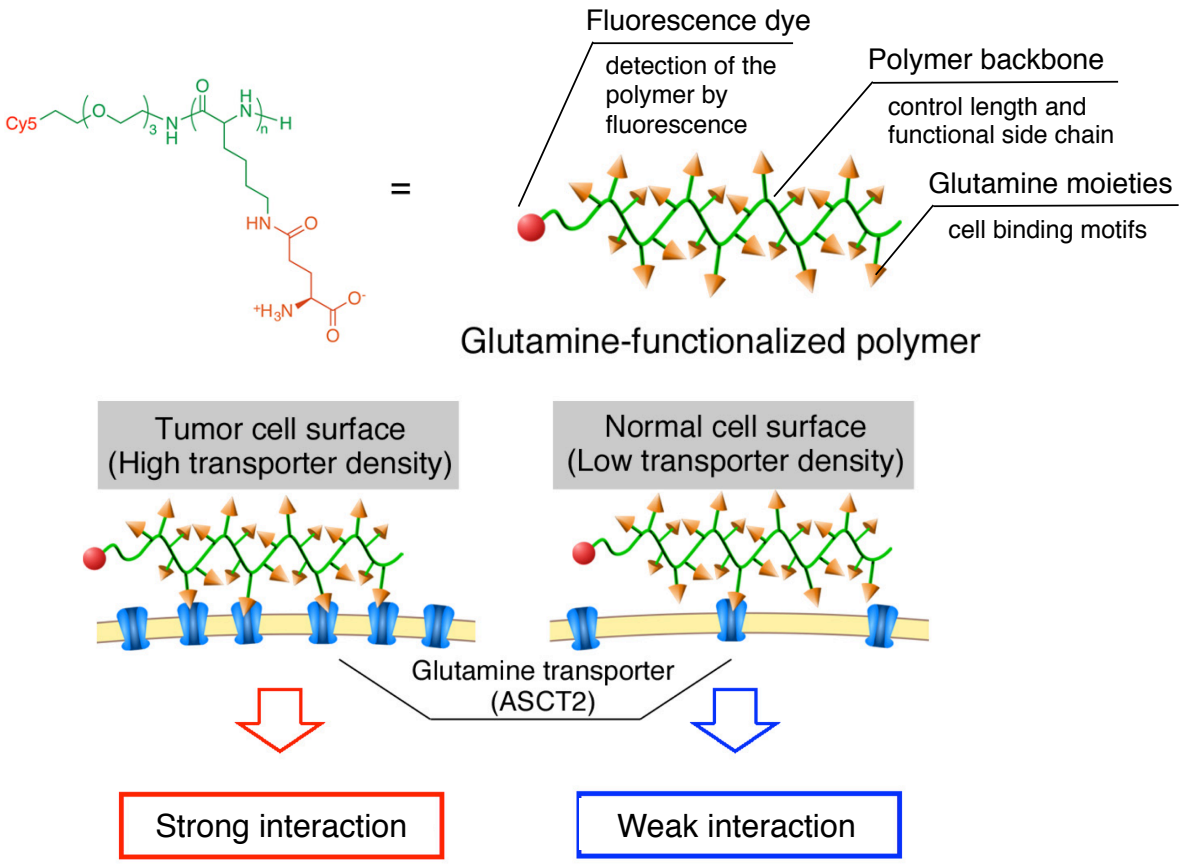

Figure 1-5. Design of glutamine-functionalized polymer and illustration of interaction between the glutamine-functionalized polymer and cell surface.

The polymer strongly interacts with tumor cell surface by multivalent interaction associated with high transporter density. In contrast, the polymer weakly interacts with normal cell surface because of low transporter density.

1.5 Outline of the Dissertation

Chapter 2 describes design, synthesis, and characterization of glutamine-functionalized polymers to achieve a high affinity to tumor cells. Through the *N*-carboxy anhydride (NCA) polymerization method and subsequent deprotection of the side

chain, azide-functionalized poly(L-lysine)s having controlled length with narrow molecular weight distribution were first prepared. Lysine residues of the synthesized polymers were then modified to have glutamine moieties through γ-amide linkage. Meanwhile, as control systems, glutamine moieties were changed to α-glutamyl moieties. Finally, Cy5 fluorescence dye was conjugated to the polymer terminus by copper-free click chemistry. The obtained polymers were characterized using ^{1}H NMR and GPC.

Chapter 3 describes the expression level of glutamine transporter ASCT2 in *in vitro* and *in vivo*. Flow cytometric analysis revealed overexpression of ASCT2 in human pancreatic cancer BxPC3 cells compared to human embryonic kidney HEK293 cells. In addition, the relative ASCT2 expression ratio between these cell lines was quantified by enzyme-linked immunosorbent assay. Moreover, this overexpression of ASCT2 was also confirmed in BxPC3 subcutaneous tumor compared to normal tissues.

Chapter 4 describes the biological activities of the glutamine-functionalized polymers in cultured cells and BxPC3 xenograft model. To investigate the cellular interaction of the synthesized polymers with cultured cells, cellular uptake efficiency of the polymers were analyzed using flow cytometer. Tumor cell specificity and transporter specificity of this interaction was also assessed. Binding affinity of the polymers to target transporters on BxPC3 cells was then estimated by cell-based competitive inhibition assay. Finally, *in vivo* interaction capacity of the polymers was evaluated by analyzing tumor retention of the polymer after intratumoral injection.

Chapter 5 describes the summary of the dissertation and future perspectives.

1.6 References

1. Allen, T. M. & Cullis, P. R. Drug delivery systems: entering the mainstream. *Science* **303,** 1818–1822 (2004).
2. Matsumura, Y. & Kataoka, K. Preclinical and clinical studies of anticancer agent-incorporating polymer micelles. *Cancer Sci.* **100,** 572–579 (2009).
3. Cabral, H., Nishiyama, N. & Kataoka, K. Supramolecular nanodevices: From design validation to theranostic nanomedicine. *Acc. Chem. Res.* **44,** 999–1008 (2011).
4. Barenholz, Y. Liposome application: problems and prospects. *Curr. Opin. Colloid Interface Sci.* **6,** 66–77 (2001).
5. Wu, L., Ficker, M., Christensen, J. B., Trohopoulos, P. N. & Moghimi, S. M. Dendrimers in Medicine: Therapeutic Concepts and Pharmaceutical Challenges. *Bioconjug. Chem.* 150213085013008 (2015). doi:10.1021/acs.bioconjchem.5b00031
6. Kopeček, J. Polymer-drug conjugates: Origins, progress to date and future directions. *Adv. Drug Deliv. Rev.* **65,** 49–59 (2013).
7. Carmeliet, P. & Jain, R. K. Angiogenesis in cancer and other diseases. *Nature* **407,** 249–257 (2000).
8. Danhier, F., Feron, O. & Préat, V. To exploit the tumor microenvironment: Passive and active tumor targeting of nanocarriers for anti-cancer drug delivery. *J. Control. Release* **148,** 135–146 (2010).
9. Moens, S., Goveia, J., Stapor, P. C., Cantelmo, A. R. & Carmeliet, P. The multifaceted activity of VEGF in angiogenesis - Implications for therapy responses. *Cytokine Growth Factor Rev.* **25,** 473–0482 (2014).
10. Bergers, G. & Benjamin, L. E. Tumorigenesis and the angiogenic switch. *Nat. Rev.*

Cancer **3,** 401–410 (2003).

11. Matsumura, Y. & Maeda, H. A new concept for macromolecular therapeutics in cnacer chemotherapy: mechanism of tumoritropic accumulatio of proteins and the antitumor agents Smancs. *Cancer Res.* **46,** 6387–6392 (1986).

12. Maeda, H., Wu, J., Sawa, T., Matsumura, Y. & Hori, K. Tumor vascular permeability and the EPR effect in macromolecular therapeutics: A review. *J. Control. Release* **65,** 271–284 (2000).

13. Maeda, H., Bharate, G. Y. & Daruwalla, J. Polymeric drugs for efficient tumor-targeted drug delivery based on EPR-effect. *Eur. J. Pharm. Biopharm.* **71,** 409–419 (2009).

14. Brusa, P., Immordino, M. L., Rocco, F. & Cattel, L. Antitumor activity and pharmacokinetics of liposomes containing lipophilic gemcitabine prodrugs. *Anticancer Res.* **27,** 195–200 (2007).

15. Cabral, H., Nishiyama, N. & Kataoka, K. Optimization of (1,2-diamino-cyclohexane)platinum(II)-loaded polymeric micelles directed to improved tumor targeting and enhanced antitumor activity. *J. Control. Release* **121,** 146–155 (2007).

16. Cabral, H., Matsumoto, Y., Mizuno, K., Chen, Q., Murakami, M., Kimura, M., Terada, Y., Kano, M. R., Miyazono, K., Uesaka, M., Nishiyama, N. & Kataoka, K. Accumulation of sub-100 nm polymeric micelles in poorly permeable tumours depends on size. *Nat. Nanotechnol.* **6,** 815–823 (2011).

17. Cabral, H., Nishiyama, N., Okazaki, S., Koyama, H. & Kataoka, K. Preparation and biological properties of dichloro(1,2-diaminocyclohexane)platinum(II)

(DACHPt)-loaded polymeric micelles. *J. Control. Release* **101,** 223–232 (2005).

18. Cabral, H., Murakami, M., Hojo, H., Terada, Y., Kano, M. R., Chung, U., Nishiyama, N. & Kataoka, K. Targeted therapy of spontaneous murine pancreatic tumors by polymeric micelles prolongs survival and prevents peritoneal metastasis. *Proc. Natl. Acad. Sci. U. S. A.* **110,** 11397–402 (2013).

19. Kataoka, K., Harada, a & Nagasaki, Y. Block copolymer micelles for drug delivery: design, characterization and biological significance. *Adv. Drug Deliv. Rev.* **47,** 113–131 (2001).

20. Uchida, S., Itaka, K., Chen, Q., Osada, K., Miyata, K., Ishii, T., Harada-Shiba, M. & Kataoka, K. Combination of chondroitin sulfate and polyplex micelles from Poly(ethylene glycol)-poly{N'-[N-(2-aminoethyl)-2-aminoethyl]aspartamide} block copolymer for prolonged in vivo gene transfection with reduced toxicity. *J. Control. Release* **155,** 296–302 (2011).

21. Hobbs, S. K., Monsky, W. L., Yuan, F., Roberts, W. G., Griffith, L., Torchilin, V. P. & Jain, R. K. Regulation of transport pathways in tumor vessels: role of tumor type and microenvironment. *Proc. Natl. Acad. Sci. U. S. A.* **95,** 4607–4612 (1998).

22. Cabral, H., Matsumoto, Y., Mizuno, K., Chen, Q., Murakami, M., Kimura, M., Terada, Y., Kano, M. R., Miyazono, K., Uesaka, M., Nishiyama, N. & Kataoka, K. Accumulation of sub-100 nm polymeric micelles in poorly permeable tumours depends on size. *Nat. Nanotechnol.* **6,** 815–23 (2011).

23. Jain, R. K. Physiological Barriers to Delivery of Monoclonal Antibodies and Other Macromolecules in Tumors1. (1990).

24. Adams, G. P., Schier, R., McCall, A. M., Simmons, H. H., Horak, E. M., Alpaugh, R.

K., Marks, J. D. & Weiner, L. M. High affinity restricts the localization and tumor penetration of single-chain fv antibody molecules. *Cancer Res.* **61,** 4750–5 (2001).

25. Huang, S. K., Mayhew, E., Gilani, S., Lasic, D. D., Martin, F. J. & Papahadjopoulos, D. Pharmacokinetics and therapeutics of sterically stabilized liposomes in mice bearing C-26 colon carcinoma. *Cancer Res.* **52,** 6774–81 (1992).

26. Low, P. S. & Kularatne, S. A. Folate-targeted therapeutic and imaging agents for cancer. *Curr. Opin. Chem. Biol.* **13,** 256–262 (2009).

27. Dube, D. H. & Bertozzi, C. R. Glycans in cancer and inflammation — potential for therapeutics and diagnostics. *Nat. Rev. Drug Discov.* **4,** 477–488 (2005).

28. Minko, T. Drug targeting to the colon with lectins and neoglycoconjugates. *Adv. Drug Deliv. Rev.* **56,** 491–509 (2004).

29. Hynes, R. O. A reevaluation of integrins as regulators of angiogenesis. *Nat. Med.* **8,** 918–921 (2002).

30. Hood, J. D. & Cheresh, D. A. Role of Integrins in Cell Invasion and Migration. *Nat. Rev. Cancer* **2,** 91–100 (2002).

31. Zhan, C., Gu, B., Xie, C., Li, J., Liu, Y. & Lu, W. Cyclic RGD conjugated poly(ethylene glycol)-co-poly(lactic acid) micelle enhances paclitaxel anti-glioblastoma effect. *J. Control. Release* **143,** 136–142 (2010).

32. Miura, Y., Takenaka, T., Toh, K., Wu, S., Nishihara, H., Kano, M. R., Ino, Y., Nomoto, T., Matsumoto, Y., Koyama, H., Cabral, H., Nishiyama, N. & Kataoka, K. Cyclic RGD-linked polymeric micelles for targeted delivery of platinum anticancer drugs to glioblastoma through the blood-brain tumor barrier. *ACS Nano* **7,** 8583–8592 (2013).

33. Diamantis, N. & Banerji, U. Antibody-drug conjugates—an emerging class of cancer

treatment. *Br. J. Cancer* **114,** 362–367 (2016).

34. Wicki, A., Witzigmann, D., Balasubramanian, V. & Huwyler, J. Nanomedicine in cancer therapy: Challenges, opportunities, and clinical applications. *J. Control. Release* **200,** 138–157 (2015).

35. Baselga, J., Cortés, J., Kim, S.-B., Im, S.-A., Hegg, R., Im, Y.-H., Roman, L., Pedrini, J. L., Pienkowski, T., Knott, A., Clark, E., Benyunes, M. C., Ross, G. & Swain, S. M. Pertuzumab plus Trastuzumab plus Docetaxel for Metastatic Breast Cancer. *N. Engl. J. Med.* **366,** 109–119 (2012).

36. Toporkiewicz, M. Toward a magic or imaginary bullet ? Ligands for drug targeting to cancer cells : principles , hopes , and challenges. 1399–1414 (2015).

37. Cairns, R. A., Harris, I. S. & Mak, T. W. Regulation of cancer cell metabolism. *Nat. Rev. Cancer* **11,** 85–95 (2011).

38. Galluzzi, L., Kepp, O., Vander Heiden, M. G. & Kroemer, G. Metabolic targets for cancer therapy. *Nat. Rev. Drug Discov.* **12,** 829–46 (2013).

39. Vander Heiden, M. G., Cantley, L. C. & Thompson, C. B. Understanding the Warburg effect: the metabolic requirements of cell proliferation. *Science (80-.).* **324,** 1029–33 (2009).

40. Dang, C. V. Rethinking the warburg effect with Myc micromanaging glutamine metabolism. *Cancer Res.* **70,** 859–862 (2010).

41. Kitajima, K., Doi, H. & Kuribayashi, K. Present and future roles of FDG-PET/CT imaging in the management of malignant pleural mesothelioma. *Jpn. J. Radiol.* **34,** 537–547 (2016).

42. Madsen, P. H., Holdgaard, P. C., Christensen, J. B. & Høilund-Carlsen, P. F. Clinical

utility of F-18 FDG PET-CT in the initial evaluation of lung cancer. *Eur. J. Nucl. Med. Mol. Imaging* 1–14 (2016). doi:10.1007/s00259-016-3407-4

43. Tennant, D. a., Durán, R. V., Boulahbel, H. & Gottlieb, E. Metabolic transformation in cancer. *Carcinogenesis* **30,** 1269–1280 (2009).

44. Vander Heiden, M. G. Targeting cancer metabolism: a therapeutic window opens. *Nat. Rev. Drug Discov.* **10,** 671–684 (2011).

45. Jin, L., Alesi, G. N. & Kang, S. Glutaminolysis as a target for cancer therapy. *Oncogene* **35,** 3619–25 (2016).

46. Namikawa, M., Kakizaki, S., Kaira, K., Tojima, H., Yamazaki, Y., Horiguchi, N., Sato, K., Oriuchi, N., Tominaga, H., Sunose, Y., Nagamori, S., Kanai, Y., Oyama, T., Takeyoshi, I. & Yamada, M. Expression of amino acid transporters (LAT1, ASCT2 and xCT) as clinical significance in hepatocellular carcinoma. *Hepatol. Res.* **45,** 1014–1022 (2015).

47. van Geldermalsen, M., Wang, Q., Nagarajah, R., Marshall, A. D., Thoeng, A., Gao, D., Ritchie, W., Feng, Y., Bailey, C. G., Deng, N., Harvey, K., Beith, J. M., Selinger, C. I., O'Toole, S. A., Rasko, J. E. J. & Holst, J. ASCT2/SLC1A5 controls glutamine uptake and tumour growth in triple-negative basal-like breast cancer. *Oncogene* **35,** 3201–8 (2016).

48. Wang, Q., Hardie, R.-A., Hoy, A. J., van Geldermalsen, M., Gao, D., Fazli, L., Sadowski, M. C., Balaban, S., Schreuder, M., Nagarajah, R., Wong, J. J.-L., Metierre, C., Pinello, N., Otte, N. J., Lehman, M. L., Gleave, M., Nelson, C. C., Bailey, C. G., Ritchie, W., Rasko, J. E. J. & Holst, J. Targeting ASCT2-mediated glutamine uptake blocks prostate cancer growth and tumour development. *J. Pathol.* **236,** 278–89

(2015).

49. Kaira, K., Sunose, Y., Arakawa, K., Sunaga, N., Shimizu, K., Tominaga, H., Oriuchi, N., Nagamori, S., Kanai, Y., Oyama, T. & Takeyoshi, I. Clinicopathological significance of ASC amino acid transporter-2 expression in pancreatic ductal carcinoma. *Histopathology* **66,** 234–243 (2015).

50. Wang, Q., Beaumont, K. a., Otte, N. J., Font, J., Bailey, C. G., van Geldermalsen, M., Sharp, D. M., Tiffen, J. C., Ryan, R. M., Jormakka, M., Haass, N. K., Rasko, J. E. J. & Holst, J. Targeting glutamine transport to suppress melanoma cell growth. *Int. J. cancer* **135,** 1060–71 (2014).

51. Gao, P., Tchernyshyov, I., Chang, T.-C., Lee, Y.-S., Kita, K., Ochi, T., Zeller, K. I., De Marzo, A. M., Van Eyk, J. E., Mendell, J. T. & Dang, C. V. c-Myc suppression of miR-23a/b enhances mitochondrial glutaminase expression and glutamine metabolism. *Nature* **458,** 762–765 (2009).

52. Reynolds, M. R., Lane, A. N., Robertson, B., Kemp, S., Liu, Y., Hill, B. G., Dean, D. C. & Clem, B. F. Control of glutamine metabolism by the tumor suppressor Rb. *Oncogene* **33,** 556–566 (2014).

53. Pochini, L., Scalise, M., Galluccio, M. & Indiveri, C. Membrane transporters for the special amino acid glutamine: structure/function relationships and relevance to human health. *Front. Chem.* **2,** 61 (2014).

54. Console, L., Scalise, M., Tarmakova, Z., Coe, I. R. & Indiveri, C. N-linked Glycosylation of human SLC1A5 (ASCT2) transporter is critical for trafficking to membrane. *Biochim. Biophys. Acta - Mol. Cell Res.* **1853,** 1636–1645 (2015).

55. Bungard, C. I. & McGivan, J. D. Glutamine availability up-regulates expression of the

amino acid transporter protein ASCT2 in HepG2 cells and stimulates the ASCT2 promoter. *Biochem. J.* **382,** 27–32 (2004).

56. Venneti, S., Dunphy, M. P., Zhang, H., Pitter, K. L., Zanzonico, P., Campos, C., Carlin, S. D., La Rocca, G., Lyashchenko, S., Ploessl, K., Rohle, D., Omuro, A. M., Cross, J. R., Brennan, C. W., Weber, W. A., Holland, E. C., Mellinghoff, I. K., Kung, H. F., Lewis, J. S. & Thompson, C. B. Glutamine-based PET imaging facilitates enhanced metabolic evaluation of gliomas in vivo. *Sci. Transl. Med.* **7,** 274ra17-274ra17 (2015).

57. Wu, Z., Zha, Z., Li, G., Lieberman, B. P., Choi, S. R., Ploessl, K. & Kung, H. F. [18 F](2 S ,4 S)-4-(3-Fluoropropyl)glutamine as a Tumor Imaging Agent. *Mol. Pharm.* **11,** 3852–3866 (2014).

58. Ploessl, K., Wang, L., Lieberman, B. P., Qu, W. & Kung, H. F. Comparative Evaluation of 18F-Labeled Glutamic Acid and Glutamine as Tumor Metabolic Imaging Agents. *J. Nucl. Med.* **53,** 1616–1624 (2012).

59. Hassanein, M., Hight, M. R., Buck, J. R., Tantawy, M. N., Nickels, M. L., Hoeksema, M. D., Harris, B. K., Boyd, K., Massion, P. P. & Manning, H. C. Preclinical Evaluation of 4-[18F]Fluoroglutamine PET to Assess ASCT2 Expression in Lung Cancer. *Mol. Imaging Biol.* **18,** 18–23 (2016).

60. Scalise, M., Pochini, L., Panni, S., Pingitore, P., Hedfalk, K. & Indiveri, C. Transport mechanism and regulatory properties of the human amino acid transporter ASCT2 (SLC1A5). *Amino Acids* **46,** 2463–2475 (2014).

61. Srinivasarao, M., Galliford, C. V. & Low, P. S. Principles in the design of ligand-targeted cancer therapeutics and imaging agents. *Nat. Rev. Drug Discov.* **14,** 203–219 (2015).

62. Pochini, L., Scalise, M., Galluccio, M. & Indiveri, C. Membrane transporters for the special amino acid glutamine: structure/function relationships and relevance to human health. *Front. Chem.* **2,** 1–23 (2014).

63. Cloninger, M. J., Bilgiçer, B., Li, L., Mangold, S. L., Phillips, S. T. & Wolfenden, M. L. in *Supramol. Chem.* **1,** 95–115 (John Wiley & Sons, Ltd, 2012).

64. Mammen, M., Choi, S.-K. & Whitesides, G. M. Polyvalent Interactions in Biological Systems: Implications for Design and Use of Multivalent Ligands and Inhibitors. *Angew. Chem. Int. Ed.* **37,** 2754–2794 (1998).

65. Kawamura, W., Miura, Y., Kokuryo, D., Toh, K., Yamada, N., Nomoto, T., Matsumoto, Y., Sueyoshi, D., Liu, X., Aoki, I., Kano, M. R., Nishiyama, N., Saga, T., Kishimura, A. & Kataoka, K. Density-tunable conjugation of cyclic RGD ligands with polyion complex vesicles for the neovascular imaging of orthotopic glioblastomas. *Sci. Technol. Adv. Mater.* **16,** 35004 (2016).

66. Dubacheva, G. V., Curk, T., Mognetti, B. M., Auzély-Velty, R., Frenkel, D. & Richter, R. P. Superselective Targeting Using Multivalent Polymers. *J. Am. Chem. Soc.* **136,** 1722–1725 (2014).

67. Dubacheva, G. V, Curk, T., Auzély-Velty, R., Frenkel, D. & Richter, R. P. Designing multivalent probes for tunable superselective targeting. *Proc. Natl. Acad. Sci. U. S. A.* **112,** 5579–84 (2015).

68. Esslinger, C. S., Cybulski, K. A. & Rhoderick, J. F. Nγ-Aryl glutamine analogues as probes of the ASCT2 neutral amino acid transporter binding site. *Bioorg. Med. Chem.* **13,** 1111–1118 (2005).

69. Schulte, M. L., Dawson, E. S., Saleh, S. a., Cuthbertson, M. L. & Manning, H. C.

2-Substituted Nγ-glutamylanilides as novel probes of ASCT2 with improved potency. *Bioorg. Med. Chem. Lett.* **25,** 113–116 (2015).

Chapter 2. Synthesis of glutamine-functionalized polymers

2.1 Introduction

Among several kinds of glutamine transporters, system ASC transporter 2 (ASCT2) plays a dominant contribution of glutamine uptake in tumor cells and was reported to be overexpressed on various kinds of tumor cells including hepatocellular carcinoma [1], breast cancer [2], prostate cancer [3], colorectal cancer [4], pancreatic cancer [5]. Thus, to achieve a high affinity to tumor cells, chemical structure of the glutamine-functionalized polymer should be designed to possess high interaction capacity with ASCT2. Considering that glutamine analogues having γ-amide modified structure inhibited ASCT2 function [6,7], γ-amide modification of glutamine is expected to tolerate ASCT2-glutamine interaction. Thus, in this study, glutamine moieties were tethered to polymer side chain through γ-amide linkage as shown in Figure 2-1.

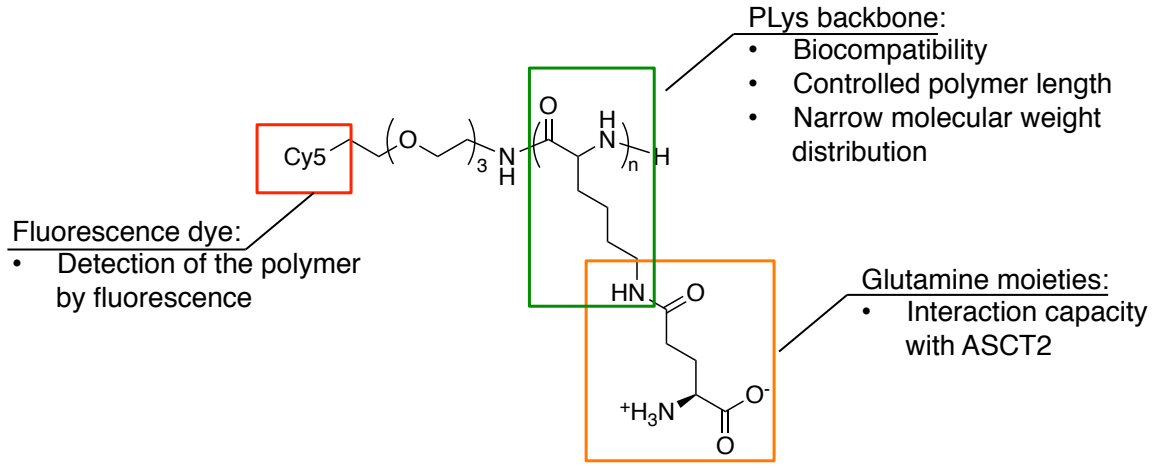

Figure 2-1. Design of glutamine-functionalized polymer.

The polymers are termed as PLys(Gln)-n, where n is the mean degree of polymerization of PLys.

In addition, polymer length should also be a crucial factor for the affinity of the glutamine-functionalized polymer to tumor cells because the interaction potency of

multivalent polymeric ligands depended on their length [8,9]. To obtain the glutamine-functionalized polymer with controlled length, a series of azide-functionalized poly(L-lysine) (PLys) having different degree of the polymerizations (DPs) were first synthesized as precursor polymers through ring-opening polymerization of *N*-carboxy anhydride (NCA) and subsequent deprotection. NCA polymerization is initiated by primary amine group as shown in Figure 2-2, and provides biocompatible poly(amino acid)s with controlled polymer length and narrow molecular weight distribution [10].

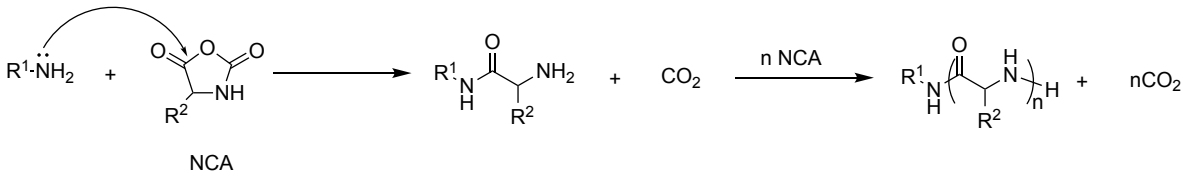

Figure 2-2. Mechanism of NCA polymerization.

Lysine residues of precursor polymers were then modified to have glutamine moieties by condensation and deprotection reaction based on the aforementioned consideration. Finally, Cy5 fluorescence dye was conjugated to the polymer terminus by copper-free click chemistry, for the detection of the polymers by fluorescence in following experiments. The resultant glutamine-functionalized polymers were termed as PLys(Gln)-n, where n is the mean degree of polymerization of PLys. Meanwhile, for control polymers, lysine residues of the precursor polymers were modified to have α-glutamyl moieties because glutamine moieties and α-glutamyl moieties have same molecular weight and neutral charge but different position of amine group. Through this chapter, I present the synthesis and characterization of a series of glutamine-functionalized polymers and control polymers.

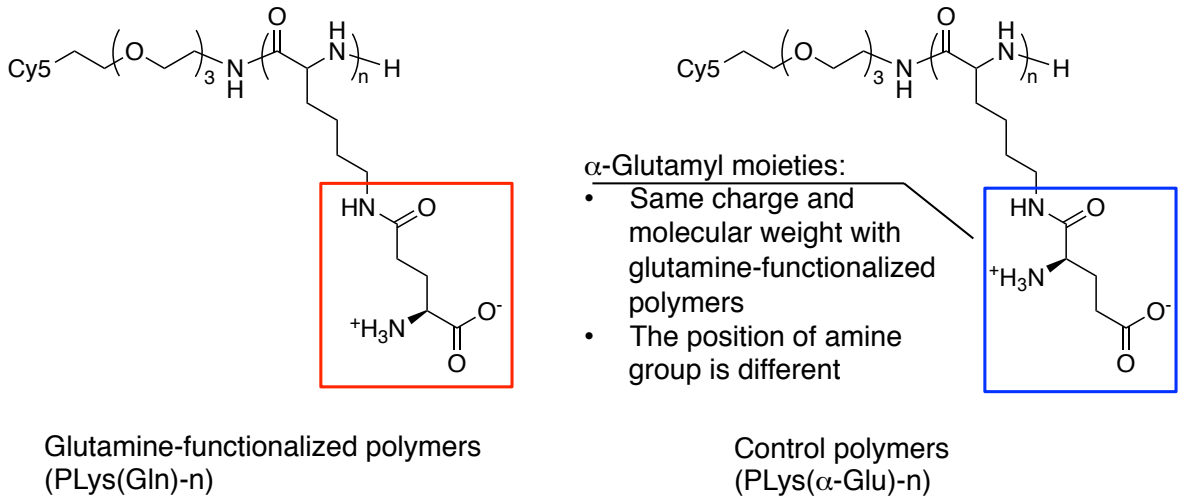

Figure 2-3. Chemical structure of glutamine-functionalized polymers and control polymers.

2.2 Materials and Methods

2.2.1 Materials

N-Carboxy anhydride of ε-trifluoroacetyl-L-lysine (NCA-Lys(TFA)) was purchased from Chuo Kasei Co. Ltd. (Osaka, Japan). 11-Azido-3,6,9-trioxaundecan-1-amine, Boc-L-glutamic acid 1-benzyl ester (Boc-Glu-OBzl), Boc-L-glutamic acid 5-benzyl ester (Boc-Glu(OBzl)-OH) were purchased from Sigma Aldrich Corporation (St. Louis, MO). Dimethylsulfoxide (DMSO), triethylamine (TEA), *N*-methyl-2-pyrolidone (NMP), 4-(4,6-dimethoxy-1,3,5-triazin-2-yl)-4-methylmorpholinium chloride (DMT-MM) were purchased from Wako Pure Chemical Industries, Ltd. (Osaka, Japan). DMSO was purified by distillation under reduced pressure before use. Dibenzocyclooctyne-Cy5 (Cy5-DBCO) was purchased from Click Chemistry Tools (Scottsdale, AZ).

2.2.2 Synthesis of azide-functionalized poly(L-lysine) (azide-PLys) with different length

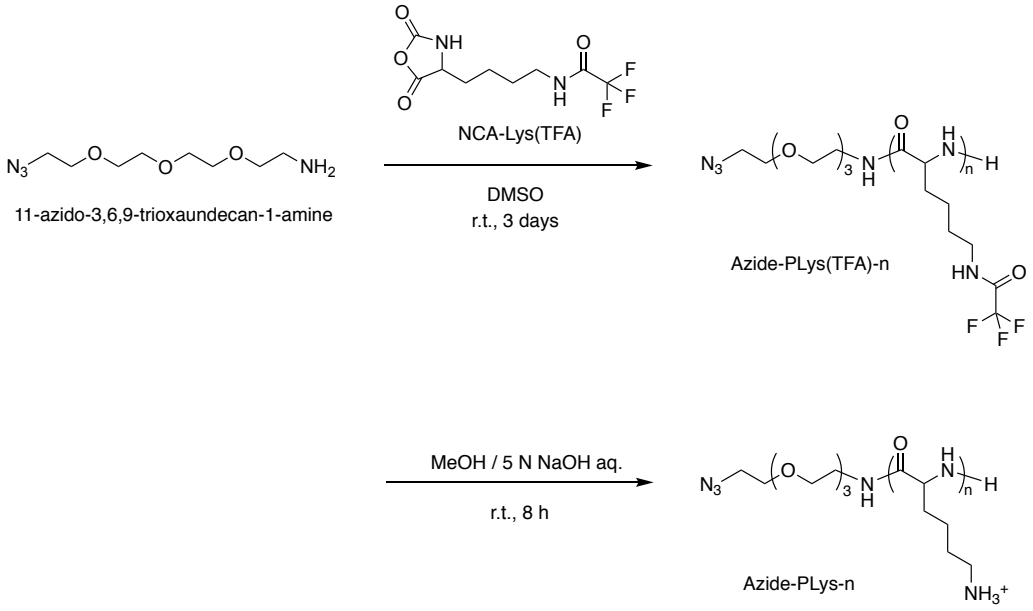

Scheme 2-1. Synthetic procedure for azide-PLys-n.

A series of azide-PLys-n (n is the polymerization degree of Lys unit) were synthesized by ring-opening polymerization of NCA-Lys(TFA) and subsequent deprotection of trifluoroacetyl group as shown in Scheme 2-1. For the synthesis of azide-PLys-100, the NCA-Lys(TFA) (2.16 g, 8.1 mmol) was polymerized in distilled DMSO (10 mL) using 11-azido-3,6,9-trioxaundecan-1-amine (16 μl, 0.081 mmol) as an initiator. After stirring at room temperature for 3 days under argon atmosphere, the reaction mixture was dialyzed against MeOH (MWCO: 1,000). The dialyzed solution in MeOH was then evaporated and dried *in vacuo* to obtain azide-PLys(TFA)-100 (1.73 g, yield = 92 %). Molecular weight distribution and polydispersity index (M_w/M_n) of the obtained polymer was estimated using gel permeation chromatography (GPC) [column: TSK-gel superAW3000, superAW4000, and

superAWL-guard column (Tosoh Corporation, Yamaguchi, Japan); eluent: NMP containing 50 mM LiBr; flow rate: 0.3 ml/min; detector: refractive index (RI); temperature: 40 ˚C].

To deprotect the trifuluoroacetyl group, the obtained azide-PLys(TFA)-100 (1.0 g) was dissolved in 5 N NaOH aqueous solution/MeOH (1:4 (v/v), 20 mL) and stirred at room temperature for 8 h. The reaction mixture was purified by dialysis against 0.01 N HCl aqueous solution and subsequent deionized water (MWCO: 1,000), followed by freeze-drying to afford azide-PLys-100 (0.545 g, yield = 74 %). The obtained polymer was characterized by size exclusion chromatography [column: Superdex 200 increase 10/300GL (GE Healthcare Ltd., UK); eluent: 10 mM phosphate buffer (pH 7.4) containing 500 mM NaCl; flow rate: 0.6 mL/min; detector: UV (220 nm); temperature: room temperature] and ^{1}H NMR, respectively. Azide-PLys-50 and Azide-PLys-30 were synthesized in the same manner.

2.2.3 Synthesis of glutamine-modified azide-PLys-n (azide-PLys(Gln)-n) and α-glutamate-modified azide-PLys-n (azide-PLys(α-Glu)-n)

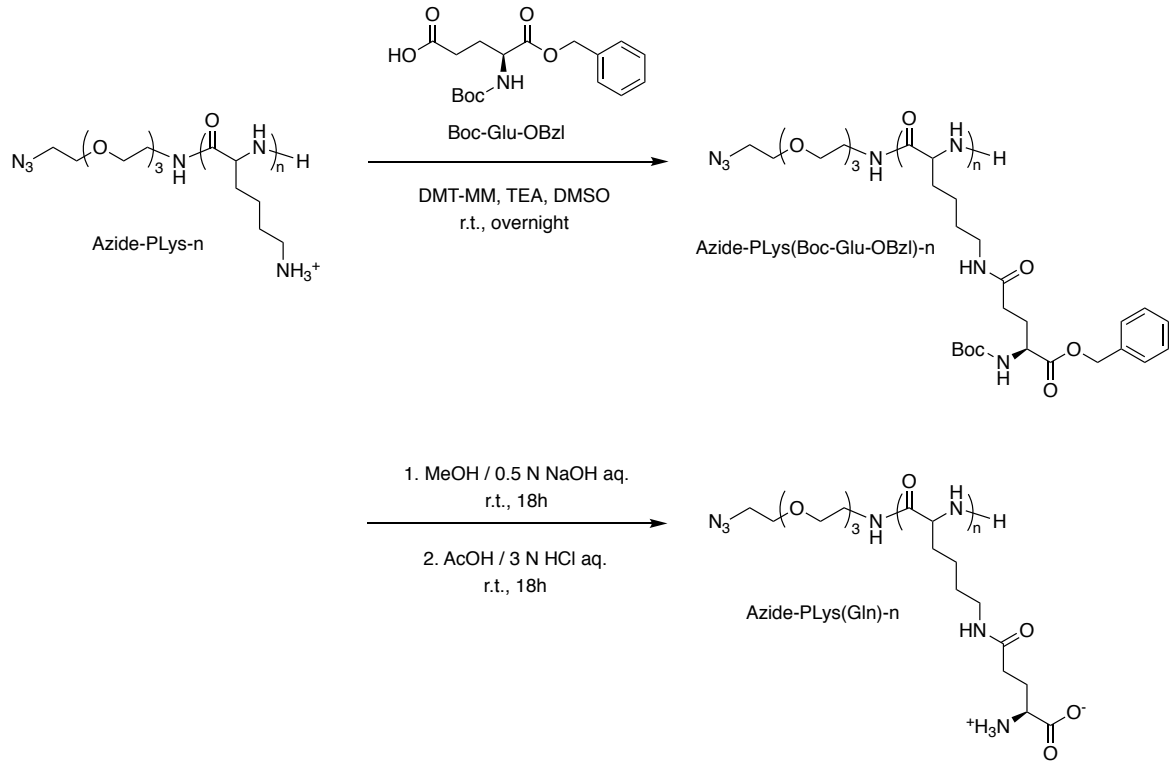

Scheme 2-2. Synthetic procedure for azide-PLys(Gln)-n.

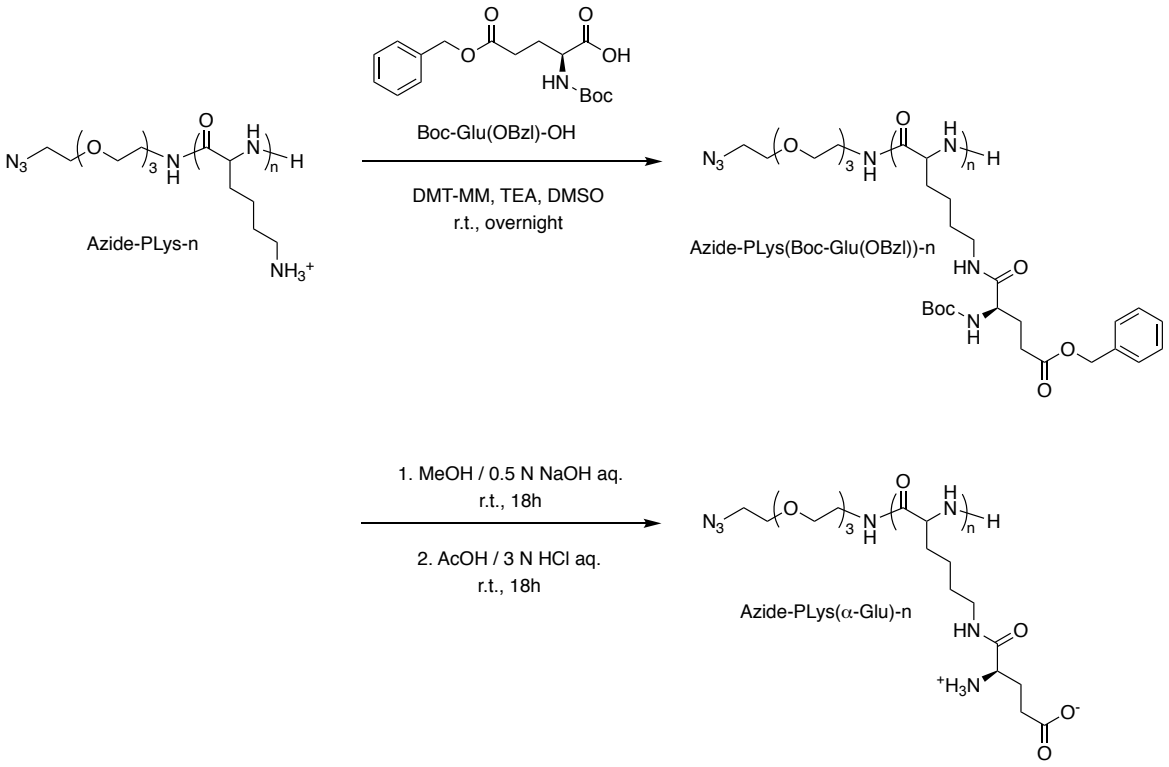

Scheme 2-3. Synthetic procedure for azide-PLys(α-Glu)-n.

Azide-PLys(Gln)-n and azide-PLys(α-Glu)-n were synthesized by condensation reaction and deprotection reaction as shown in Scheme 2-2 and Scheme 2-3. For the synthesis of azide-PLys(Gln)-100, Boc-Glu-OBzl (121 mg, 0.36 mmol) and DMT-MM (249 mg, 0.90 mmol) were added to a solution of azide-PLys-100 (30 mg, 0.0017 mmol) in a mixture of DMSO (5 mL) and TEA (0.5 mL). The reaction mixture was stirred overnight at room temperature, and then purified by dialysis against MeOH (MWCO: 6-8,000). After dialysis, the residue was evaporated and dried *in vacuo* to obtain azide-PLys(Boc-Glu-OBzl)-100 (83 mg, yield > 99%). To deprotect Bzl group, the obtained polymer was dissolved in a mixture of 0.5 N NaOH aqueous solution (3 mL) and MeOH (3 mL). After stirring at room temperature for 18h, the reaction mixture was purified by dialysis against deionized water (MWCO: 6-8,000), followed by lyophilization. Complete deprotection of Bzl group was

confirmed by ^{1}H NMR spectrum (solvent: D_2O). To deprotect the Boc group, the polymer was dissolved in a mixture of 3 N HCl aqueous solution (3 mL) and AcOH (3 mL), and stirred at room temperature for 18h. The reaction mixture was purified by dialysis against deionized water (MWCO: 6-8,000), and freeze-dried to afford azide-PLys(Gln)-100 (46 mg, yield = 85 %). The obtained polymer was characterized by ^{1}H NMR. Azide-PLys(Gln)-50 and azide-PLys(Gln)-30 were synthesized in the same procedure. For the synthesis of a series of azide-PLys(α-Glu)-n, Boc-Glu(OBzl)-OH was used instead of Boc-Glu-OBzl.

2.2.4 Cy5 conjugation to azide-PLys(Gln)-n and azide-PLys(α-Glu)-n

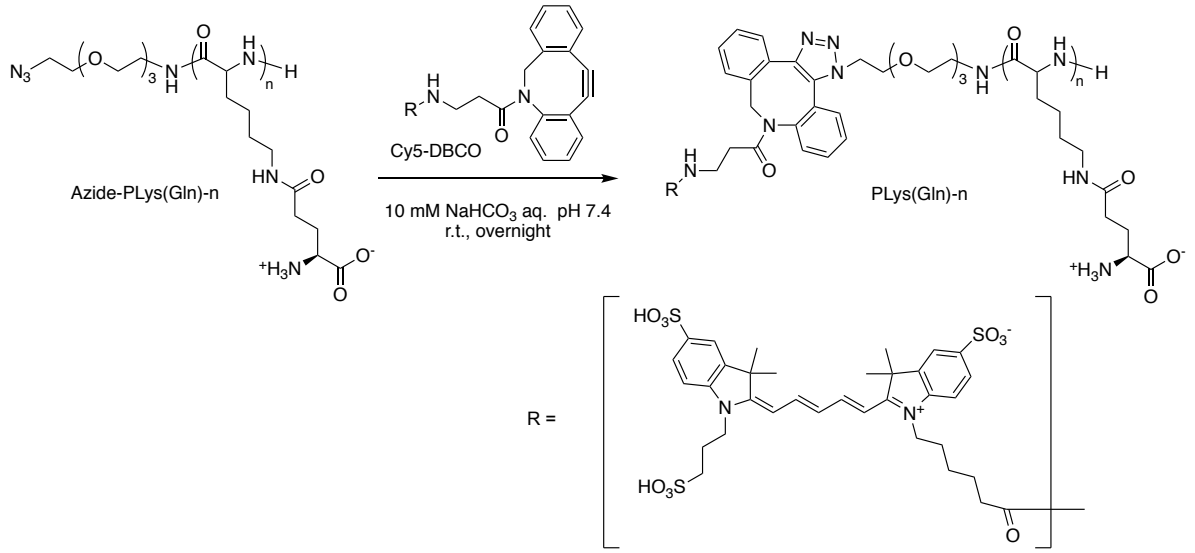

Scheme 2-4. Synthetic procedure for PLys(Gln)-n.

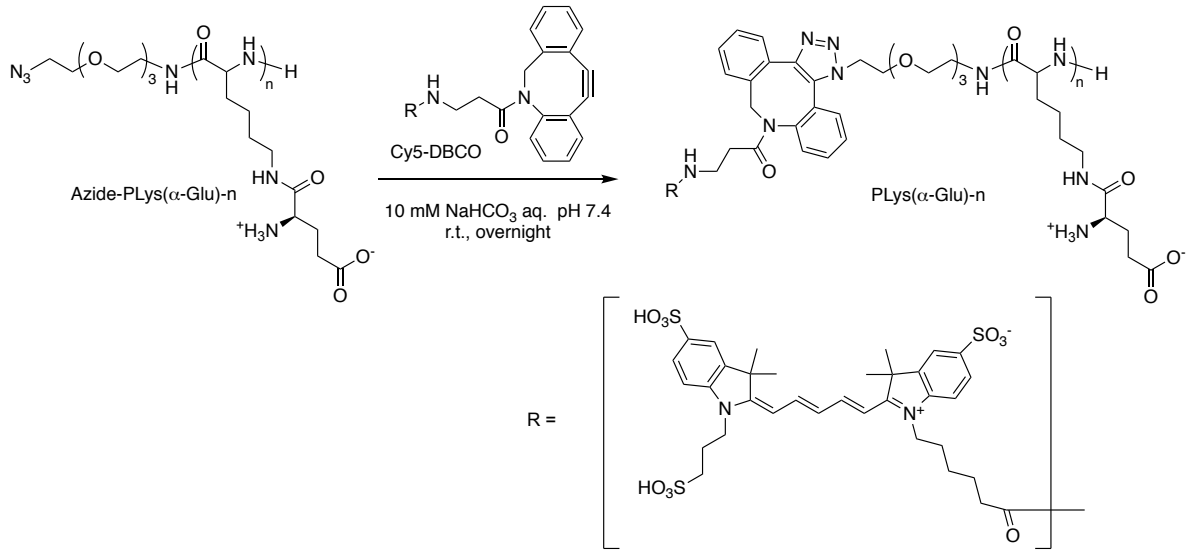

Scheme 2-5. Synthetic procedure for PLys(α-Glu)-n.

Dibenzocyclooctyne-Cy5 dye (Cy5-DBCO) was conjugated to azide-PLys(Gln)-n and azide-PLys(α-Glu)-n by copper-free click chemistry to afford fluorescence-labeled polymers as shown in Scheme 2-4 and Scheme 2-5. The resultant polymers were termed as PLys(Gln)-n and PLys(α-Glu)-n, respectively. For the synthesis of PLys(Gln)-100, azide-PLys(Gln)-100 (46 mg, 0.0015 mmol) and Cy5-DBCO (0.5 mg, 0.00050 mmol) was dissolved in 10 mM $NaHCO_3$ aqueous solution (2 mL, pH 7.4) and stirred overnight at room temperature. The reaction mixture was purified by dialysis against deionized water (MWCO: 6-8,000). After freeze-drying, the crude product was dissolved in 1 M NaCl aqueous solution and further purified by PD-10 column (Sephadex G-25, GE Healthcare Ltd.), followed by dialysis against deionized water (MWCO: 6-8,000) and lyophilization. The PLys(Gln)-100 was obtained as a blue powder (32 mg, yield = 70 %). PLys(Gln)-n (n = 50, 30) or PLys(α-Glu)-n (n=100, 50, 30) were synthesized in the same procedure. The final products were characterized by size exclusion chromatography [column: Superdex 200 increase

10/300GL; eluent: 10 mM phosphate buffer (pH 7.4) containing 150 mM NaCl; flow rate: 0.6 ml/min; temperature: room temperature; detector: fluorescence (ex/em = 620 nm/670 nm)].

2.3 Results and Discussion

2.3.1 Synthesis of azide-functionalized poly(L-lysine) (azide-PLys)

To synthesize the glutamine-functionalized polymers with controlled polymer length, azide-PLys having different degree of polymerizations (DPs) were synthesized in accordance with Scheme 2-1. First, NCA-PLys(TFA) was polymerized by 11-azido-3,6,9-trioxaundecan-1-amine to afford a series of azide-PLys(TFA)-n with target DP of 100, 50, and 30. Molecular weight distribution of the obtained polymers were characterized using gel permeation chromatography, and polydispersity index (Mw/Mn) of the polymers were calculated based on the poly(ethylene glycol) standard. As shown in Figure 2-1, all of the obtained polymers possessed narrow molecular weight distribution (M_w/M_n = 1.22, 1.20, and 1.16 for azide-PLys(TFA)-100, azide-PLys(TFA)-50, and azide-PLys(TFA)-30, respectively.)

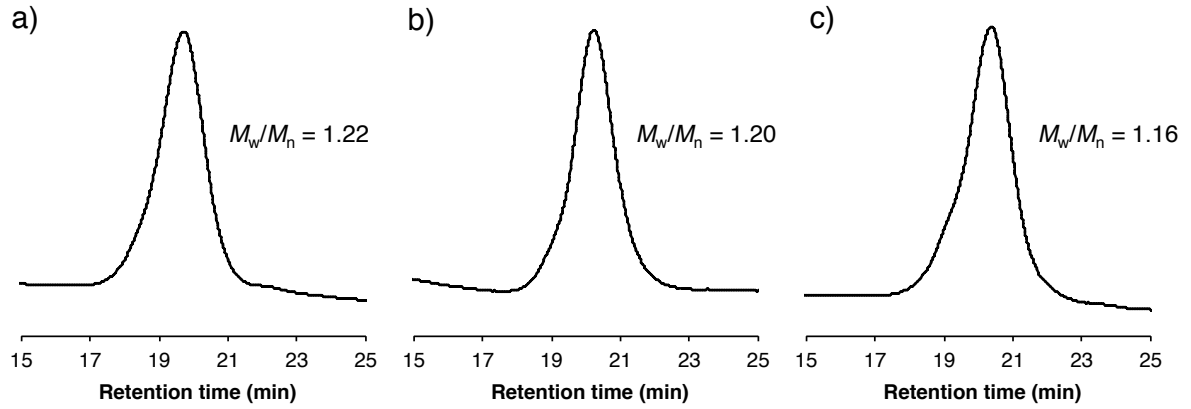

Figure 2-4. GPC chart of a series azide-PLys(TFA)-n.

(a) azide-PLys(TFA)-100, (b) azide-PLys(TFA)-50, and (c) azide-PLys(TFA)-30. [column: TSK-gel superAW3000, superAW4000, and superAWL-guard column; eluent: NMP containing 50 mM LiBr; flow rate: 0.3 ml/min; detector: refractive index (RI); temperature: 40 ˚C].

Trifluoroacetyl groups were then deprotected in basic condition, and the resultant polymers were characterized using size exclusion chromatography and ^{1}H NMR. As shown in Figure 2-2, all of the polymers maintained narrow molecular weight distribution after deprotection reaction. Complete deprotection of the trifluoroacetyl group was confirmed by the chemical shift of methylene protons adjacent to the ε-amino group (δ = 3.0 ppm), which is consistent with previous study[ref]. By comparing the integration value of the ethylene protons in the initiator (δ = 3.4-3.8 ppm) and that of the butylene protons of Lys (δ = 1.3-1.9 and 2.9 ppm), the DPs were calculated to be 103, 51, and 29 for azide-PLys-100, azide-PLys-50, and azide-PLys-30, respectively.

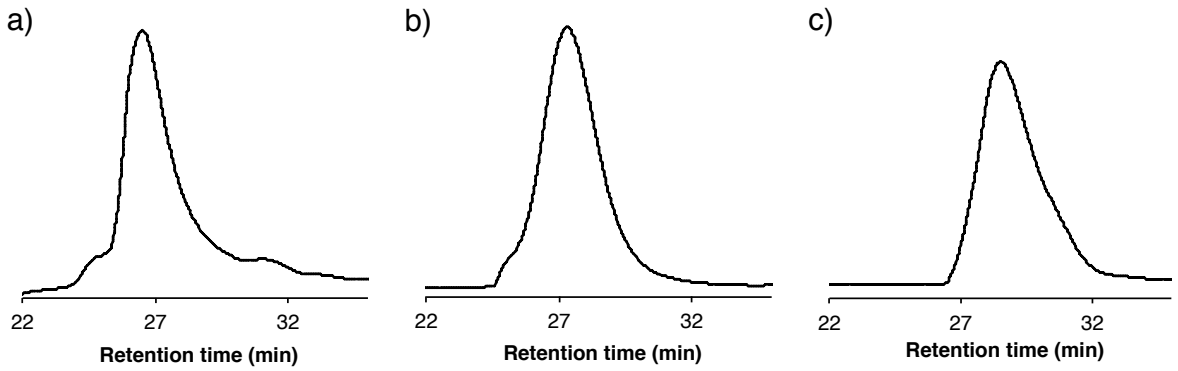

Figure 2-5. GPC chart of a series azide-PLys-n.

a) azide-PLys-100, b) azide-PLys-50, and c) azide-PLys-30. [column: Superdex 200 increase 10/300GL; eluent: 10 mM phosphate buffer (pH 7.4) containing 500 mM NaCl; flow rate: 0.6 mL/min; detector: UV (220 nm); temperature: room temperature].

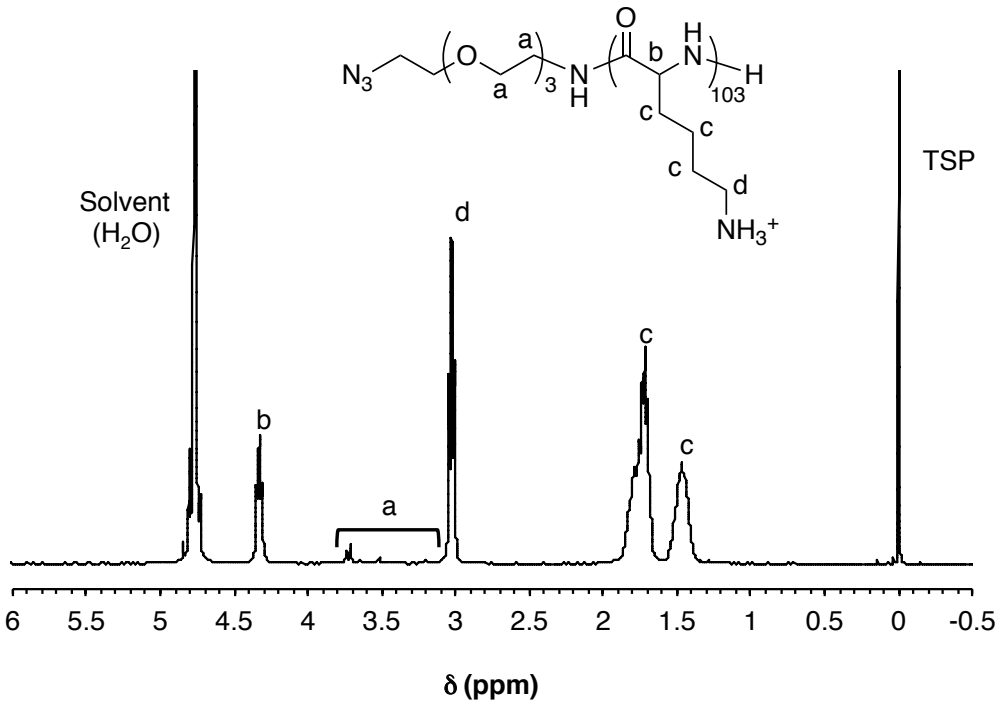

Figure 2-6. ^{1}H NMR spectrum of azide-PLys-100 (in D_2O, room temperature).

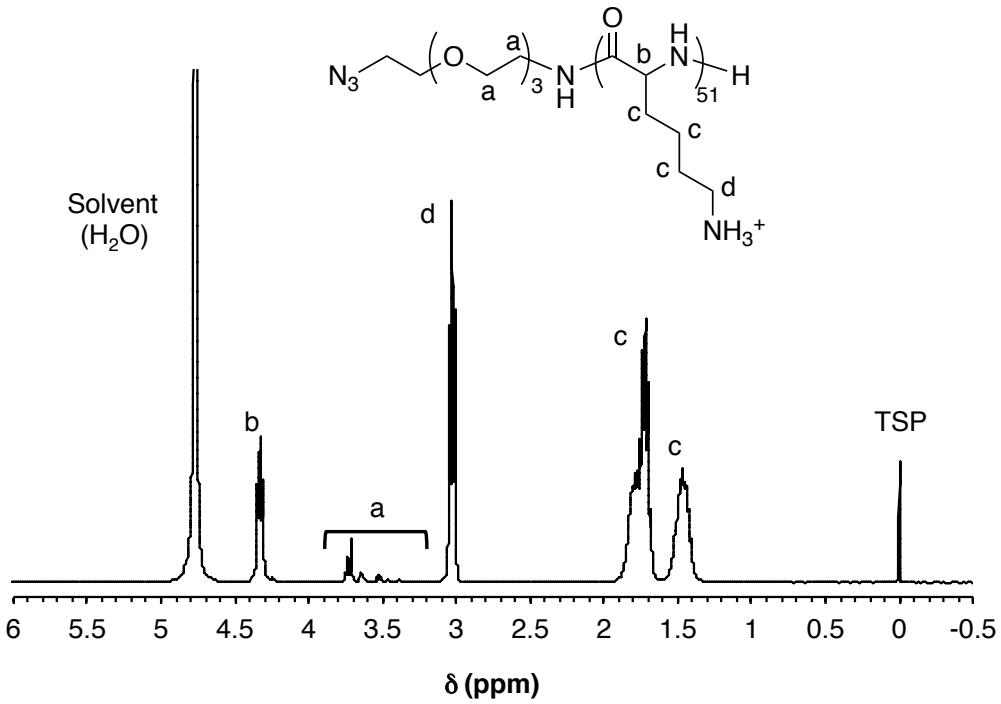

Figure 2-7. ^{1}H NMR spectrum of azide-PLys-50 (in D_2O, room temperature).

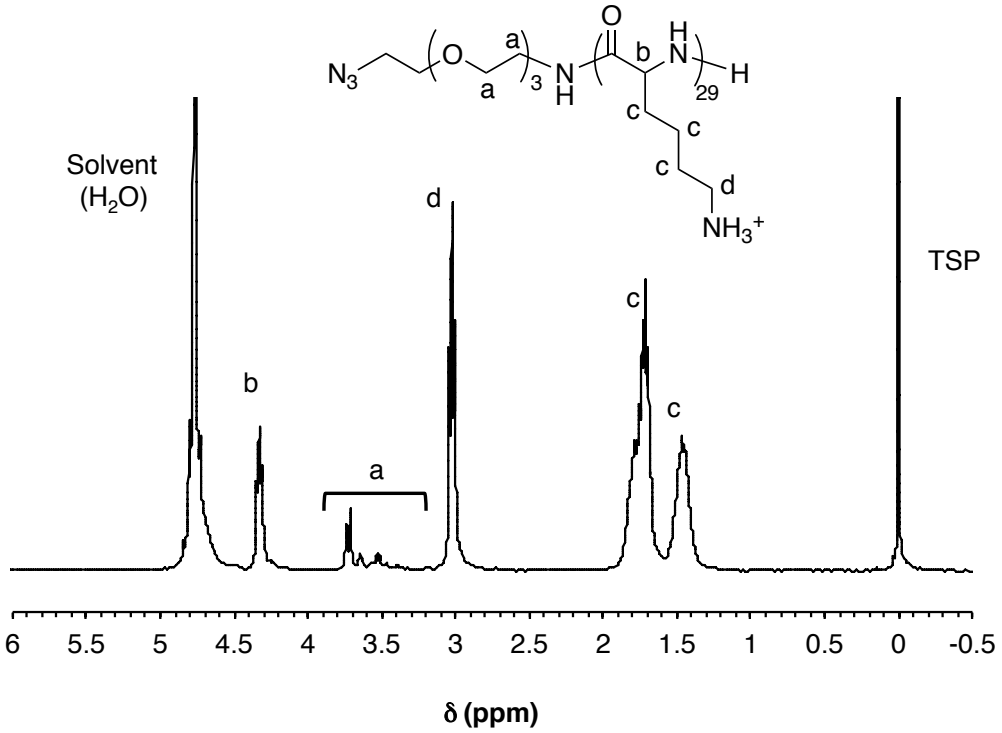

Figure 2-8. ^{1}H NMR spectrum of azide-PLys-30 (in D_2O, room temperature).

2.3.2 Synthesis of glutamine-modified azide-PLys-n (azide-PLys(Gln)-n) and α-glutamate-modified azide-PLys-n (azide-PLys(α-Glu)-n)

The side chain of the azide-PLys was modified to have glutamine moieties for glutamine-functionalized polymers and α-glutamate moieties for control polymers. Quantitative installation of Boc-Glu-OBzl or Boc-Glu(OBzl)-OH was confirmed by the proton ratio of phenyl group (δ = 7.3 ppm) and methylene group of Lys (δ = 3.1 ppm) in the ^{1}H NMR spectrum (solvent: MeOD). Representative ^{1}H NMR spectrum (azide-PLys(Boc-Glu-OBzl)-100) was shown in Figure 2-6.

Then, benzyl groups were deprotected in the mixture of NaOH aqueous solution and MeOH. Complete deprotection of the benzyl group was confirmed by the absence of the peaks from benzyl group (δ = 5.1 and 7.3 ppm). Representative ^{1}H NMR spectrum (azide-PLys(Boc-Glu)-100) was shown in Figure 2-7. Finally, boc groups were deprotected in acidic condition and the resultant polymers (azide-PLys(Gln)-n and azide-PLys(α-Glu)-n) were characterized using ^{1}H NMR as shown in Figure 2-8 to Figure 2-13. The absence of the peaks from boc groups (δ = 1.4 ppm) in all ^{1}H NMR spectrums indicated successful deprotection of the boc groups. In addition, almost quantitative modification of the side chain was confirmed for all polymers from the proton ratio of the ethylene groups (δ = 3.4-3.8 ppm) to the butylene groups of Lys (δ = 1.3-1.9 and 2.9 ppm).

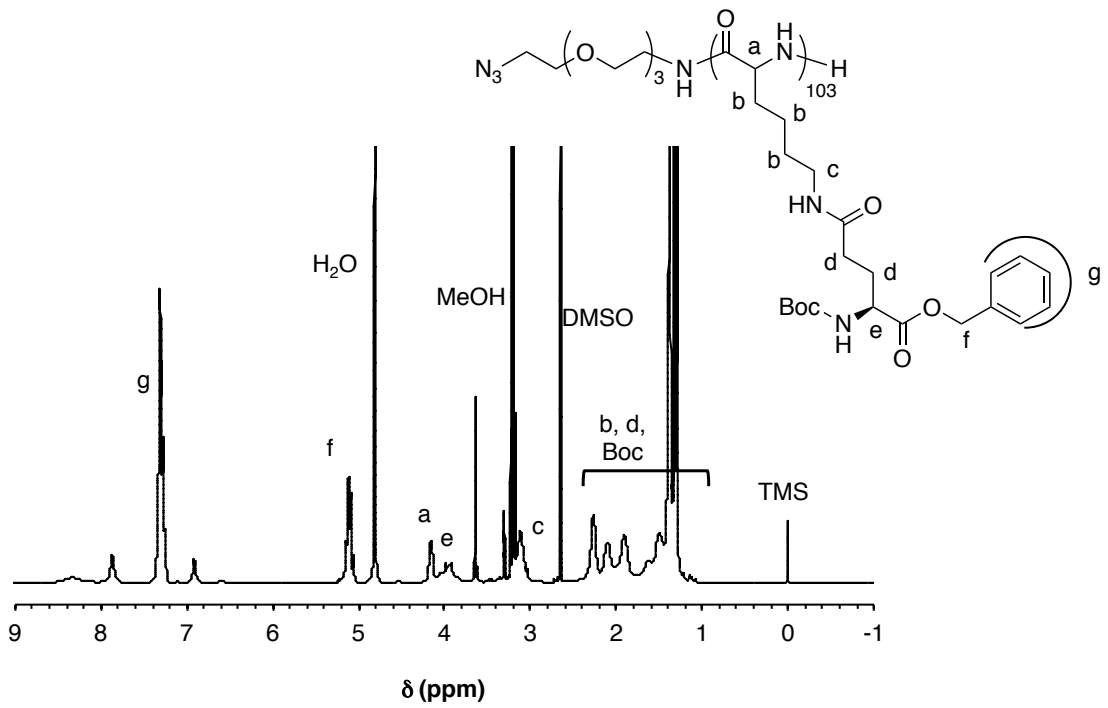

Figure 2-9. ^{1}H NMR spectrum of azide-PLys(Boc-Glu-OBzl)-100 (in MeOD, room temperature).

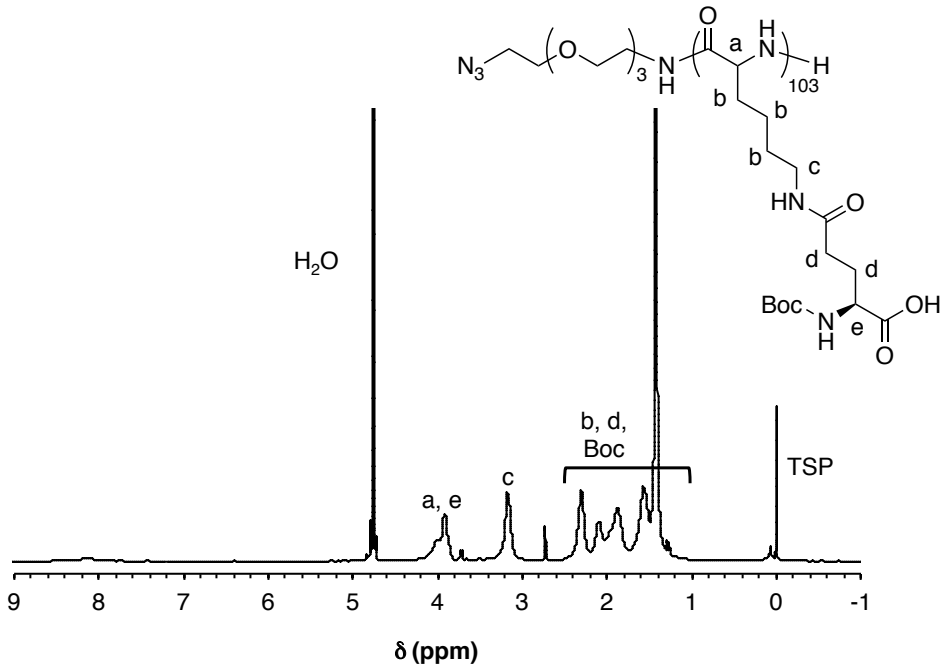

Figure 2-10. ^{1}H NMR spectrum of azide-PLys(Boc-Glu)-100 (in D_2O, room temperature).

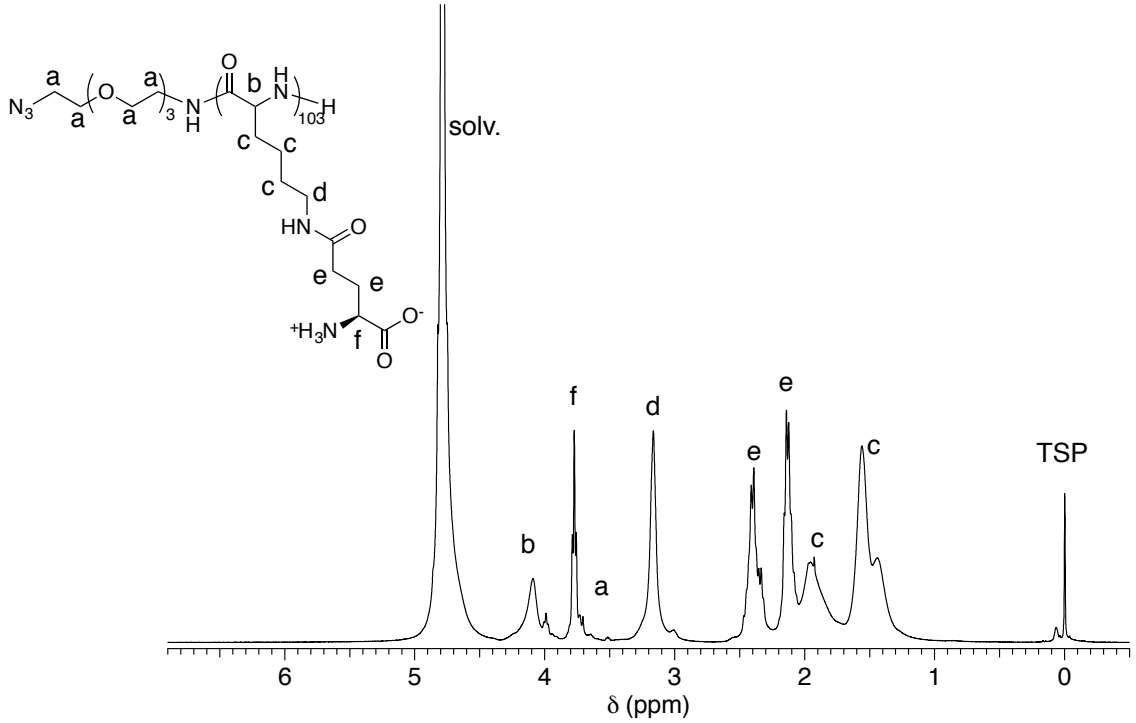

Figure 2-11. ^{1}H NMR spectrum of azide-PLys(Gln)-100 (in D_2O, room temperature).

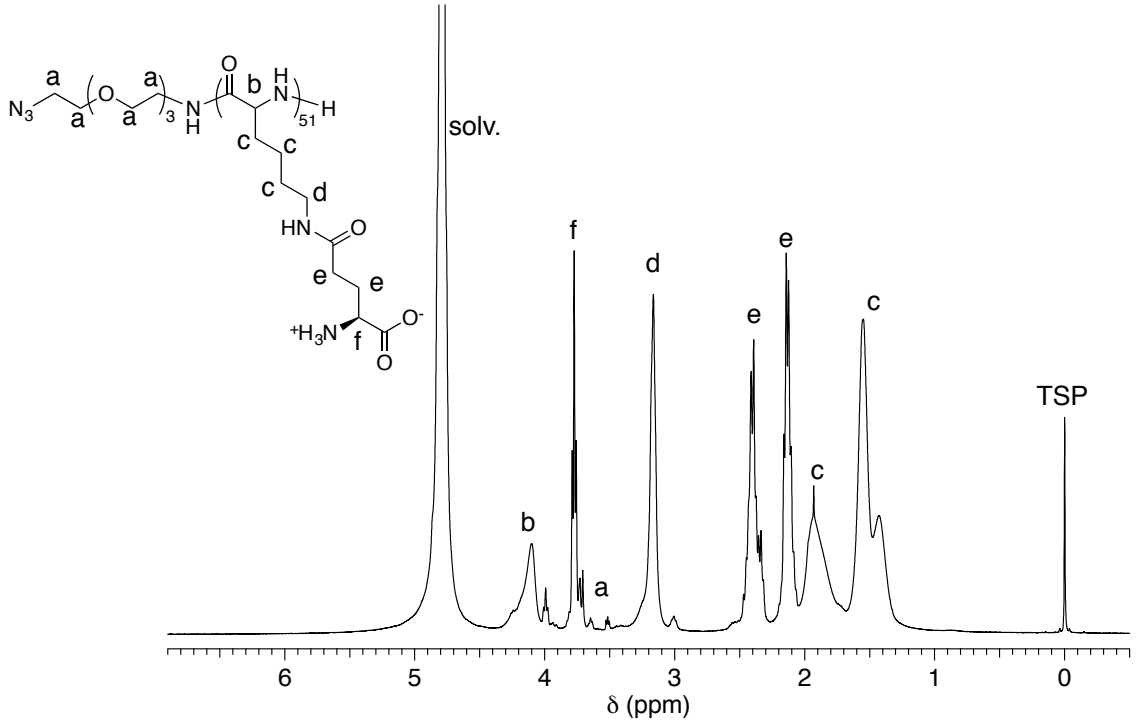

Figure 2-12. ^{1}H NMR spectrum of azide-PLys(Gln)-50 (in D_2O, room temperature).

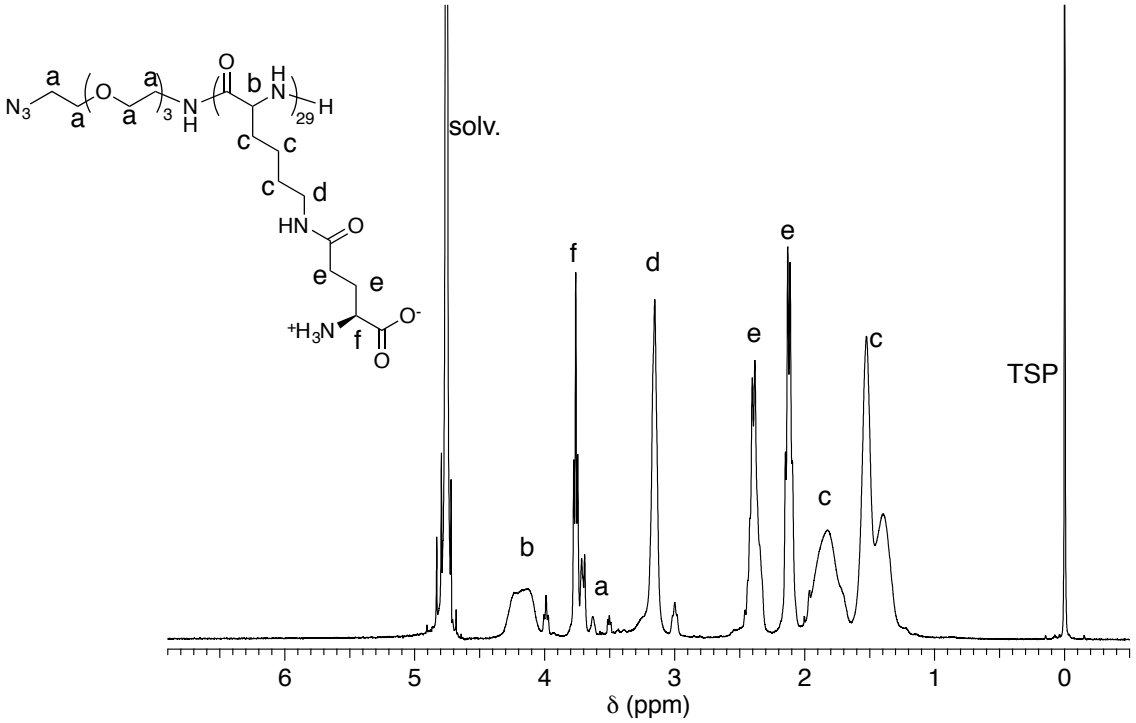

Figure 2-13. ^{1}H NMR spectrum of azide-PLys(Gln)-30 (in D_2O, room temperature).

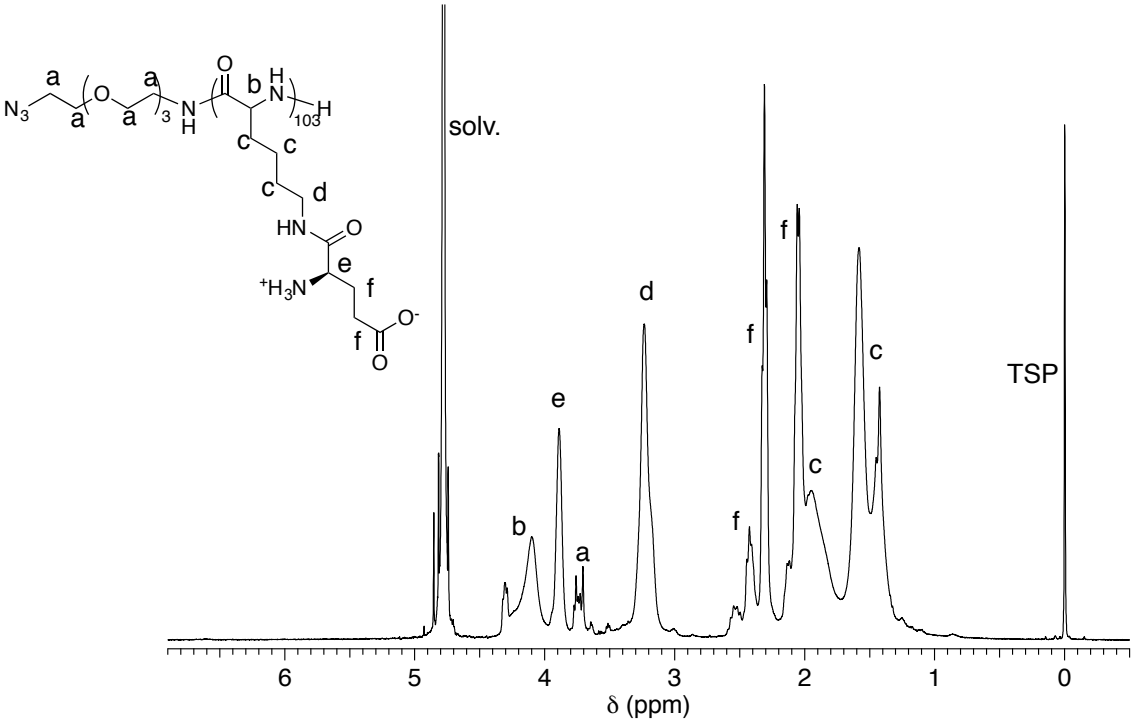

Figure 2-14. ^{1}H NMR spectrum of azide-PLys(α-Glu)-100 (in D_2O, room temperature).

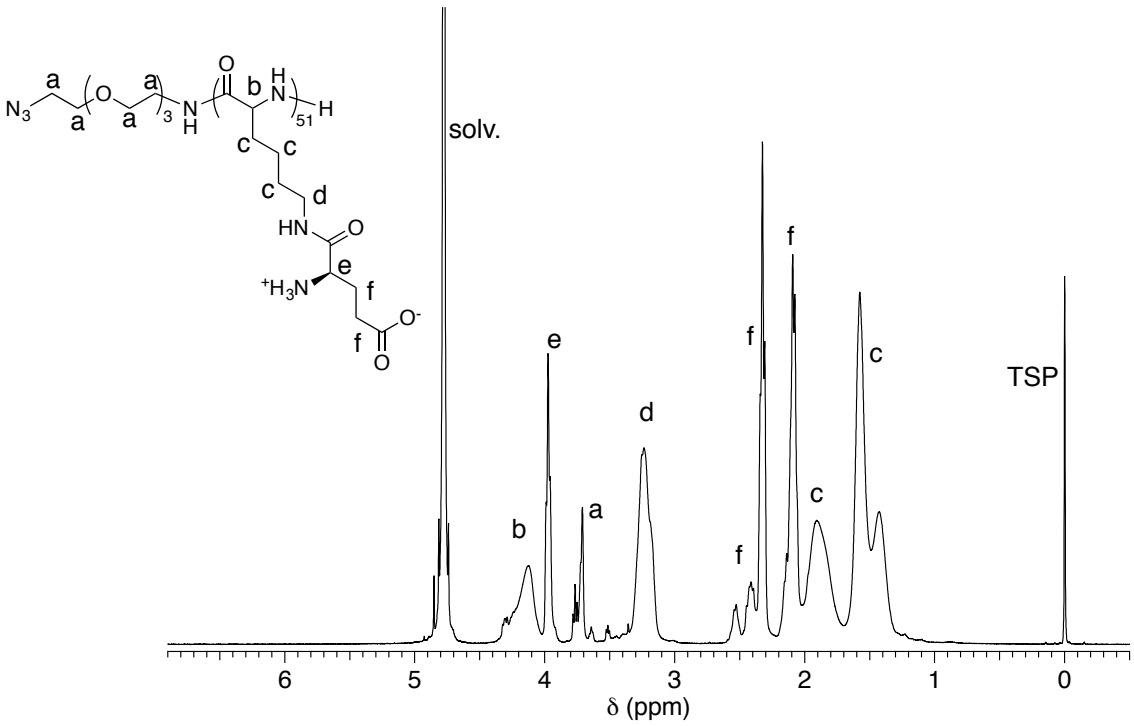

Figure 2-15. ^{1}H NMR spectrum of azide-PLys(α-Glu)-50 (in D_2O, room temperature).

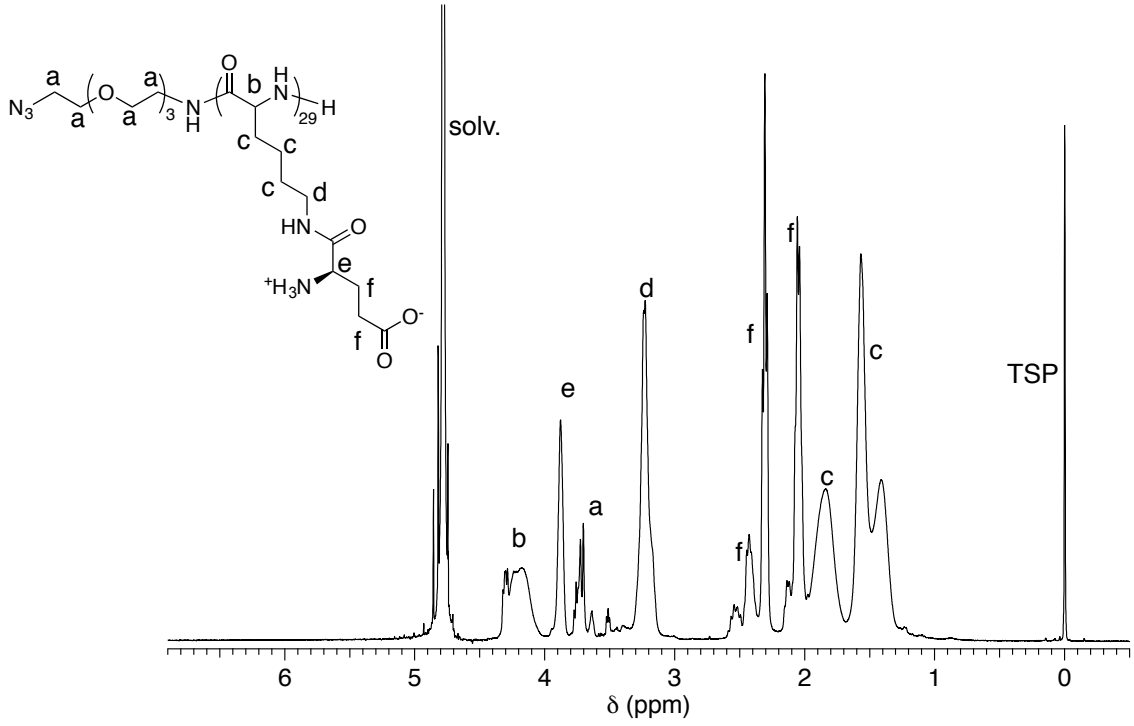

Figure 2-16. ^{1}H NMR spectrum of azide-PLys(α-Glu)-30 (in D_2O, room temperature).

2.3.3 Cy5 conjugation to azide-PLys(Gln)-n and azide-PLys(α-Glu)-n

Finally, to detect the synthesized polymers by fluorescence in following experiments, Cy5-DBCO was conjugated to azide group at the polymer terminus by copper-free click chemistry. All of the obtained polymers showed monodispersed molecular weight distribution (Figure 2-14), indicating no obvious aggregation and degradation after the introduction of Cy5 fluorescence dye to the polymers.

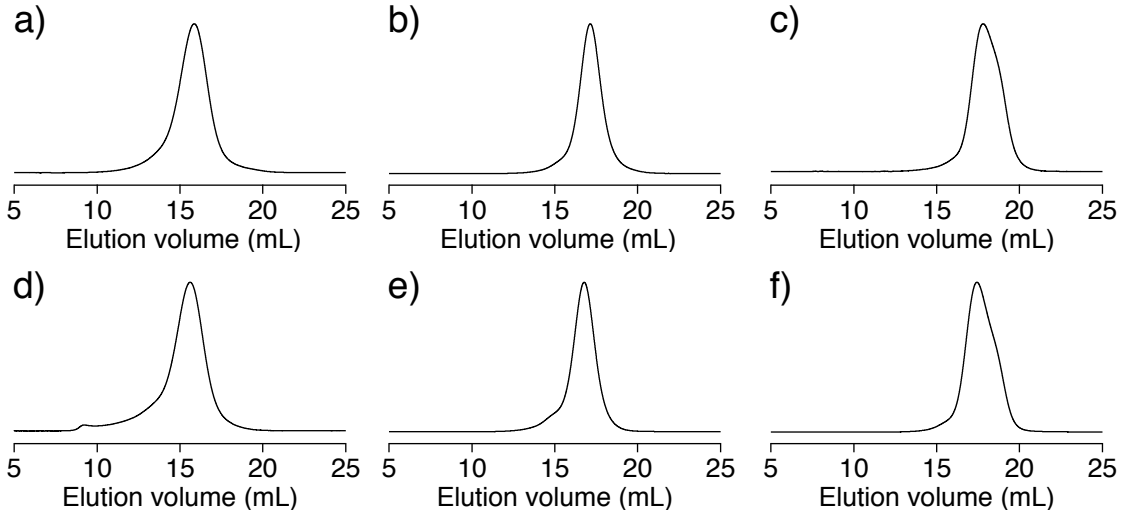

Figure 2-17. Size exclusion chromatography of a series of PLys(Gln)-n and PLys(α-Glu)-n.

a) PLys(Gln)-100, b) PLys(Gln)-50, c) PLys(Gln)-30, d) PLys(α-Glu)-100, e) PLys(α-Glu)-50, f) PLys(α-Glu)-30. [Column, Superdex 200 increase 10/300GL; eluent, 10 mM phosphate buffer (pH 7.4) containing 150 mM NaCl; flow rate, 0.6 ml/min; temperature, room temperature; detector, fluorescence (ex/em = 620 nm/670 nm)]

2.4 Conclusion

In conclusion, a series of glutamine-functionalized polymers (PLys(Gln)-n) and control polymers (PLys(α-Glu)-n) were successfully synthesized by ring-opening polymerization of NCA and subsequent side chain modification. All polymers showed

quantitative modification of the side chain and narrow molecular weight distribution.

2.5 References

1. Namikawa, M., Kakizaki, S., Kaira, K., Tojima, H., Yamazaki, Y., Horiguchi, N., Sato, K., Oriuchi, N., Tominaga, H., Sunose, Y., Nagamori, S., Kanai, Y., Oyama, T., Takeyoshi, I. & Yamada, M. Expression of amino acid transporters (LAT1, ASCT2 and xCT) as clinical significance in hepatocellular carcinoma. *Hepatol. Res.* **45,** 1014–1022 (2015).
2. van Geldermalsen, M., Wang, Q., Nagarajah, R., Marshall, A. D., Thoeng, A., Gao, D., Ritchie, W., Feng, Y., Bailey, C. G., Deng, N., Harvey, K., Beith, J. M., Selinger, C. I., O'Toole, S. A., Rasko, J. E. J. & Holst, J. ASCT2/SLC1A5 controls glutamine uptake and tumour growth in triple-negative basal-like breast cancer. *Oncogene* **35,** 3201–8 (2016).
3. Wang, Q., Hardie, R.-A., Hoy, A. J., van Geldermalsen, M., Gao, D., Fazli, L., Sadowski, M. C., Balaban, S., Schreuder, M., Nagarajah, R., Wong, J. J.-L., Metierre, C., Pinello, N., Otte, N. J., Lehman, M. L., Gleave, M., Nelson, C. C., Bailey, C. G., Ritchie, W., Rasko, J. E. J. & Holst, J. Targeting ASCT2-mediated glutamine uptake blocks prostate cancer growth and tumour development. *J. Pathol.* **236,** 278–89 (2015).
4. Huang, F., Zhao, Y., Zhao, J., Wu, S., Jiang, Y., Ma, H. & Zhang, T. Upregulated SLC1A5 promotes cell growth and survival in colorectal cancer. *Int J Clin Exp Pathol* **7,** 6006–6014 (2014).
5. Kaira, K., Sunose, Y., Arakawa, K., Sunaga, N., Shimizu, K., Tominaga, H., Oriuchi,

N., Nagamori, S., Kanai, Y., Oyama, T. & Takeyoshi, I. Clinicopathological significance of ASC amino acid transporter-2 expression in pancreatic ductal carcinoma. *Histopathology* **66,** 234–243 (2015).

6. Esslinger, C. S., Cybulski, K. A. & Rhoderick, J. F. Nγ-Aryl glutamine analogues as probes of the ASCT2 neutral amino acid transporter binding site. *Bioorg. Med. Chem.* **13,** 1111–1118 (2005).

7. Schulte, M. L., Dawson, E. S., Saleh, S. a., Cuthbertson, M. L. & Manning, H. C. 2-Substituted Nγ-glutamylanilides as novel probes of ASCT2 with improved potency. *Bioorg. Med. Chem. Lett.* **25,** 113–116 (2015).

8. Kanai, M., Mortell, K. H. & Kiessling, L. L. Varying the Size of Multivalent Ligands: The Dependence of Concanavalin A Binding on Neoglycopolymer Length. *J. Am. Chem. Soc.* **119,** 9931–9932 (1997).

9. Gestwicki, J. E., Cairo, C. W., Strong, L. E., Oetjen, K. A. & Kiessling, L. L. Influencing receptor-ligand binding mechanisms with multivalent ligand architecture. *J. Am. Chem. Soc.* **124,** 14922–14933 (2002).

10. Cheng, J. & Deming, T. J. Synthesis of polypeptides by ring-opening polymerization of α-amino acid N-carboxyanhydrides. *Top. Curr. Chem.* **310,** 1–26 (2012).

Chapter 3. *In vitro* and *in vivo* expression of ASCT2

3.1 Introduction

Transporters are generally characterized by their function, their specificity of the substrates, and their sensitivity to inhibitors. Based on these characteristics, glutamine transporters are classified to several systems: system ASC, system A, system N, and system L [1]. Among them, system ASC transporter 2 (ASCT2), a Na^+-dependent transporter for neutral amino acids transporter, is considered to play an essential role of glutamine uptake towards elevated glutamine metabolism (glutaminoelysis) in tumor cells. Indeed, inhibition of ASCT2 function has resulted in a decrease of glutamine uptake in tumor cells and suppression of tumor cell growth [2-4]. In addition, ASCT2 was up-regulated by oncogene Myc [5] and down-regulated by retinoblastoma protein (Rb, a tumor suppressor protein) [6], indicating the strong relationship between ASCT2 overexpression and tumor genesis. Consistent with this, previous studies have demonstrated the overexpression of ASCT2 in many kinds of tumor tissue [2, 3, 7]. Thus, ASCT2 can be a potential target transporter of glutamine-functionalized polymers for sensing tumor cells.

Surface plasmon resonance (SPR) is a widely used technique to evaluate affinity between ligands and their receptors. The other methods including isothermal titration calorimetry (ITC) and fluorescence correlation spectroscopy (FCS) are also used for this purpose. These analytical methods allow kinetic/thermodynamic analysis of the ligand-protein interaction; however, to perform these analytical methods, the target protein should be isolated and purified. In this regard, the difficulty of isolation and purification of membrane proteins including transporters limit the use of these methods. In addition, because the exact density and distribution of ASCT2 on cell surface are not fully understood, establishment of appropriate models for assessing the interaction between synthesized

polymers and ASCT2 with different density is also difficult. Based on these considerations, the interaction between the synthesized polymers and ASCT2 should be evaluated using cultured cells and animal models. Thus, in this chapter, to select the appropriate cell lines and animal models for the assessment of the biological activities of the synthesized polymers, ASCT2 expression levels in cultured cells as well as in tissues from xenograft model were evaluated. As aforementioned, ASCT2 overexpression was reported in various kinds of tumor cells including prostate cancer [3], breast cancer [2], and pancreatic cancer [8]. Among them, effective delivery of therapeutic agents to pancreatic cancer is urgently needed because pancreatic cancer is characterized by low vascularization, poor drug permeability, and poor prognosis [9, 10]. Thus, in this study, I used human pancreatic cancer cells as ASCT2-overexpressing cell lines. For detecting ASCT2 on cellular membrane in cultured cells, flow cytometric analysis of human pancreatic cancer BxPC3 cells and human non-cancerous HEK293 cells (as cell lines having moderate expression level of ASCT2) were performed. The overexpression ratio of ASCT2 in these cell lines were then quantified using enzyme-linked immunosorbent assay (ELISA) to examine whether these cell lines well mimic the *in vivo* situation. Finally, the ASCT2 overexpression of BxPC3 subcutaneous tumor was confirmed by immunohistochemical analysis.

3.2 Materials and Methods

3.2.1 Materials

RPMI 1640 medium, Dulbecco's modified Eagle's medium (DMEM), penicillin/streptomycin, trypsin/EDTA, and NP-40 were purchased from Sigma Aldrich Corporation. Fetal bovine serum (FBS), and Hoechst 33342 were purchased from Thermo

Fisher Scientific, Inc. (Waltham, MA). D-PBS(-) (PBS) were purchased from Wako Pure Chemical Industries, Ltd. Bovine serum albumin (BSA) was purchased from Nacalai Tesque, Inc. (Kyoto, Japan).

3.2.2 Cell lines and animals

BxPC3 cells and HEK293 cells were purchased from ATCC (Manassas, VA). BxPC3 cells were cultured under a humidified atmosphere containing 5% CO_2 at 37 °C in RPMI 1640 supplemented with 10 % FBS and 1 % penicillin/streptomycin. HEK293 cells were cultured under a humidified atmosphere containing 5% CO_2 at 37 °C in DMEM supplemented with 10 % FBS and 1 % penicillin/streptomycin. BALB/c nu/nu mice (female, 4 weeks old) were purchased from Charles River Laboratories Japan, Inc. (Yokohama, Japan). All animal experiments were approved by the Animal Care and Use Committee of Tokyo Institute of Technology, and performed in accordance with the Guidelines for the Care and Use of Laboratory Animals as stated by Tokyo Institute of Technology.

3.2.3 Flow cytometric analysis of ASCT2 expression

BxPC3 cells and HEK293 cells (2.0×10^5 cells) were transferred into 1.5 mL tube and washed with assay buffer (PBS containing 1 % BSA). Then, the cells were resuspended in 100 μL of rabbit anti-human ASCT2 polyclonal antibody solution (1:50 dilution in the assay buffer, Santa Cruz Biotechnology, Dallas, TX) or isotype control rabbit IgG solution (1:250 dilution in the assay buffer, abcam, Cambridge, MA) and incubated for 1.5 h on ice. The cells were washed twice with 500 μL of the assay buffer and resuspended in 100 μL of DyLight 650-conjugated anti-rabbit IgG solution (1: 500 dilution in the assay buffer, abcam).

After 45 min incubation on ice in the dark, the cells were washed twice with 500 μL of the assay buffer and resuspended in the 500 μL of the assay buffer, followed by analysis using flow cytometer (Guava easyCyte 6-2L, Merck Millipore, Billerica, MA) (ex/em = 642 nm/661 nm).

3.2.4 Enzyme-linked immunosorbent assay (ELISA)

The relative expression level of ASCT2 in cultured cells was quantified using ELISA Starter Accessory Kit (Bethyl Laboratories, Inc., Montgomery, TX) according to the manufacture's procedure. To prepare the cell lysates, the cells (5.0×10^6 cells) were transferred to 1.5 mL tubes, washed three times with cold PBS, and then lysed by sonication in 500 μL of lysis buffer (tris-buffered saline (TBS) containing 1 mM EDTA, 0.1% NP-40, and protease inhibitor cocktail (Roche, Mannheim, Germany), pH 7.5). The resulting solutions were centrifuged (4˚C, 10,000 g, 15 min) to collect the supernatants. Protein concentration of the collected supernatants was quantified using BCA assay (Thermo Fischer Scientific). To perform the ELISA, microtiter plates were coated with 50 μg of the protein lysates by incubating overnight at 4 ˚C. The plates were washed three times with washing buffer (TBS with 0.05% Tween 20, pH 8.0) and treated with 1% BSA in TBS at ambient temperature for 30 min. After washing three times with washing buffer, the plates were incubated with 100 μL of rabbit anti-human ASCT2 polyclonal antibody solution (1:300 dilution in TBS containing 1% BSA and 0.05% Tween 20, Santa Cruz Biotechnology) at ambient temperature for 1.5 h. The plates were washed three times with washing buffer and incubated with 100 μL of horseradish peroxidase (HRP)-conjugated goat anti-rabbit IgG antibody (1:800 dilution in TBS containing 1% BSA and 0.05% Tween 20, Thermo Fischer

Scientific) at ambient temperature for 1 h. After washing five times with washing buffer, 100 μL of 3,3',5,5'-tetramethylbenzidine (TMB) substrate solution was added to each wells for the reaction with HRP. The reaction was stopped by the addition of 100 μL of 0.18 M H_2SO_4, and the absorbance at 450 nm was measured.

3.2.5 Immunohistochemistry

To establish the BxPC3 xenograft model, the BxPC3 cells (5.0×10^6 cells) were subcutaneously inoculated to BALB/c nu/nu mice. When tumor volume reached approximately 150 mm^3, the mice were perfused using saline and fixed using 4% paraformaldehyde. Tissues were excised and frozen in OCT compound (Sakura Finetek Japan Co., Ltd., Tokyo, Japan). The frozen samples were sectioned at 4-μm thickness and washed with PBS. After 1 h blocking treatment using 5% skim milk in PBS, the sections were incubated with rabbit anti-human/murine ASCT2 polyclonal antibody (1:100 dilution in PBS containing 5% skim milk, LSBio, Seattle, WA) overnight at 4 °C. Then, the sections were washed with PBS three times, incubated with Alexa Fluor 568-conjugated goat anti-rabbit IgG (1:800 dilution in PBS containing 5% skim milk, Thermo Fischer Scientific) at ambient temperature for 45 min. After washing with PBS three times, the sections were incubated with Hoechst 33342 (1:1000 dilution in PBS) for staining the nuclei, and mounted in Vectashield mounting media (Vector Laboratories, Burlingame, CA). The obtained tissue sections were observed using a fluorescence microscope (BZ-X710, Keyence, Osaka, Japan).

3.3 Results and Discussion

3.3.1 ASCT2 expression in cultured cells

To select appropriate cell lines for the evaluation of biological activities of synthesized polymers, ASCT2 expression level in cultured cells were analyzed using flow cytometer. As shown in Figure 3-1, human pancreatic cancer BxPC3 cells overexpressed ASCT2 compared to HEK293 cells.

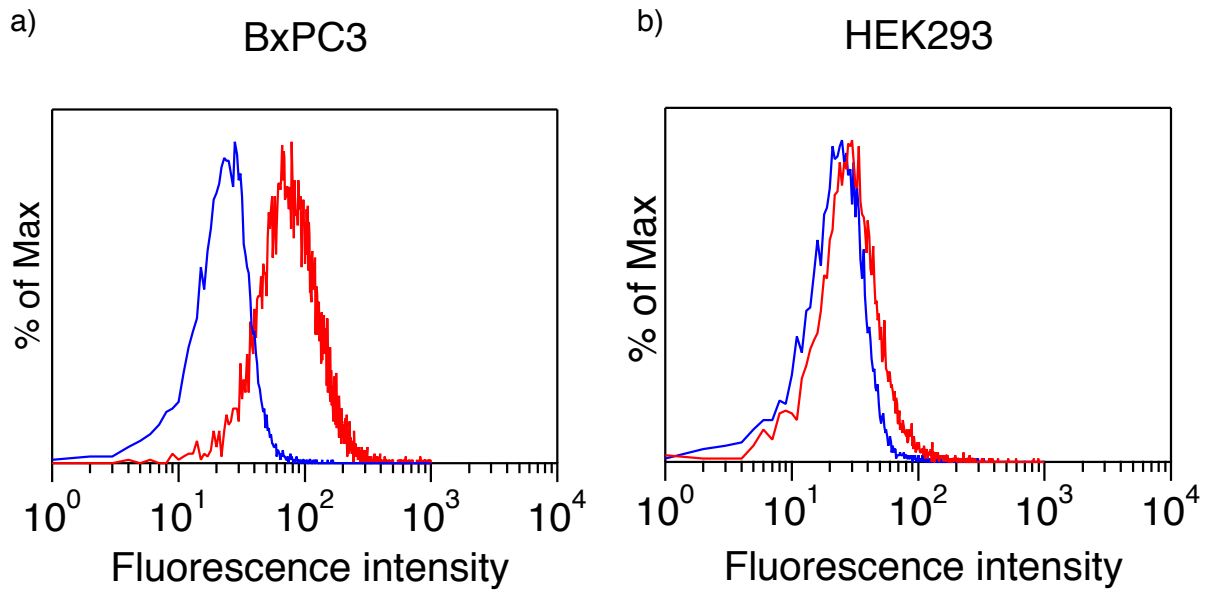

Figure 3-1. Flow cytometric analysis of ASCT2 expression on cultured cells.

ASCT2 expression of BxPC3 cells (human pancreatic cancer cells, a) and HEK293 cells (human embryonic kidney cells, b) were analyzed using flow cytometry. Red, anti-human ASCT2 antibody; blue, isotype control IgG.

Moreover, enzyme-linked immunosorbent assay (ELISA) revealed 4.8-fold higher expression of ASCT2 on BxPC3 cells compared to HEK293 cells (Figure 3-2). This overexpression ratio is consistent with previous studies, where tumor tissues showed approximately 2- to 10-fold higher ASCT2 expression compared to their normal counterparts [3, 11, 12]. Thus, these cell lines should be suitable models to predict the *in vivo* biological

activities of the synthesized polymers although HEK293 cells possess the immortalized characteristics.

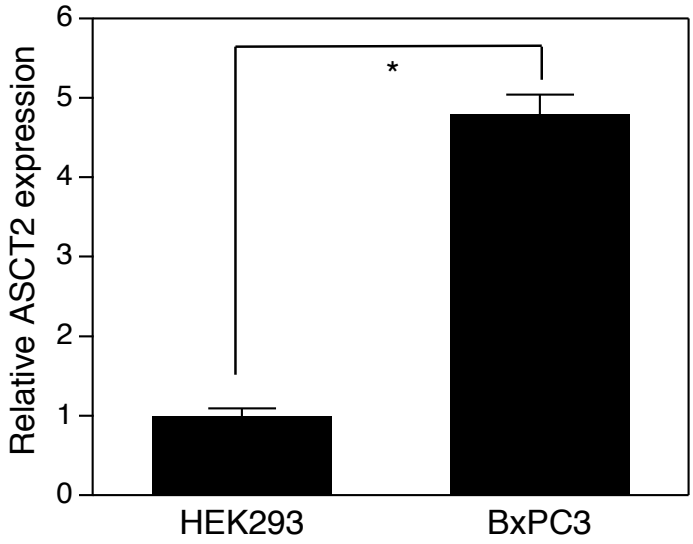

Figure 3-2. Quantification of ASCT2 expression level by ELISA.

Data are mean ± S.D. (n=3). $p^{*} < 0.001$ (Student *t*-test).

3.3.2 ASCT2 expression level in BxPC3

As aforementioned, flow cytometric analysis and ELISA revealed augmented expression of ASCT2 on BxPC3 cells compared to HEK29 cells, suggesting the validity of using these cell lines in *in vitro* studies. To examine whether this BxPC3 cells can be used in *in vivo* studies, BxPC3 subcutaneous xenograft model were prepared and ASCT2 expression of tissues from the mice was assessed using anti-murine/human ASCT2 antibody. As shown in Figure 3-3, ASCT2 was distinctly overexpressed in BxPC3 tumor tissue while the other tissues showed low/undetectable ASCT2 expression, indicating that this model can be used in *in vivo* evaluation on the biological activities of the synthesized polymers.

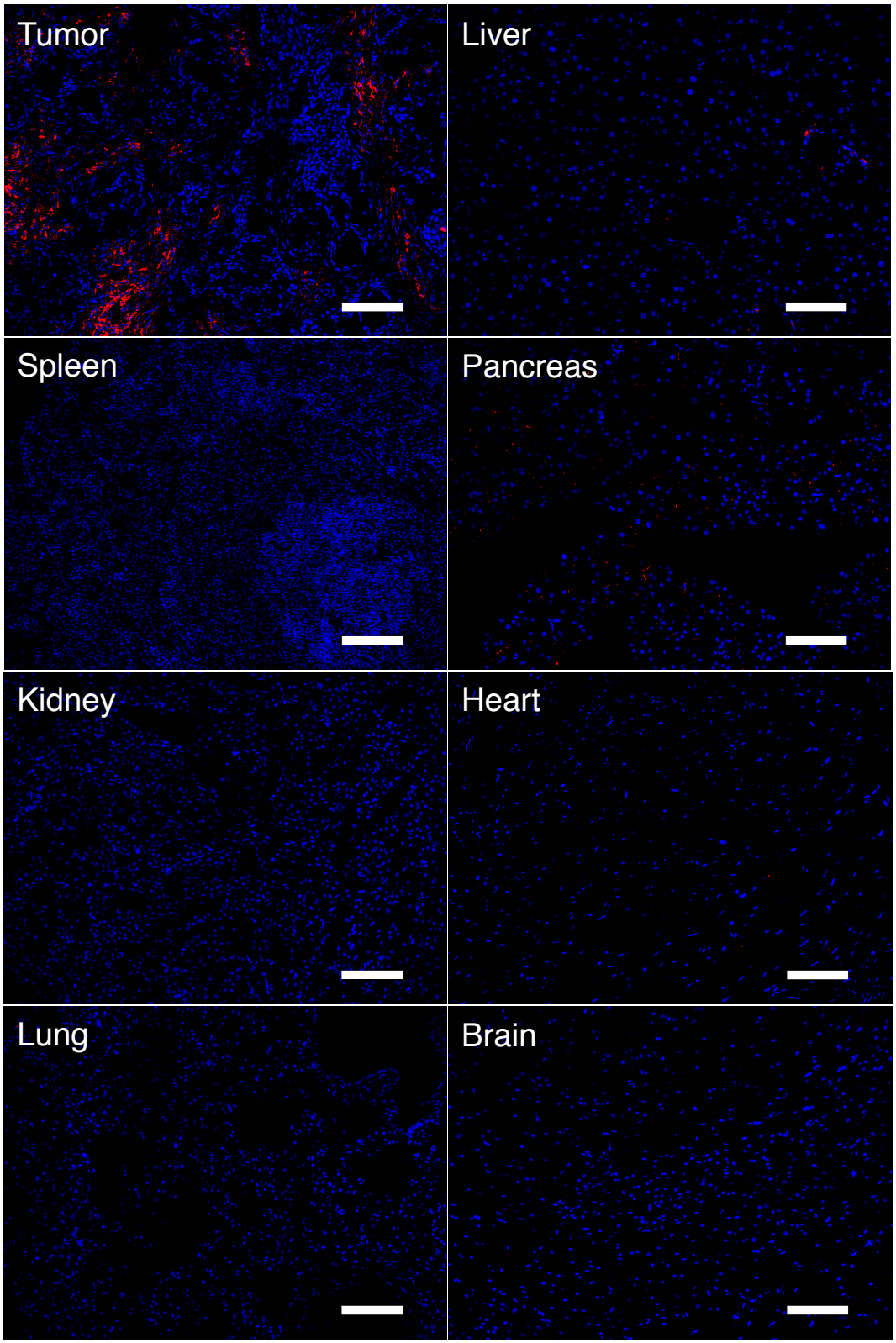

Figure 3-3. Immunohistochemical analysis of tissues in mice bearing subcutaneous BxPC3 tumors.

Red, anti-human/murine ASCT2 antibody; blue, nucleus. Scale bar, 100 μm.

3.4 Conclusion

This chapter highlights the expression level of ASCT2, which is the dominant glutamine transporter in tumor tissue. Flow cytometric analysis showed the overexpression of ASCT2 on human pancreatic cancer BxPC3 cells compared to non-cancerous HEK293 cells. The ASCT2 overexpression ratio between these cell lines (4.8-fold higher expression in BxPC3 cells than that in HEK293 cells) is in line with the *in vivo* situation described in previous studies [3, 11, 12]. Furthermore, ASCT2 overexpression in BxPC3 tumor was also observed in *in vivo* environment. Based on these results, BxPC3 cells and HEK293 cells were used in the subsequent experiments.

3.5 References

1. Pochini, L., Scalise, M., Galluccio, M. & Indiveri, C. Membrane transporters for the special amino acid glutamine: structure/function relationships and relevance to human health. *Front. Chem.* **2,** 61 (2014).
2. van Geldermalsen, M., Wang, Q., Nagarajah, R., Marshall, A. D., Thoeng, A., Gao, D., Ritchie, W., Feng, Y., Bailey, C. G., Deng, N., Harvey, K., Beith, J. M., Selinger, C. I., O'Toole, S. A., Rasko, J. E. J. & Holst, J. ASCT2/SLC1A5 controls glutamine uptake and tumour growth in triple-negative basal-like breast cancer. *Oncogene* **35,** 3201–8 (2016).
3. Wang, Q., Hardie, R.-A., Hoy, A. J., van Geldermalsen, M., Gao, D., Fazli, L., Sadowski, M. C., Balaban, S., Schreuder, M., Nagarajah, R., Wong, J. J.-L., Metierre, C., Pinello, N., Otte, N. J., Lehman, M. L., Gleave, M., Nelson, C. C., Bailey, C. G., Ritchie, W., Rasko, J. E. J. & Holst, J. Targeting ASCT2-mediated glutamine uptake

blocks prostate cancer growth and tumour development. *J. Pathol.* **236,** 278–89 (2015).

4. Wang, Q., Beaumont, K. a., Otte, N. J., Font, J., Bailey, C. G., van Geldermalsen, M., Sharp, D. M., Tiffen, J. C., Ryan, R. M., Jormakka, M., Haass, N. K., Rasko, J. E. J. & Holst, J. Targeting glutamine transport to suppress melanoma cell growth. *Int. J. cancer* **135,** 1060–71 (2014).
5. Gao, P., Tchernyshyov, I., Chang, T.-C., Lee, Y.-S., Kita, K., Ochi, T., Zeller, K. I., De Marzo, A. M., Van Eyk, J. E., Mendell, J. T. & Dang, C. V. c-Myc suppression of miR-23a/b enhances mitochondrial glutaminase expression and glutamine metabolism. *Nature* **458,** 762–765 (2009).
6. Reynolds, M. R., Lane, A. N., Robertson, B., Kemp, S., Liu, Y., Hill, B. G., Dean, D. C. & Clem, B. F. Control of glutamine metabolism by the tumor suppressor Rb. *Oncogene* **33,** 556–566 (2014).
7. Bode, B. P., Fuchs, B. C., Hurley, B. P., Conroy, J. L., Suetterlin, J. E., Tanabe, K. K., Rhoads, D. B., Abcouwer, S. F. & Souba, W. W. Molecular and functional analysis of glutamine uptake in human hepatoma and liver-derived cells. *Am. J. Physiol. Gastrointest. Liver Physiol.* **283,** G1062-73 (2002).
8. Kaira, K., Sunose, Y., Arakawa, K., Sunaga, N., Shimizu, K., Tominaga, H., Oriuchi, N., Nagamori, S., Kanai, Y., Oyama, T. & Takeyoshi, I. Clinicopathological significance of ASC amino acid transporter-2 expression in pancreatic ductal carcinoma. *Histopathology* **66,** 234–243 (2015).
9. Cabral, H., Matsumoto, Y., Mizuno, K., Chen, Q., Murakami, M., Kimura, M., Terada, Y., Kano, M. R., Miyazono, K., Uesaka, M., Nishiyama, N. & Kataoka, K.

Accumulation of sub-100 nm polymeric micelles in poorly permeable tumours depends on size. *Nat. Nanotechnol.* **6,** 815–823 (2011).

10. Cabral, H., Murakami, M., Hojo, H., Terada, Y., Kano, M. R., Chung, U., Nishiyama, N. & Kataoka, K. Targeted therapy of spontaneous murine pancreatic tumors by polymeric micelles prolongs survival and prevents peritoneal metastasis. *Proc. Natl. Acad. Sci. U. S. A.* **110,** 11397–402 (2013).

11. Huang, F., Zhao, Y., Zhao, J., Wu, S., Jiang, Y., Ma, H. & Zhang, T. Upregulated SLC1A5 promotes cell growth and survival in colorectal cancer. *Int J Clin Exp Pathol* **7,** 6006–6014 (2014).

12. Alves, M. J. F., Uno, M., Silva, R. da, Oba-Shinjo, S. M. & Marie, S. K. N. The expression of the aminoacid transporters ASCT2 (SLC1A5) and LAT1 (SLC7A5) in astrocytomas. *Med. Express* **3,** 1–8 (2016).

Chapter 4. Biological activities of glutamine-functionalized polymers

4.1 Introduction

Previous studies revealed the significance of glutamine metabolism in cancer cells and characteristics of cancer cells associated with glutamine metabolism; this elevated glutamine metabolism is accompanied with overexpression of specific glutamine transporter ASCT2 and increased glutamine uptake. Considering the overexpression of ASCT2 in a wide variety of tumor tissues [1-6], glutamine can be used as a versatile ligand molecule with tumor specificity. However, the weak affinity of glutamine to ASCT2 limits the application of glutamine for this purpose.

To overcome this problem, multivalent interaction is a promising strategy because multiple glutamine-ASCT2 interaction is expected to dramatically enhance the binding affinity associated with dense ASCT2 on tumor cells. To examine this hypothesis, a series of glutamine-functionalized polymers (PLys(Gln)-n) were designed and prepared as described in chapter 2.

Consequently, the aim of this chapter is biological evaluation of the interaction between synthesized glutamine-functionalized polymers and tumor cells in *in vitro* and *in vivo*. The enhanced interaction between the glutamine-functionalized polymer and the cells potentially improves the cellular uptake efficiency of the polymers. Accordingly, to examine the cellular interaction of the synthesized polymers in cultured cells, cellular uptake efficiency of the polymers were evaluated using flow cytometer. Through this flow cytometric analysis, the effects of DP and chemical structure at the side chain of the polymers on the cellular uptake were first evaluated. Next, target transporter of the polymers was investigated by evaluating their cellular uptake efficiency in the presence of transporter inhibitors. Confocal laser scanning microscopic observation was also performed to examine

the subcellular distribution and internalized pathway of the polymers. Based on cell-based competitive inhibition assay, apparent binding affinity of the polymers to target transporters on tumor cells was estimated. Finally, to assess the *in vivo* interaction between the polymers and tumor tissue, the polymers were intratumorally injected to subcutaneous tumor and their retention at the tumor site was evaluated.

4.2 Materials and Methods

4.2.1 Materials

2-(methylamino)isobutyric acid (MeAIB) was purchased from Tokyo Chemical Industry Co., Ltd. RPMI 1640 medium, Dulbecco's modified Eagle's medium (DMEM), penicillin/streptomycin, trypsin/EDTA, and 2-amino-2-norbornanecarboxylic acid (BCH) were purchased from Sigma Aldrich Corporation. *O*-benzyl-L-serine (BzlSer), L-glutamine (Gln), and D-PBS(-) (PBS) were purchased from Wako Pure Chemical Industries, Ltd.

4.2.2 Cell lines and animals

BxPC3 cells and HEK293 cells were purchased from ATCC (Manassas, VA). BxPC3 cells were cultured under a humidified atmosphere containing 5% CO_2 at 37 °C in RPMI 1640 supplemented with 10 % FBS and 1 % penicillin/streptomycin. HEK293 cells were cultured under a humidified atmosphere containing 5% CO_2 at 37 °C in DMEM supplemented with 10 % FBS and 1 % penicillin/streptomycin. BALB/c nu/nu mice (female, 4 weeks old) were purchased from Charles River Laboratories Japan, Inc. (Yokohama, Japan). All animal experiments were approved by the Animal Care and Use Committee of Tokyo Institute of Technology, and performed in accordance with the Guidelines for the Care and

Use of Laboratory Animals as stated by Tokyo Institute of Technology.

4.2.3 General procedure for cellular uptake analysis

The cells (5.0×10^4 cells/well) were seeded into 24-well plates and incubated at 37 °C for 24 h. The cells were washed with PBS, and incubated in 500 μl of assay buffer (PBS containing 10% FBS) with 1 μM of polymers. After 3 h incubation at 37 °C, the cells were washed twice with PBS, treated with 150 μL of trypsin, and suspended with 300 μl of the assay buffer. Cy5 fluorescence intensities of the cells were measured using the flow cytometer (ex/em = 642 nm/664 nm).

4.2.4 Time-dependent cellular uptake analysis

The time-dependent cellular uptake study was conducted in accordance with the general procedure for cellular uptake analysis described in 4.2.3 except for incubation time with the polymers. Incubation time with the polymers was changed to 1, 2, 4, or 8 h.

4.2.4 Cellular uptake analysis with transporter inhibitors

Cellular uptake of the polymers was evaluated in the presence of specific transporter inhibitors (BzlSer, ASCT2 inhibitor; MeAIB, system A inhibitor; BCH, system L inhibitor; Gln, system N inhibitor) in a concentration ranging from 2.5 mM to 10 mM. The procedure was same as the general procedure for cellular uptake analysis described in 4.2.3 except for the addition of inhibitors to the polymer solution. The data are expressed as a percentage of fluorescence intensity obtained from the cells treated without any inhibitor.

4.2.5 Cellular uptake analysis at pH 6.5

To investigate the effect of pH on the cellular uptake behavior of PLys(α-Glu)-100 and PLys(Gln)-100 in BxPC3 cells, the pH of the assay buffer (PBS containing 10% FBS) was adjusted to 6.5 using HCl aqueous solution. The procedure was same as the general procedure for cellular uptake analysis described above except for the pH of the assay buffer.

4.2.6 Confocal laser scanning microscopic observation

To visualize the subcellular distribution of the polymers, BxPC3 cells treated with each polymer at 37 °C or 4 °C were observed using a confocal laser scanning microscope (LSM710, Carl Zeiss, Oberkochen, Germany). BxPC3 cells (5×10^4 cells/dish) were seeded into 35 mm glass-based dish (Asahi Glass Co., Ltd., Tokyo, Japan) and incubated at 37 °C for 24 h. For the treatment at 37 °C, the cells were washed with PBS, and incubated in 1 mL of PBS containing 10% FBS and 1 μM of the polymer at 37 °C for 2.5 h. To stain late endosome/lysosome and nuclei, LysoTracker Red (Thermo Fischer Scientific) and Hoechst 33342 were added to the solution. After additional 30 min incubation at 37 °C, the cells were washed twice with PBS, and observed in fresh medium using LSM710 equipped with an incubator (37 °C, 5% CO_2 in humidified atmosphere).

For the treatment at 4 °C, the cells were cooled at 4 °C for 10 min and washed with cold PBS, followed by incubation in 1 mL of PBS containing 10% FBS and 1 μM of the polymers at 4 °C for 2.5 h. Then, LysoTracker Red and Hoechst 33342 were added to the solution, and the cells were incubated at 4 °C for another 30 min. The cells were washed twice with cold PBS, fixed with 4% paraformaldehyde in PBS, and observed in fresh PBS using LSM710.

Cy5, LysoTracker Red, and Hoechst 33342 were excited using laser light at 633 nm, 561 nm, and 405 nm, respectively.

4.2.7 Cellular uptake at 4 °C

BxPC3 cells (5.0×10^4 cells/well) were seeded into 24-well plates and incubated at 37 °C for 24 h. The cells were cooled at 4 °C for 10 min and washed with cold PBS, followed by the incubation in 500 μl of the assay buffer (10% FBS in PBS) containing 1 μM of the polymers. After 3 h incubation at 4 °C, the cells were washed twice with cold PBS, detached with 150 μL of trypsin, and suspended with 300 μL of the assay buffer. The cells were analysed using flow cytometer, and the obtained Cy5 fluorescence intensities were expressed as a percentage of the fluorescence intensity obtained from cells treated at 37 °C.

4.2.8 Cell-based competitive inhibition

To estimate the binding affinity of the polymers to ASCT2 on BxPC3 cells, cell-based competitive inhibition assay was performed. BxPC3 cells (5.0×10^4 cells/well) were seeded into 24-well plates and incubated at 37 °C for 24 h. For the inhibition of PLys(Gln)-100, the cells were cooled at 4 °C for 10 min, washed with cold PBS, followed by incubation at 4 °C for 2 h in 500 μL of the assay buffer (10% FBS in PBS) containing 1 μM of PLys(Gln)-100 and BzlSer in a concentration ranging from 30 mM to 0.04 mM. After the incubation, the cells were washed with cold PBS, treated with 150 μL of trypsin, and suspended with 300 μL of the assay buffer. The cells were analyzed using flow cytometer, and half maximal inhibitory concentrations (IC_{50}) of BzlSer were calculated. Apparent

dissociation constant (K_d) of the polymers were estimated using the obtained IC_{50} values, following Cheng-Prusoff equation [7, 8]:

$$K_d = K_i \times [L] / (IC_{50} - K_i)$$

where K_i is the apparent inhibition constant of BzlSer for ASCT2 (0.9 mM), and [L] is the polymer concentration in this assay. For the inhibition of PLys(Gln)-50 and PLys(α-Glu)-100, concentration of both polymers was changed to 3 μM.

4.2.9 In vivo tumor retention

To establish the BxPC3 xenograft model, the BxPC3 cells (5.0×10^6 cells) were subcutaneously inoculated to BALB/c nu/nu mice (female, 4 weeks old). When average tumor volume reached approximately 150 mm^3, 20 μl of PLys(Gln)-100, PLys(Gln)-50, or PLys(α-Glu)-100 solution (40 μM in PBS) was intratumorally injected (n = 3). At 0.25, 1, 4, and 8 h after injection, the mice were imaged by in vivo imaging system (IVIS, Perkin Elmer, Waltham, MA) using 640 nm/680 nm ex/em filter. Average radiant efficiency of the tumour region was quantified using Living Image software.

4.3 Results and Discussion

4.3.1 Cellular uptake analysis

To investigate the interaction between glutamine-functionalized polymers (PLys(Gln)-n) and cultured cells, the cellular uptake efficiency of the polymers was evaluated using flow cytometer.

First, to examine the effect of DP on the cellular uptake efficiency, BxPC3 cells were treated with a series of PLys(Gln)-n, and then Cy5 intensities from the cells were

measured to quantify the cellular uptake. As shown in Figure 4-1, a series of PLys(Gln)-n showed DP-dependent uptake behavior; PLys(Gln)-100 exhibited the highest uptake in BxPC3 cells, which was 9.7-fold and 18-fold higher than that of PLys(Gln)-50 and PLys(Gln)-30, respectively. According to a previous study, the interaction potency of multivalent polymeric ligand was exponentially enhanced by an increase of the polymer length [9, 10]. Thus, this drastically high cellular uptake of PLys(Gln)-100 in ASCT2-overexpressing cells is probably due to the multivalent interaction between the polymer and the cells.

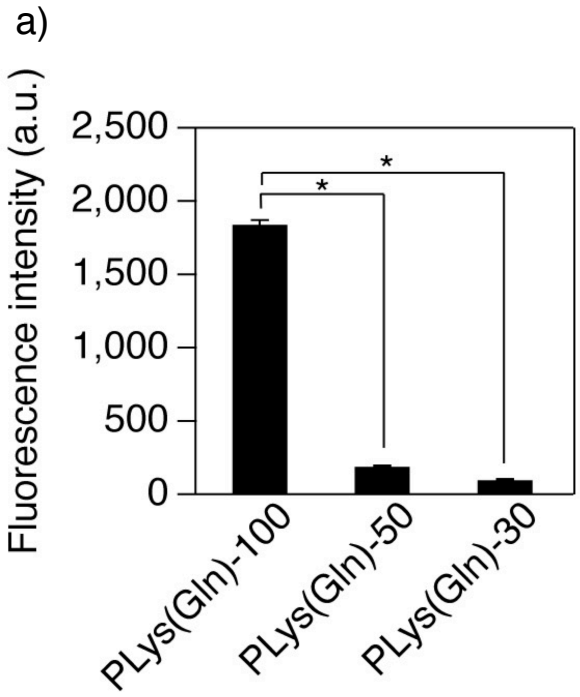

Figure 4-1. Cellular uptake analysis of a series of PLys(Gln)-n in BxPC3 cells.

BxPC3 cells were incubated with the polymers for 3 h at 37 ˚C, and analyzed using flow cytometer. Data are mean ± S.D. (n=3). $p^{\star} < 0.001$ (one-way ANOVA with Tukey's multiple comparison test).

Next, to investigate the tumor specificity of this enhanced interaction between PLys(Gln)-100 and cultured cells, the time-dependent cellular uptake was evaluated using

HEK293 cells (moderate expression level of ASCT2) as well as BxPC3 cells (Figure 4-2 a). PLys(Gln)-100 exhibited faster uptake in BxPC3 cells compared to HEK293 cells. After 8 h incubation, PLys(Gln)-100 uptake in BxPC3 cells was 4.7-fold higher than that in HEK293 cells. These results are consistent with the scheme that PLys(Gln)-100 might strongly interact with tumor cells overexpressing ASCT2 through the strong multivalent effect, while weakly interacting with normal cells because of low ASCT2 density as illustrated in Figure 1-5.

To get insight about the effect of glutamine-like structure of the side chain on this cellular interaction, the time-dependent cellular uptake of control polymer PLys(α-Glu)-100 was also investigated. This polymer has same molecular weight and charge with PLys(Gln)-100 under examined condition, but has the different position of free amine group at the side chain. Thus, this polymer was used as a control polymer. As shown in Figure 4-2 b, PLys(α-Glu)-100 showed slightly higher uptake in BxPC3 cells compared to HEK293 cells. Given that glutamate weakly interacted with ASCT2 [11, 12], it could be assumed that PLys(α-Glu)-100 having glutamate-like structure at the side chain might interact with ASCT2 to some extent and exhibit multivalent effect. Indeed, a series of PLys(α-Glu)-n also exhibited DP-dependent uptake behavior in cultured BxPC3 cells (Figure 4-3). However, compared to PLys(Gln)-100, PLys(α-Glu)-100 exhibited slower uptake in BxPC3 cells and lower uptake ratio between BxPC3 and HEK293 cells. The relatively high affinity of PLys(Gln)-100 to tumor cells is probably due to its chemical structure at the side chain, which is similar to potent ASCT2 inhibitor having γ-amide modified glutamine structure [13, 14].

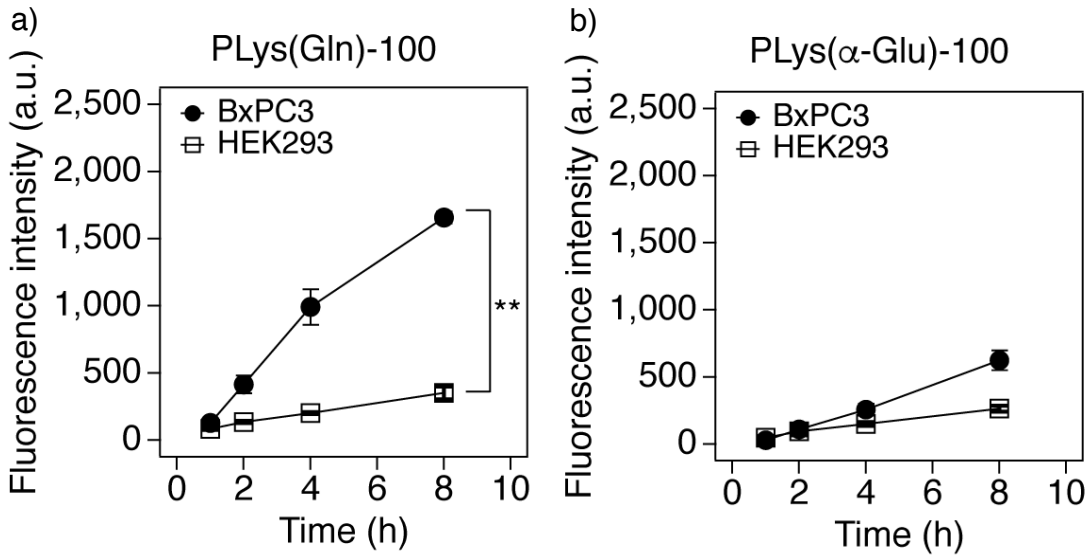

Figure 4-2. Time-dependent cellular uptake analysis in BxPC3 cells and HEK293 cells.

The cells were treated with PLys(Gln)-100 (a) or PLys(α-Glu)-100 (b), and analyzed by flow cytometer. Data are mean ± S.D. (n=3). $p^{**} < 0.001$ (one-way ANOVA with Tukey's multiple comparison test).

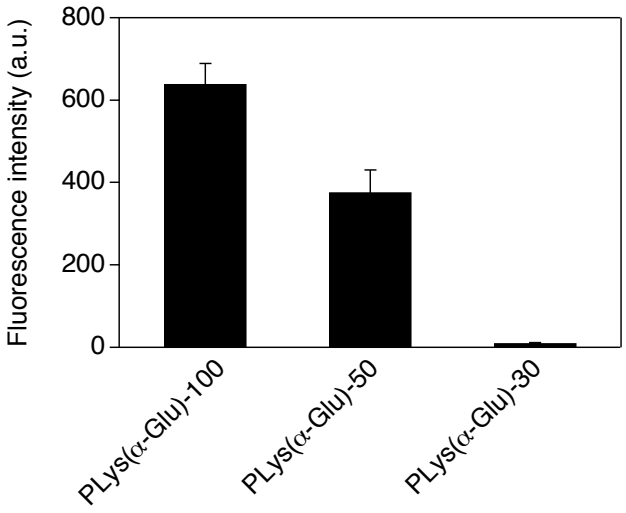

Figure 4-3. Cellular uptake analysis of a series of PLys(α-Glu)-n in BxPC3 cells.

BxPC3 cells were incubated with a series of PLys(α-Glu)-n for 3 h at 37 ˚C, and analyzed using flow cytometer. Data are mean ± S.D. (n=3).

4.3.2 Transporter specificity

To examine the transporter specificity of the developed polymers, cellular uptake was evaluated in the presence of several inhibitors for glutamine transporters: ASCT2, system A, system L, and system N transporters. For their inhibitors, *O*-benzyl-L-serine (BzlSer, ASCT2 inhibitor), 2-(methylamino)isobutyric acid (MeAIB, system A inhibitor), 2-amino-2-norbornanecarboxylic acid (BCH, system L inhibitor), and L-glutamine (Gln, system N inhibitor) were used. As shown in Figure 4-4 a, only BzlSer inhibited PLys(Gln)-100 uptake in a concentration-dependent manner, while the other inhibitors showed negligible inhibitory effect, indicating the dominant contribution of ASCT2 to the uptake of PLys(Gln)-100. Similar inhibitory effects were also observed for PLys(Gln)-50 (Figure 4-4 b). Among above-mentioned glutamine transporters, ASCT2 has relatively high affinity with glutamine (Michaelis constant (K_m) is 20-60 μM [12, 15], whereas the other transporters has K_m in the range of approximately 150-1600 μM [16-19]). Because of this relatively strong interaction between ASCT2 and glutamine molecule, ASCT2 could be a dominant target transporter for PLys(Gln)-n. Moreover, the overexpression of ASCT2 on BxPC3 cells as shown in Figure 3-1 may also contribute to the dominant role of ASCT2 for tumor cell-selective interaction of PLys(Gln)-n.

Cellular uptake of PLys(α-Glu)-100 was also inhibited by only BzlSer while its inhibitory effect was higher compared to that of PLys(Gln)-100 (Figure 4-4 c), suggesting that PLys(α-Glu)-100 modestly interacted with ASCT2. Given that PLys(Gln)-100 and PLys(α-Glu)-100 has the same valency and density of the binding motifs, this moderate interaction between PLys(α-Glu)-100 and ASCT2 might be attributed to the recognition of glutamate-like structure at the side chain by ASCT2. This explanation is consistent with

previous reports, where glutamate did not interact with system L and system N glutamine transporters but weakly interacted with ASCT2 [11, 12, 18, 20]. In addition, this glutamate-ASCT2 interaction was reported to be pH-dependent; a decrease of pH could enhance the interaction capacity of glutamate with ASCT2 [12, 13]. In line with this report, PLys(α-Glu)-100 showed higher uptake in BxPC3 cells at pH 6.5 compared to that at pH 7.4 (Figure 4-5). However, this increased cellular uptake of PLys(α-Glu)-100 at pH 6.5 was still lower than that of PLys(Gln)-100, indicating that even at the intratumoral pH (~ 6.5) PLys(Gln)-100 should be the preferred structure for achieving high affinity to ASCT2.

These results also provide insight about recognition mechanism of ASCT2-polymer interaction. Although exact mechanism of interaction between ASCT2 and glutamine or glutamine-analogues is not fully understood, a previous study has proposed key structures of glutamine-analogues to get a high affinity to ASCT2: α-amine and α-carboxyl groups for charge interaction, γ-amide group for hydrogen bonding, and modified side chain for hydrophobic interaction [13]. As most potent ASCT2 inhibitors have α-amine and α-carboxyl groups, these chemical structures appeared to be important for glutamine-ASCT2 interaction. Indeed, PLys(Gln)-100 that has α-amine and α-carboxyl groups at the side chain showed higher interaction capacity with ASCT2 compared to PLys(α-Glu)-100 although the difference between these polymers is just the position of amine group at the side chain. In addition to α-amine and α-carboxyl groups, glutamine-like structure should be important for achieving ASCT2 selective interaction because amino acids transporters generally recognize these functional groups. For instance, α-amine and α-carboxyl groups are key components for the substrates of system L transporter 1 (LAT1) [21], which is overexpressed on a variety of tumor cells [22-24]. Given that LAT1 is reported to be expressed on BxPC3 cells [25],

PLys(Gln)-100 was expected to interact with LAT1 as well as ASCT2 if amino acids transporters recognize just the side chain terminus of the polymers. However, as shown in Figure 4-4 a, LAT1 inhibitor BCH did not inhibit the PLys(Gln)-100 uptake in BxPC3 cells while ASCT2 inhibitor BzlSer strongly inhibited the uptake. This ASCT2-selective interaction of PLys(Gln)-100 suggests that ASCT2 may recognize not merely α-amine and α-carboxyl groups but whole glutamine-like structure (including γ-amide groups) of the side chain.

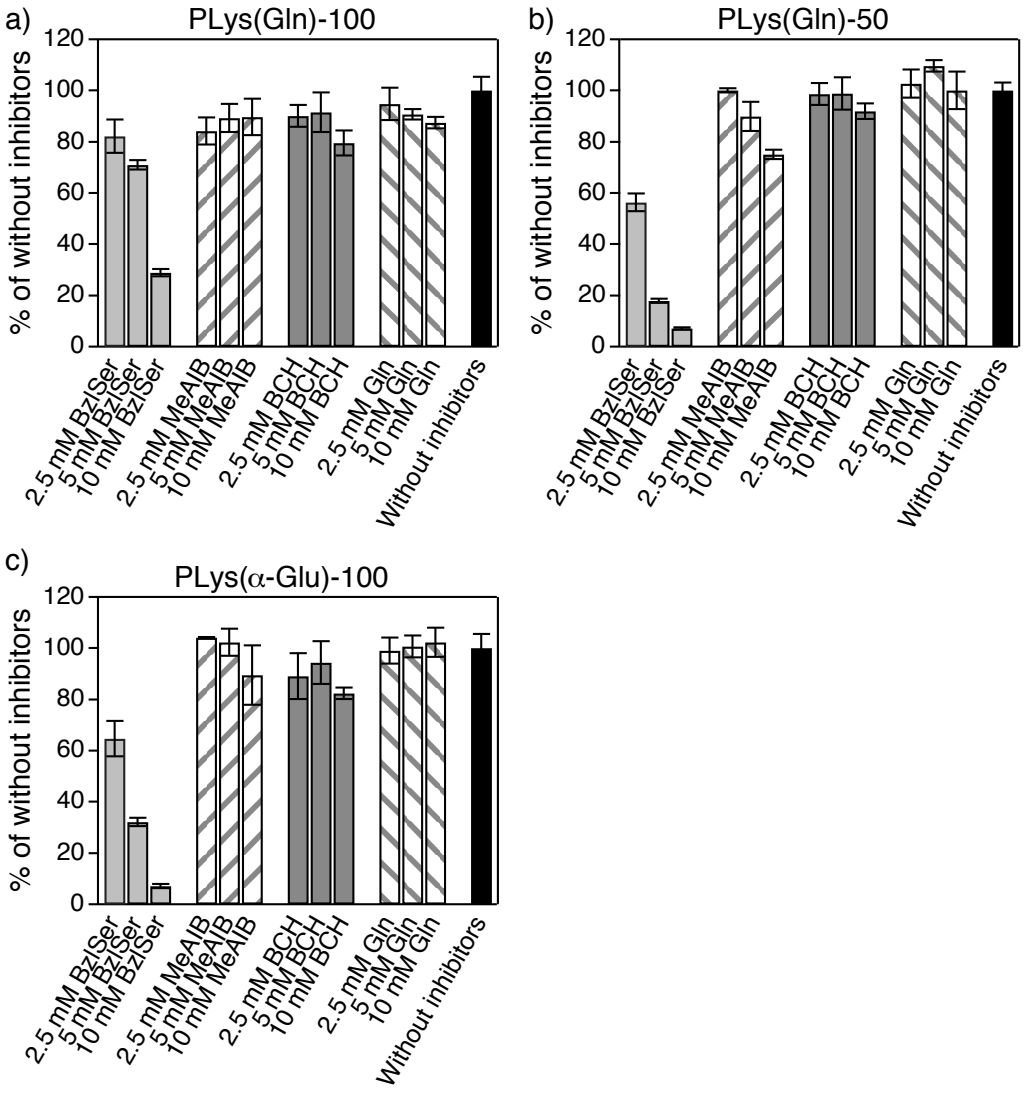

Figure 4-4. Cellular uptake analysis of the polymers in the presence of transporter inhibitors.

Effect of transporter inhibitors on cellular uptake of PLys(Gln)-100 (a), PLys(Gln)-50 (b), and PLys(α-Glu)-100 (c) in BxPC3 cells (BzlSer, ASCT2 inhibitor; MeAIB, system A inhibitor; BCH, system L inhibitor; Gln, system N inhibitor). Data are mean ± S.D. (n=3).

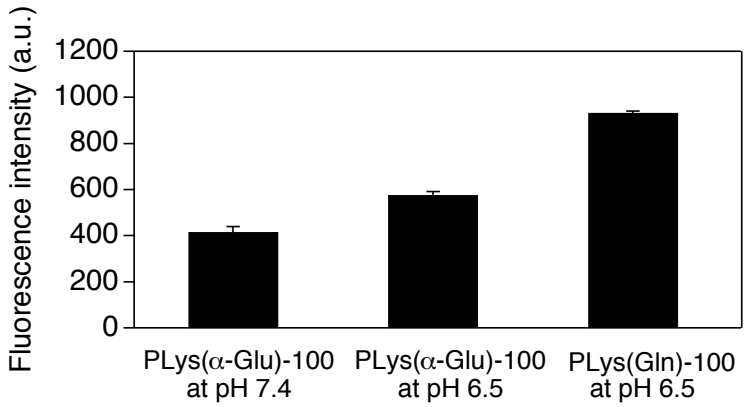

Figure 4-5. Cellular uptake analysis of PLys(Gln)-100 and PLys(α-Glu)-100 in BxPC3 cells at pH 6.5.

BxPC3 cells were incubated with PLys(Gln)-100 or PLys(α-Glu)-100 for 3 h at indicated pH, and analyzed using flow cytometer. Data are mean ± S.D. (n=3).

4.3.3 Subcellular distribution

Subcellular distribution of the polymer was then investigated using confocal laser scanning microscopy (CLSM) to assess the internalization of the polymers. As shown in Figure 4-6 a, in the BxPC3 cells incubated with PLys(Gln)-100 at 37 °C, the polymer (red) was located at intracellular space, and colocalized (yellow) with the late endosome/lysosome indicator, Lysotracker Red (green). In contrast, when BxPC3 cells were incubated with the polymer at 4 °C to suppress the endocytosis, the polymer was located only on the cellular membrane, and did not colocalize with the late endosome/lysosomes. In addition, mean fluorescence intensity from the cells incubated with the polymer at 4 °C was significantly lower compared to that of 37 °C incubation (Figure 4-6 d). These results indicate that PLys(Gln)-100 first attached to the cell membrane through the polymer-ASCT2 interaction, and the attached polymer was internalized by endocytosis. Note that similar behaviors in subcellular distribution were observed for PLys(α-Glu)-100 and PLys(Gln)-50 (Figure 4-6 b,

c, e, f), indicating that these polymers were also internalized by endocytosis after interacting with ASCT2 on cell surface.

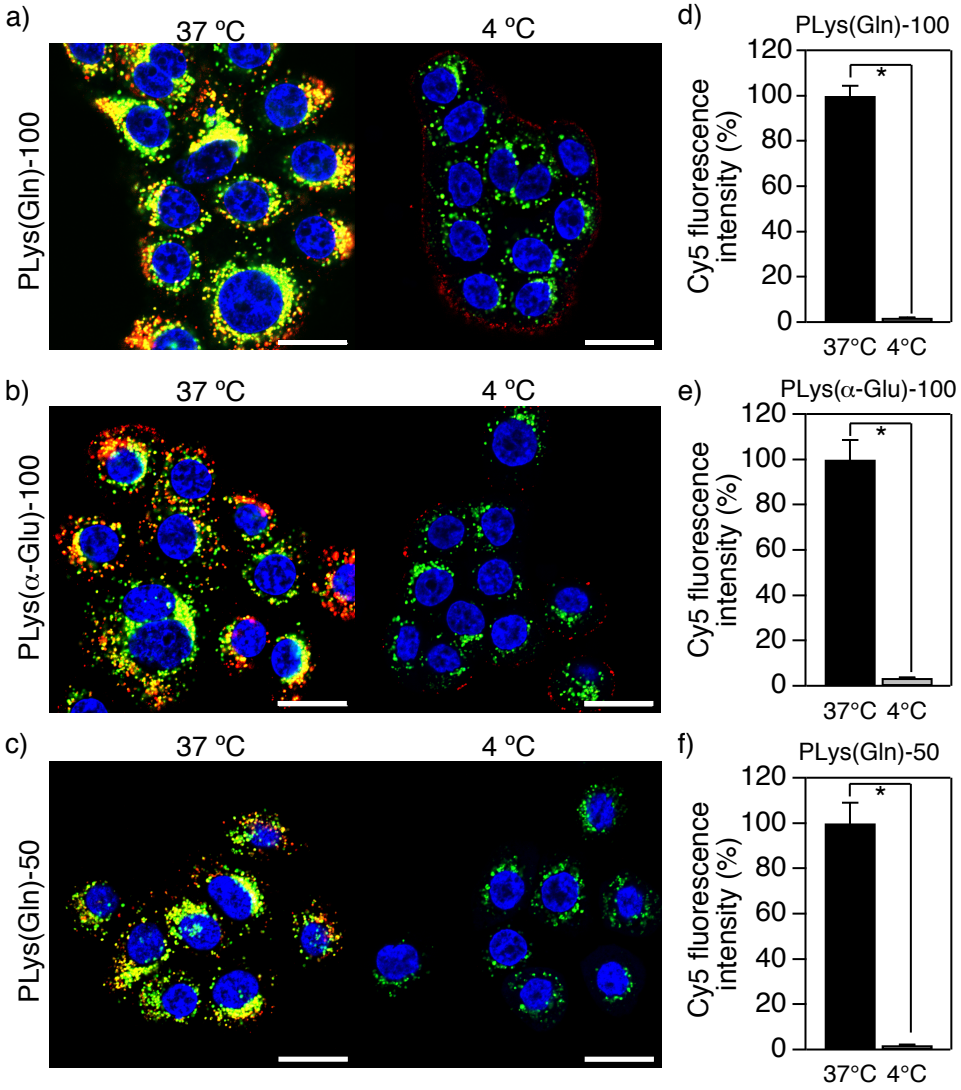

Figure 4-6. Subcellular distribution of the polymers in BxPC3 cells.

(a-c) Confocal laser scanning microscopic images of BxPC3 cells after 3 h treatment with PLys(Gln)-100 (a), PLys(α-Glu)-100 (b), and PLys(Gln)-50 (c) at 37 °C (left) and 4 °C (right). Red, Cy5-labeld polymers; green, late endosome/lysosome; blue, nucleus. Scale bar, 20 μm. (d-f) Cy5 fluorescence intensities of BxPC3 cells after 3 h treatment with PLys(Gln)-100 (d), PLys(α-Glu)-100 (e), and PLys(Gln)-50 (f) at 37 °C and 4 °C. The cells were analyzed using flow cytometer. Data are mean ± S.D. (n=3). $p^* < 0.001$ (Student's *t*-test).

4.3.4 Binding affinities of the polymers to ASCT2 on BxPC3 cells

To estimate the binding affinity of the polymers to ASCT2, cell-based competitive inhibition study was carried out using ASCT2 inhibitor BzlSer. Because BzlSer is a competitive inhibitor for ASCT2 with an inhibition constant (K_i) of 0.9 mM [26], apparent K_d values of these polymers can be estimated by assuming a simple inhibition model [8]. Under this assumption, PLys(Gln)-100 showed apparent K_d value of 62 nM, which is comparable to the K_d value of potent ligands [27]. By contrast, K_d for PLys(Gln)-50 could not be estimated in this method since the inhibition curve of PLys(Gln)-50 indicated incomplete inhibition within the examined BzlSer concentration (Figure 4-7 b). Meanwhile, PLys(α-Glu)-100 showed apparent K_d value of 250 nM. The K_d values of PLys(Gln)-100 and PLys(α-Glu)-100 were consistent with cellular uptake behavior as shown in Figure 4-2.

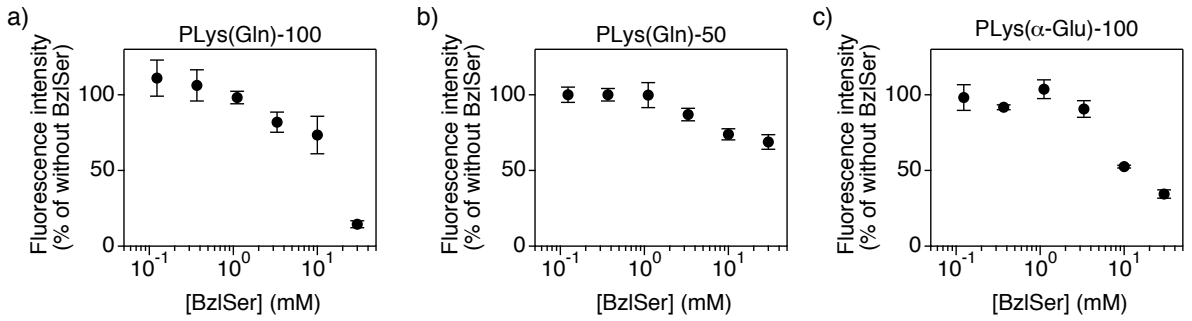

Figure 4-7. Cell-based competitive inhibition curve of the polymers.

(a) PLys(Gln)-100, (b) PLys(Gln)-50, and (c) PLys(α-Glu)-100. Data are mean ± S.D. (n=3). IC_{50} values were calculated using these curves. Apparent Kd values of these polymers to ASCT2 on BxPC3 cells were estimated using Cheng-Prusoff equation [7, 8].

4.3.5 Tumor retention

Finally, to examine *in vivo* interaction capacity of the polymers, the polymers were

intratumorally injected to subcutaneous BxPC3 tumors in mice, and their retention in the tumor was evaluated by measuring fluorescence intensity at tumor site using in vivo imaging system (Figure 4-8). PLys(Gln)-50 was most rapidly eliminated from the tumor because PLys(Gln)-50 had low binding affinity to ASCT2 on BxPC3 cells as discussed above. Compared with PLys(α-Glu)-100, PLys(Gln)-100 exhibited longer retention in the tumor. Considering that these polymers have same molecular weight and neutral charge, this prolonged retention of PLys(Gln)-100 can be attributed to its higher binding affinity to the tumor cells, which is in line with the apparent K_d values.

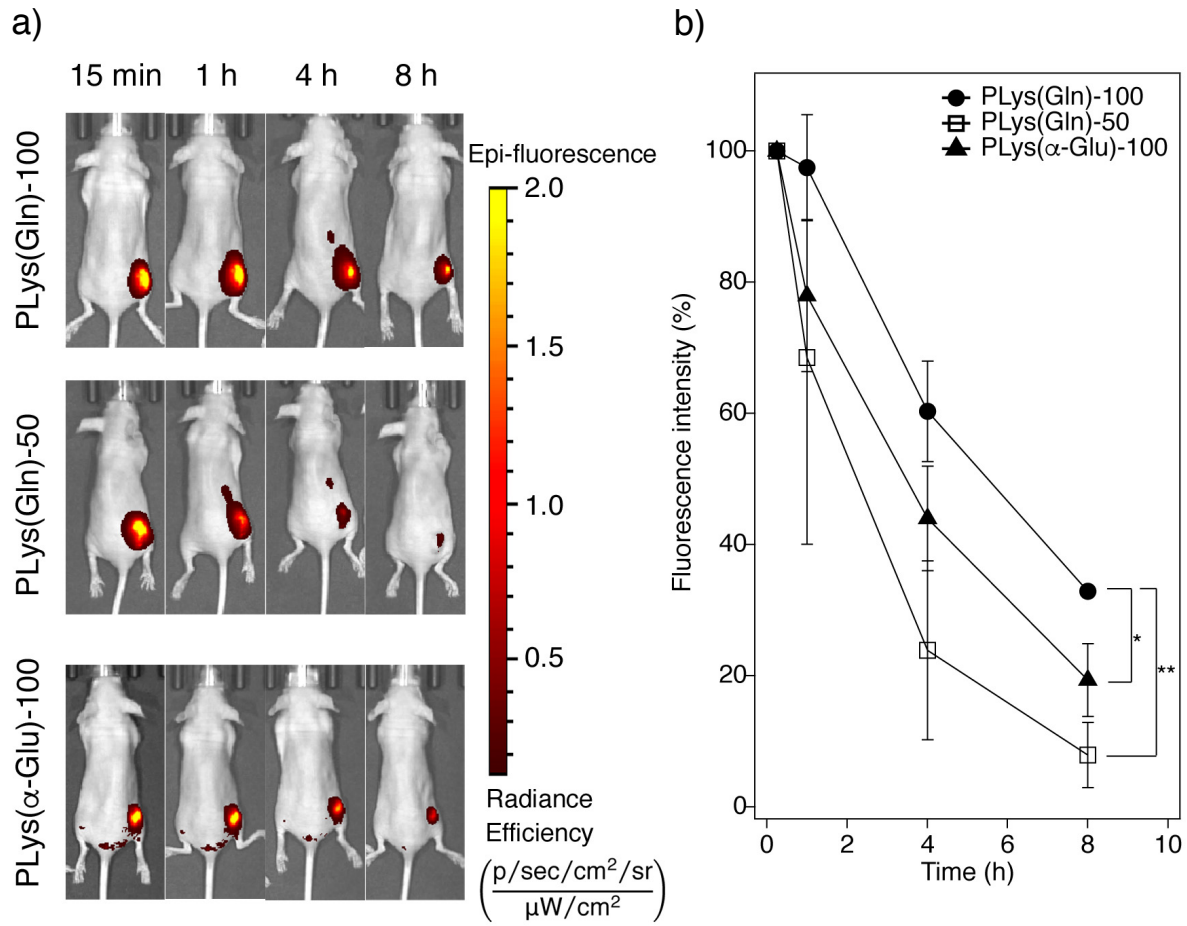

Figure 4-8. *In vivo* tumor retention of the polymers after intratumoral injection.

(a) Representative images of mice bearing subcutaneous BxPC3 tumors after intratumoral injection of the polymers. Images were taken by in vivo imaging system (IVIS). (b) Cy5 fluorescence intensities from the intratumorally injected polymers at subcutaneous BxPC3 tumor. Data are mean ± S.D. (n=3). $p^* < 0.05$, $p^{**} < 0.01$ (two-way ANOVA with Tukey's multiple comparison test).

4.4 Conclusion

The developed glutamine-functionalized polymer PLys(Gln)-100 showed drastically enhanced cellular uptake efficiency (9.7-fold and 18-fold higher compared to PLys(Gln)-50 and PLys(Gln)-30, respectively) possibly due to the multivalent interaction with target transporter on tumor cells. In addition, this enhanced cellular interaction was

selectively achieved in tumor cells overexpressing ASCT2; PLys(Gln)-100 exhibited fast and higher (4.7-fold higher) uptake behavior in BxPC3 cells (overexpressing ASCT2) compared to non-cancerous HEK293 cells (moderate expression level of ASCT2). Furthermore, the glutamine-like structure of the side chain

4.5 References

1. Kaira, K., Sunose, Y., Arakawa, K., Sunaga, N., Shimizu, K., Tominaga, H., Oriuchi, N., Nagamori, S., Kanai, Y., Oyama, T. & Takeyoshi, I. Clinicopathological significance of ASC amino acid transporter-2 expression in pancreatic ductal carcinoma. *Histopathology* **66,** 234–243 (2015).
2. van Geldermalsen, M., Wang, Q., Nagarajah, R., Marshall, A. D., Thoeng, A., Gao, D., Ritchie, W., Feng, Y., Bailey, C. G., Deng, N., Harvey, K., Beith, J. M., Selinger, C. I., O'Toole, S. A., Rasko, J. E. J. & Holst, J. ASCT2/SLC1A5 controls glutamine uptake and tumour growth in triple-negative basal-like breast cancer. *Oncogene* **35,** 3201–8 (2016).
3. Wang, Q., Hardie, R.-A., Hoy, A. J., van Geldermalsen, M., Gao, D., Fazli, L., Sadowski, M. C., Balaban, S., Schreuder, M., Nagarajah, R., Wong, J. J.-L., Metierre, C., Pinello, N., Otte, N. J., Lehman, M. L., Gleave, M., Nelson, C. C., Bailey, C. G., Ritchie, W., Rasko, J. E. J. & Holst, J. Targeting ASCT2-mediated glutamine uptake blocks prostate cancer growth and tumour development. *J. Pathol.* **236,** 278–89 (2015).
4. Alves, M. J. F., Uno, M., Silva, R. da, Oba-Shinjo, S. M. & Marie, S. K. N. The expression of the aminoacid transporters ASCT2 (SLC1A5) and LAT1 (SLC7A5) in

astrocytomas. *Med. Express* **3,** 1–8 (2016).

5. Shimizu, K., Kaira, K., Tomizawa, Y., Sunaga, N., Kawashima, O., Oriuchi, N., Tominaga, H., Nagamori, S., Kanai, Y., Yamada, M., Oyama, T. & Takeyoshi, I. ASC amino-acid transporter 2 (ASCT2) as a novel prognostic marker in non-small cell lung cancer. *Br. J. Cancer* **110,** 2030–9 (2014).
6. Wang, Q., Beaumont, K. a., Otte, N. J., Font, J., Bailey, C. G., van Geldermalsen, M., Sharp, D. M., Tiffen, J. C., Ryan, R. M., Jormakka, M., Haass, N. K., Rasko, J. E. J. & Holst, J. Targeting glutamine transport to suppress melanoma cell growth. *Int. J. cancer* **135,** 1060–71 (2014).
7. Yung-Chi, C. & Prusoff, W. H. Relationship between the inhibition constant (KI) and the concentration of inhibitor which causes 50 per cent inhibition (I50) of an enzymatic reaction. *Biochem. Pharmacol.* **22,** 3099–3108 (1973).
8. Monestier, M., Charbonnier, P., Gateau, C., Cuillel, M., Robert, F., Lebrun, C., Mintz, E., Renaudet, O. & Delangle, P. ASGPR-Mediated Uptake of Multivalent Glycoconjugates for Drug Delivery in Hepatocytes. *ChemBioChem* **17,** 590–594 (2016).
9. Kanai, M., Mortell, K. H. & Kiessling, L. L. Varying the Size of Multivalent Ligands: The Dependence of Concanavalin A Binding on Neoglycopolymer Length. *J. Am. Chem. Soc.* **119,** 9931–9932 (1997).
10. Gestwicki, J. E., Cairo, C. W., Strong, L. E., Oetjen, K. A. & Kiessling, L. L. Influencing receptor-ligand binding mechanisms with multivalent ligand architecture. *J. Am. Chem. Soc.* **124,** 14922–14933 (2002).
11. Bröer, A., Brookes, N., Ganapathy, V., Dimmer, K. S., Wagner, C. A., Lang, F. &

Bröer, S. The astroglial ASCT2 amino acid transporter as a mediator of glutamine efflux. *J. Neurochem.* **73,** 2184–94 (1999).

12. Utsunomiya-Tate, N., Endou, H. & Kanai, Y. Cloning and functional characterization of a system ASC-like Na+-dependent neutral amino acid transporter. *J. Biol. Chem.* **271,** 14883–90 (1996).

13. Esslinger, C. S., Cybulski, K. A. & Rhoderick, J. F. Nγ-Aryl glutamine analogues as probes of the ASCT2 neutral amino acid transporter binding site. *Bioorg. Med. Chem.* **13,** 1111–1118 (2005).

14. Schulte, M. L., Dawson, E. S., Saleh, S. a., Cuthbertson, M. L. & Manning, H. C. 2-Substituted Nγ-glutamylanilides as novel probes of ASCT2 with improved potency. *Bioorg. Med. Chem. Lett.* **25,** 113–116 (2015).

15. Scalise, M., Pochini, L., Panni, S., Pingitore, P., Hedfalk, K. & Indiveri, C. Transport mechanism and regulatory properties of the human amino acid transporter ASCT2 (SLC1A5). *Amino Acids* **46,** 2463–2475 (2014).

16. Mackenzie, B. & Erickson, J. D. Sodium-coupled neutral amino acid (System N/A) transporters of the SLC38 gene family. *Pflugers Arch.* **447,** 784–95 (2004).

17. Yao, D., Mackenzie, B., Ming, H., Varoqui, H., Zhu, H., Hediger, M. A. & Erickson, J. D. A Novel System A Isoform Mediating Na+/Neutral Amino Acid Cotransport. *J. Biol. Chem.* **275,** 22790–22797 (2000).

18. Yanagida, O., Kanai, Y., Chairoungdua, A., Kim, D. K., Segawa, H., Nii, T., Cha, S. H., Matsuo, H., Fukushima, J., Fukasawa, Y., Tani, Y., Taketani, Y., Uchino, H., Kim, J. Y., Inatomi, J., Okayasu, I., Miyamoto, K., Takeda, E., Goya, T. & Endou, H. Human L-type amino acid transporter 1 (LAT1): characterization of function and

expression in tumor cell lines. *Biochim. Biophys. Acta* **1514,** 291–302 (2001).

19. Segawa, H., Fukasawa, Y., Miyamoto, K., Takeda, E., Endou, H. & Kanai, Y. Identification and functional characterization of a Na+-independent neutral amino acid transporter with broad substrate selectivity. *J. Biol. Chem.* **274,** 19745–51 (1999).

20. Nakanishi, T., Sugawara, M., Huang, W., Martindale, R. G., Leibach, F. H., Ganapathy, M. E., Prasad, P. D. & Ganapathy, V. Structure, Function, and Tissue Expression Pattern of Human SN2, a Subtype of the Amino Acid Transport System N. *Biochem. Biophys. Res. Commun.* **281,** 1343–1348 (2001).

21. Rautio, J., Gynther, M. & Laine, K. LAT1-mediated prodrug uptake: a way to breach the blood–brain barrier? *Ther. Deliv.* **4,** 281–284 (2013).

22. Wang, Q. & Holst, J. L-type amino acid transport and cancer: targeting the mTORC1 pathway to inhibit neoplasia. *Am. J. Cancer Res.* **5,** 1281–94 (2015).

23. Wongthai, P., Hagiwara, K., Miyoshi, Y., Wiriyasermkul, P., Wei, L., Ohgaki, R., Kato, I., Hamase, K., Nagamori, S. & Kanai, Y. Boronophenylalanine, a boron delivery agent for boron neutron capture therapy, is transported by ATB 0,+ , LAT1 and LAT2. *Cancer Sci.* **106,** 279–286 (2015).

24. Wiriyasermkul, P., Nagamori, S., Tominaga, H., Oriuchi, N., Kaira, K., Nakao, H., Kitashoji, T., Ohgaki, R., Tanaka, H., Endou, H., Endo, K., Sakurai, H. & Kanai, Y. Transport of 3-Fluoro-L- -Methyl-Tyrosine by Tumor-Upregulated L-Type Amino Acid Transporter 1: A Cause of the Tumor Uptake in PET. *J. Nucl. Med.* **53,** 1253–1261 (2012).

25. Hitoshi, E., Yoshikatsu, K., Kunio, S. & Koji, O. Aromatic Amino Acid Derivative with LAT1 Inhibitory Activity, LAT1 Inhibitor Containing the Same and Method for

Producing the Same. (2008). at <http://www.freepatentsonline.com/WO2008081537.html%0A%0A>

26. Grewer, C. & Grabsch, E. New inhibitors for the neutral amino acid transporter ASCT2 reveal its Na + -dependent anion leak. *J. Physiol.* **557,** 747–759 (2004).

27. Srinivasarao, M., Galliford, C. V. & Low, P. S. Principles in the design of ligand-targeted cancer therapeutics and imaging agents. *Nat. Rev. Drug Discov.* **14,** 203–219 (2015).

Chapter 5. Summary and future perspectives

5.1 Summary of the Dissertation

Previous studies have revealed potential of aberrant glutamine metabolism as a target of cancer therapy and diagnosis [1-7], and overexpression of glutamine transporters including ASCT2 [5,6,8] associated with this aberrant glutamine metabolism. While previous researches utilized increased cellular uptake of glutamine to visualize accelerated metabolism [1-3], this study focused on these overexpressed transporters on tumor cells, and developed the polymer functionalized with glutamine molecules for exerting selective affinity to tumor cells through multivalent effect with ASCT2.

Chapter 2 presented the synthesis and characterization of glutamine-functionalized polymers to achieve a high affinity to tumor cells. These functional polymers were synthesized in three steps as follows: (i) ring-opening polymerization of *N*-carboxy anhydride (NCA) to obtain biocompatible precursor polymers with controlled length and narrow molecular weight distribution, (ii) side chain modification of the precursor polymers to have glutamine moieties, and (iii) introduction of fluorescence dye to the polymer terminus for subsequent experiments. Through the NCA polymerization method, azide-functionalized poly(L-lysine)s having controlled length (the mean degree of polymerization (DP) was 30, 50, and 100) with narrow molecular weight distribution (M_w/M_n ~ 1.2) were successfully obtained. Lysine residues of the synthesized polymers were then modified to have glutamine moieties through γ-amide linkage because this modification is expected to tolerate glutamine-ASCT2 interaction according to previous studies [9,10]. Meanwhile, as control systems, glutamine moieties were changed to α-glutamyl moieties because α-glutamyl moieties have same charge and molecular weight with γ-modified glutamine moieties. ^{1}H NMR analysis revealed almost quantitative modification of the side chain for all polymers.

Finally, Cy5 fluorescence dye was conjugated to the polymer terminus by copper-free click chemistry. Even after fluorescence dye conjugation, all polymers showed monodisperse molecular weight distribution, indicating no obvious aggregation and/or degradation of the final products.

Chapter 3 described the expression level of glutamine transporter ASCT2 in *in vitro* and *in vivo*. Flow cytometric analysis revealed distinct overexpression of ASCT2 in human pancreatic cancer cell lines (BxPC3 cells) compared to human non-cancerous cell lines (HEK293 cells). From enzyme-linked immunosorbent assay (ELISA), the relative ASCT2 expression ratio between these cell lines was calculated to be 4.8-fold, which is in line with the previous clinical studies [6,11,12], indicating the validity of using these cell lines for the biological evaluation of the synthesized polymers. Moreover, this overexpression of ASCT2 was also confirmed in BxPC3 subcutaneous tumor compared to normal tissues. Based on these results, BxPC3 cells and HEK293 cells were used for the assessment of biological activities of synthesized polymers.

In **Chapter 4**, biological activities of the glutamine-functionalized polymers in *in vitro* and *in vivo* were assessed. To investigate the cellular interaction of the synthesized polymers with cultured cells, cellular uptake efficiency of the polymers was analyzed using flow cytometer. A series of glutamine-functionalized polymers PLys(Gln)-n exhibited DP-dependent cellular uptake behavior in BxPC3 cells; PLys(Gln)-100 showed significantly higher cellular uptake (9.7-fold and 18-fold higher compared to PLys(Gln)-50 and PLys(Gln)-30, respectively). In addition, this enhanced cellular uptake of PLys(Gln)-100 possessed tumor specificity; PLys(Gln)-100 showed rapid and higher cellular uptake (4.8-fold higher after 8 h incubation) in BxPC3 cells (ASCT2-overexpressing cancer cells)

compared to HEK293 cells (non-cancerous cells having moderate expression level of ASCT2). Cellular uptake analysis with transporter inhibitors demonstrated the dominant contribution of ASCT2 for the cellular interaction of PLys(Gln)-n. Interestingly, although the side chain structure of PLys(α-Glu)-100 is close to glutamate rather than glutamine, ASCT2 was also target transporter for PLys(α-Glu)-100. Confocal laser scanning microscopic observation indicated that both PLys(Gln)-100 and PLys(α-Glu)-100 could be internalized into BxPC3 cells *via* endocytosis. Based on these results, the high cellular uptake efficiency of PLys(Gln)-100 compared to PLys(α-Glu)-100 might be attributed to the high affinity to ASCT2 on tumor cells. To quantify the ability of the synthesized polymers as ligands, binding affinity of the polymers to ASCT2 on BxPC3 cells was estimated by cell-based competitive inhibition assay. Consistent with cellular uptake analysis, PLys(Gln)-100 showed high binding affinity to ASCT2 on BxPC3 cells (Dissociation constant (K_d) was estimated to be 62 nM) compared to that of PLys(α-Glu)-100 (K_d = 250 nM). It should be noted that the apparent K_d value of PLys(Gln)-100 is comparable to that of potent ligands in literature [13], indicating the potential of PLys(Gln)-100 as a tumor targeting ligand. Finally, *in vivo* interaction capacity of the polymers was evaluated by analyzing tumor retention of the polymer after intratumoral injection. Compared to PLys(α-Glu)-100, PLy(Gln)-100 showed significantly longer retention in the tumor tissue, indicating that PLys(Gln)-100 could exert its high affinity to tumor cells even in harsh *in vivo* environment.

Overall, I developed the novel glutamine-functionalized polymer with a high affinity to tumor cells overexpressing glutaminolysis-related transporter ASCT2. The glutamine-functionalized polymer exhibited enhanced cellular uptake in the cultured cancer cells by interacting with dense ASCT2. The apparent binding affinity of the

glutamine-functionalized polymer to ASCT2 on tumor cells was comparable to that of potent ligands. Even in *in vivo* environment, the glutamine-functionalized polymer showed prolonged retention at tumor site after intratumoral injection, indicating the potent interaction capacity of the glutamine-functionalized polymer to tumor tissue.

5.2 Future perspectives

To the best of my knowledge, this is the first study utilizing glutamine as a functional molecule showing a high affinity to tumor cells, inspired by tumor-associated metabolism. Given that the overexpression ratio of ASCT2 between BxPC3 and HEK293 cells is comparable to that in previous clinical studies [6, 11, 12], the tumor-selective interaction of the glutamine-functionalized polymer strongly indicates the potential *in vivo* activity of the synthesized polymer as a tumor-targeting ligand. In the synthetic strategy of the polymer, the Cy5 fluorescence dye can be easily replaced with the other functional molecules including therapeutic molecules, diagnostic agents, and functional macromolecules. Hence, the glutamine-functionalized polymer would be potentially useful as a versatile platform for delivering such functional molecules to diseased sites overexpressing ASCT2. However, the application of this polymer for this purpose still requires further optimization. For instance, PLys(Gln)-100, the most potent glutamine-functionalized polymer in this study, will be rapidly eliminated from the body after systemic administration because the molecular weight of the polymer is lower than the threshold of renal clearance [14], and therefore the polymer have few chances for interacting tumor tissues. Furthermore, in this study, glutamine moieties were tethered to polymer side chain by γ-amide linkage based on previous studies [9, 10]. This modification tolerated ASCT2-glutamine interaction and thereby showing tumor

selective high affinity; however, there is still room to consider the chemical structure of glutamine moieties at polymer side chain. For example, in addition to γ-amide group, glutamine molecule has α-amine and α-carboxyl group as the conjugation sites with polymers. Although α-amine and α-carboxyl group are appeared to be important for the interaction between amino acids and their corresponding transporters, the effect of glutamine conjugation to polymers using these functional groups on cellular interaction (e.g., cellular uptake behavior, target transporters, and binding affinity to the target transporters) should be evaluated in the future study.

The other possible application of the glutamine-functionalized polymer is a shell molecule for nanoparticle-based drug carriers. Nanoparticles such as polymeric micelles are commonly used as drug carriers in drug delivery systems due to their unique core-shell structure; the drug-loaded core is surrounded by biocompatible shell molecules. Poly(ethylene glycol) (PEG) is frequently used as shell molecules because the PEG shell can prevent non-specific protein absorption and recognition by reticuloendothelial system, thereby providing stealth ability to the nanoparticles in bloodstream [15, 16]. However, PEG also potentially prevents the interaction between PEG-modified nanoparticles and target cells, thereby decreasing the cellular uptake efficiency of the nanoparticles. Recently, zwitterionic polymers have attracted a great attention as a new class of biocompatible shell molecules because zwitterionic shell provides non-adhesive properties and colloidal stability to nanoparticles. Indeed, previous study demonstrated that 2-methacryloyloxyethyl phosphorylcholine (MPC)-coated nanoparticles inhibited non-specific protein absorption [17] and showed potential ability as a drug carrier [18]. Considering the zwitterionic structure of the developed glutamine-functionalized polymer, this polymer is expected to show suppress

non-specific interaction. In addition, the glutamine-functionalized polymer has the promising tumor-targeting ability as described in chapter 4. Thus, this glutamine-functionalized polymer has a huge potential as a novel shell molecule possessing stealth properties as well as tumor-targeting ability.

Moreover, this study offers a fundamental molecular design to target dense transporters on tumor cells by utilizing their substrates. In this study, I focused on glutamine transporter ASCT2 as a target transporter because of its important role in tumor cells and overexpression in a wide variety of tumor cells. In addition to this ASCT2, the other amino acids transporters including LAT1 (system L transporter 1) and xCT (system xc- transporter) were also reported to be overexpressed in various kinds of tumor cells [19-21], suggesting the potentials of these transporters as targets for sensing tumor cells. By utilizing their substrates (e.g., methionine and phenylalanine for LAT1, and cystine for xCT) instead of glutamine, the developed methodology in this study can provide functional polymers with a high affinity to these transporters on tumor cells.

5.3 References

1. Wu, Z., Zha, Z., Li, G., Lieberman, B. P., Choi, S. R., Ploessl, K. & Kung, H. F. [18 F](2 S ,4 S)-4-(3-Fluoropropyl)glutamine as a Tumor Imaging Agent. *Mol. Pharm.* **11,** 3852–3866 (2014).
2. Venneti, S., Dunphy, M. P., Zhang, H., Pitter, K. L., Zanzonico, P., Campos, C., Carlin, S. D., La Rocca, G., Lyashchenko, S., Ploessl, K., Rohle, D., Omuro, A. M., Cross, J. R., Brennan, C. W., Weber, W. A., Holland, E. C., Mellinghoff, I. K., Kung, H. F., Lewis, J. S. & Thompson, C. B. Glutamine-based PET imaging facilitates enhanced

metabolic evaluation of gliomas in vivo. *Sci. Transl. Med.* **7,** 274ra17-274ra17 (2015).

3. Ploessl, K., Wang, L., Lieberman, B. P., Qu, W. & Kung, H. F. Comparative Evaluation of 18F-Labeled Glutamic Acid and Glutamine as Tumor Metabolic Imaging Agents. *J. Nucl. Med.* **53,** 1616–1624 (2012).

4. Jin, L., Alesi, G. N. & Kang, S. Glutaminolysis as a target for cancer therapy. *Oncogene* **35,** 3619–25 (2016).

5. van Geldermalsen, M., Wang, Q., Nagarajah, R., Marshall, A. D., Thoeng, A., Gao, D., Ritchie, W., Feng, Y., Bailey, C. G., Deng, N., Harvey, K., Beith, J. M., Selinger, C. I., O'Toole, S. A., Rasko, J. E. J. & Holst, J. ASCT2/SLC1A5 controls glutamine uptake and tumour growth in triple-negative basal-like breast cancer. *Oncogene* **35,** 3201–8 (2016).

6. Wang, Q., Hardie, R.-A., Hoy, A. J., van Geldermalsen, M., Gao, D., Fazli, L., Sadowski, M. C., Balaban, S., Schreuder, M., Nagarajah, R., Wong, J. J.-L., Metierre, C., Pinello, N., Otte, N. J., Lehman, M. L., Gleave, M., Nelson, C. C., Bailey, C. G., Ritchie, W., Rasko, J. E. J. & Holst, J. Targeting ASCT2-mediated glutamine uptake blocks prostate cancer growth and tumour development. *J. Pathol.* **236,** 278–89 (2015).

7. Wang, Q., Beaumont, K. a., Otte, N. J., Font, J., Bailey, C. G., van Geldermalsen, M., Sharp, D. M., Tiffen, J. C., Ryan, R. M., Jormakka, M., Haass, N. K., Rasko, J. E. J. & Holst, J. Targeting glutamine transport to suppress melanoma cell growth. *Int. J. cancer* **135,** 1060–71 (2014).

8. Bode, B. P., Fuchs, B. C., Hurley, B. P., Conroy, J. L., Suetterlin, J. E., Tanabe, K. K., Rhoads, D. B., Abcouwer, S. F. & Souba, W. W. Molecular and functional analysis of

glutamine uptake in human hepatoma and liver-derived cells. *Am. J. Physiol. Gastrointest. Liver Physiol.* **283,** G1062-73 (2002).

9. Esslinger, C. S., Cybulski, K. A. & Rhoderick, J. F. Nγ-Aryl glutamine analogues as probes of the ASCT2 neutral amino acid transporter binding site. *Bioorg. Med. Chem.* **13,** 1111–1118 (2005).

10. Schulte, M. L., Dawson, E. S., Saleh, S. a., Cuthbertson, M. L. & Manning, H. C. 2-Substituted Nγ-glutamylanilides as novel probes of ASCT2 with improved potency. *Bioorg. Med. Chem. Lett.* **25,** 113–116 (2015).

11. Huang, F., Zhao, Y., Zhao, J., Wu, S., Jiang, Y., Ma, H. & Zhang, T. Upregulated SLC1A5 promotes cell growth and survival in colorectal cancer. *Int J Clin Exp Pathol* **7,** 6006–6014 (2014).

12. Alves, M. J. F., Uno, M., Silva, R. da, Oba-Shinjo, S. M. & Marie, S. K. N. The expression of the aminoacid transporters ASCT2 (SLC1A5) and LAT1 (SLC7A5) in astrocytomas. *Med. Express* **3,** 1–8 (2016).

13. Srinivasarao, M., Galliford, C. V. & Low, P. S. Principles in the design of ligand-targeted cancer therapeutics and imaging agents. *Nat. Rev. Drug Discov.* **14,** 203–219 (2015).

14. Fox, M. E., Szoka, F. C. & Fréchet, J. M. J. Soluble Polymer Carriers for the Treatment of Cancer: The Importance of Molecular Architecture. *Acc. Chem. Res.* **42,** 1141–1151 (2009).

15. Jokerst, J. V, Lobovkina, T., Zare, R. N. & Gambhir, S. S. Nanoparticle PEGylation for imaging and therapy. *Nanomedicine* **6,** 715–728 (2011).

16. Cho, K., Wang, X., Nie, S., Chen, Z. & Shin, D. M. Therapeutic Nanoparticles for

Drug Delivery in Cancer. *Clin. Cancer Res.* **14,** 1310–1316 (2008).

17. Konno, T., Kurita, K., Iwasaki, Y., Nakabayashi, N. & Ishihara, K. Preparation of nanoparticles composed with bioinspired 2-methacryloyloxyethyl phosphorylcholine polymer. *Biomaterials* **22,** 1883–9 (2001).

18. Miyata, R., Ueda, M., Jinno, H., Konno, T., Ishihara, K., Ando, N. & Kitagawa, Y. Selective targeting by preS1 domain of hepatitis B surface antigen conjugated with phosphorylcholine-based amphiphilic block copolymer micelles as a biocompatible, drug delivery carrier for treatment of human hepatocellular carcinoma with paclitaxel. *Int. J. Cancer* **124,** 2460–2467 (2009).

19. Namikawa, M., Kakizaki, S., Kaira, K., Tojima, H., Yamazaki, Y., Horiguchi, N., Sato, K., Oriuchi, N., Tominaga, H., Sunose, Y., Nagamori, S., Kanai, Y., Oyama, T., Takeyoshi, I. & Yamada, M. Expression of amino acid transporters (LAT1, ASCT2 and xCT) as clinical significance in hepatocellular carcinoma. *Hepatol. Res.* **45,** 1014–1022 (2015).

20. Wiriyasermkul, P., Nagamori, S., Tominaga, H., Oriuchi, N., Kaira, K., Nakao, H., Kitashoji, T., Ohgaki, R., Tanaka, H., Endou, H., Endo, K., Sakurai, H. & Kanai, Y. Transport of 3-Fluoro-L- -Methyl-Tyrosine by Tumor-Upregulated L-Type Amino Acid Transporter 1: A Cause of the Tumor Uptake in PET. *J. Nucl. Med.* **53,** 1253–1261 (2012).

21. Oda, K., Hosoda, N., Endo, H., Saito, K., Tsujihara, K., Yamamura, M., Sakata, T., Anzai, N., Wempe, M. F., Kanai, Y. & Endou, H. L-Type amino acid transporter 1 inhibitors inhibit tumor cell growth. *Cancer Sci.* **101,** 173–179 (2010).

Achievements

Publications

Publication for this study

1. Yamada, N., Honda, Y., Takemoto, H., Nomoto, T., Matsui, M., Tomoda, K., Konno, M., Ishii, H., Mori, M. & Nishiyama, N.
   Engineering Tumour Cell-Binding Synthetic Polymers with Sensing Dense Transporters Associated with Aberrant Glutamine Metabolism. *Sci. Rep.***7,** 6077 (2017).

Publications for the other studies

1. Wu, H., Cabral, H., Toh, K., Mi, P., Chen, Y. C., Matsumoto, Y., Yamada, N., Liu, X., Kinoh, H., Miura, Y., Kano, M. R., Nishihara, H., Nishiyama, N. & Kataoka, K.
   Polymeric micelles loaded with platinum anticancer drugs target preangiogenic micrometastatic niches associated with inflammation. *J. Control. Release* **189,** 1–10 (2014).

2. Ahn, J., Miura, Y., Yamada, N., Chida, T., Liu, X., Kim, A., Sato, R., Tsumura, R., Koga, Y., Yasunaga, M., Nishiyama, N., Matsumura, Y., Cabral, H. & Kataoka, K.
   Antibody fragment-conjugated polymeric micelles incorporating platinum drugs for targeted therapy of pancreatic cancer. *Biomaterials* **39,** 23–30 (2015).

3. Cabral, H., Makino, J., Matsumoto, Y., Mi, P., Wu, H., Nomoto, T., Toh, K., Yamada, N., Higuchi, Y., Konishi, S., Kano, M. R., Nishihara, H., Miura, Y., Nishiyama, N. &

Kataoka, K. Systemic targeting of lymph node metastasis through the blood vascular system by using size-controlled nanocarriers. *ACS Nano* **9,** 4957–4967 (2015).

4. Kawamura, W., Miura, Y., Kokuryo, D., Toh, K., Yamada, N., Nomoto, T., Matsumoto, Y., Sueyoshi, D., Liu, X., Aoki, I., Kano, M. R., Nishiyama, N., Saga, T., Kishimura, A. & Kataoka, K. Density-tunable conjugation of cyclic RGD ligands with polyion complex vesicles for the neovascular imaging of orthotopic glioblastomas. *Sci. Technol. Adv. Mater.* **16,** 35004 (2016).

5. Matsumoto, Y., Nichols, J. W., Toh, K., Nomoto, T., Cabral, H., Miura, Y., Christie, R. J., Yamada, N., Ogura, T., Kano, M. R., Matsumura, Y., Nishiyama, N., Yamasoba, T., Bae, Y. H. & Kataoka, K. Vascular bursts enhance permeability of tumour blood vessels and improve nanoparticle delivery. *Nat. Nanotechnol.* **11,** 533–8 (2016).

Patents

1. 発明者: 山田直生, 西山伸宏, 武元宏泰, 野本貴大, 友田敬士郎, 松井誠, 本田雄士, 石井秀始, 森正樹, 今野雅充
   発明の名称: グルタミントランスポーターと多価結合することができるリガンド, 及び当該リガンドを含む組成物
   出願人: 東京工業大学, 大阪大学
   出願日: 2016 年 8 月 22 日
   出願番号: 特願 2016-161774

Presentations

International conference

1. ○Yuto Honda, Naoki Yamada, Hiroyasu Takemoto, Takahiro Nomoto, Makoto Matsui, Keishiro Tomoda, Nobuhiro Nishiyama.
   “Novel design of glutamine-derived polymer with a high affinity to cancer cells based on aberrant glutamine metabolism”
   253rd American Chemical Society National Meeting & Exposition, BIOT-321, San Francisco, CA, USA (April 2017)

2. ○Naoki Yamada, Yuto Honda, Hiroyasu Takemoto, Takahiro Nomoto, Makoto Matsui, Keishiro Tomoda, Nobuhiro Nishiyama.
   “Glutamine-functionalized polymer having tumor-selective high affinity by interacting with dense glutamine transporters based on aberrant metabolism”
   International Symposium on Drug Delivery and Pharmaceutical Sciences: Beyond the History, P-33, Kyoto, Japan (March 2017)

3. ○Naoki Yamada, Yuto Honda, Hiroyasu Takemoto, Takahiro Nomoto, Makoto Matsui, Keishiro Tomoda, Nobuhiro Nishiyama.
   “Novel glutamine-based polymeric ligand for transporter-mediated tumor targeting”
   3rd International Conference on Biomaterials Science (ICBS2016), P036, Tokyo, Japan (November 2016)

Domestic conference

1. ○山田直生、本田雄士、武元宏泰、野本貴大、松井誠、友田敬士郎、西山伸宏
   「がん細胞選択的な相互作用を目指したグルタミン導入高分子の設計と機能評価」
   『第 46 回医用高分子シンポジウム』、東京、2017 年 7 月

2. ○Naoki Yamada, Yuto Honda, Hiroyasu Takemoto, Takahiro Nomoto, Makoto Matsui, Keishiro Tomoda, Nobuhiro Nishiyama
   “Design of synthetic polymer toward achieving a selective high affinity to tumor cells by interacting with dense glutaminolysis-related transporters”

『第 66 回高分子学会年次大会』、千葉、2017 年 5 月

Awards

1. Poster prizes at 3rd International Conference on Biomaterials Science (ICBS2016)

Acknowledgment

First and foremost, I would like to express the deepest appreciation to Prof. Nobuhiro Nishiyama for the sophisticated discussion, insightful suggestions, and offering me the best opportunity to proceed with this study in wonderful laboratory.

I also express the greatest appreciation to Prof. Hiroshi Ueda, Prof. Atsushi Shishido, Prof. Atsushi Maruyama, and Prof. Takeo Yamaguchi for reviewing this thesis. Their insightful suggestions and careful comments were very helpful to improve the thesis.

I appreciate for all staffs in Nishiyama Laboratory, Dr. Takahiro Nomoto for his insightful advices and encouragement, Dr. Hiroyasu Takemoto for his help in polymer synthesis and thoughtful discussion, Dr. Makoto Matsui for his help in biological experiments, Dr. Keishiro Tomoda for motivating me.

I also express my gratitude to colleagues in Nishiyama Laboratory, especially to Mr. Yuto Honda, Mr. Takanori Inaba, Mr. Junhyun Kim, Mr. Tsukasa Nishimori, Ms. Wang Chih-ling, Dr. Noor Faizah, and Dr. Huang Chi-hao for their help in the experiments, overnight discussion about researches as well as daily life, and each other encouragement.

I appreciate Honjo International Scholarship Foundation for financial support. This study was supported by Basic Science and Platform Technology Program for Innovative Biological Medicine from Japan Agency for Medical Research and Development (AMED), the Project for Cancer Research And Therapeutic Evolution (P-CREATE) from AMED, Center of Innovation (COI) program from Japan Science and Technology Agency (JST), and JSPS KAKENHI Grant-in-Aid from the Japan Society for the Promotion of Science (JSPS).

Finally, I am grateful to my family, my father Katsunao Yamada, my mother Yumi Yamada, my sister Yuki Yamada, and my wife Nanako Yamada for their warm support and encouragement.

Naoki Yamada

Department of Environmental Chemistry and Engineering
Interdisciplinary Graduate School of Science and Engineering
Tokyo Institute of Technology
September 2018